Journal of Baku Engineering University

P-ISSN :3134-6081
E-ISSN 3134-8866

Volume 9
Number 2
2025

ADVANCES in CHEMISTRY and CHEMICAL ENGINEERING

Journal is published twice a year
Number - 1. June, Number - 2. December
An International Journal

http://journal.beu.edu.az

Contact address

Journal of Baku Engineering University
AZ0101, Khirdalan city, Hasan Aliyev str. 120, Absheron, Baku, Azerbaijan
Tel: *00 994 12 - 349 99 95* ***Fax:*** *00 994 12 349-99-90/91*
e-mail: *chemstrybiology@beu.edu.az,* *journal@beu.edu.az*
web: *http://journal.beu.edu.az*
facebook: *Journal Of Baku Engineering University*

P-ISSN: 3134-6081
E-ISSN: 3134-8866

P-ISSN: 3134-6081
E-ISSN: 3134-8866

Journal of Baku Engineering University

ADVANCES IN CHEMISTRY AND CHEMICAL ENGINEERING

Baku - AZERBAIJAN

J O U R N A L O F B A K U E N G I N E E R I N G U N I V E R S I T Y
ADVANCES IN CHEMISTRY AND CHEMICAL ENGINEERING
2025. Volume 9, Number 2

CONTENTS

2025. Volume 9, Number 2 Pages 81-85

UDC: 661.183.12:628.34
DOI: https://doi.org/10.30546/2521-6317.2025.02.538

TECHNOLOGY FOR THE PRODUCTION OF ION-EXCHANGE POLYMERS BASED ON FURFURAL AND ITS DERIVATIVES AND THEIR APPLICATION IN THE TREATMENT OF WASTEWATER FROM HYDROMETALLURGICAL INDUSTRIES

Mizrobjon Khalim ugli ZARIPOV,

Vokhid Nizomovich AKHMEDOV,

Niginabonu Qobil qizi JAMILOVA

[1] *Assistant, Bukhara State Technical University,Bukhara, Republic of Uzbekistan*

[2] *Professor, Bukhara State Technical University,Bukhara, Republic of Uzbekistan*

[3] *Doctoral Candidate, Bukhara State Technical University,Bukhara, Republic of Uzbekistan*

ARTICLE INFO

Article history:
Received:2025-08-01
Received in revised form :2025-08-13
Accepted:2025-09-10
Available online:2025-12-25

Keywords:
furfural, furan compounds, thiourea, phosphoric acid derivatives, polysilicic acid, dinitrile-azobisiminodiacetic acid (DAA), potassium hydroxide (KOH), cryoscopic method, oligo(polymer), molecular weight, vinylacetylene.

ABSTRACT

The article substantiates the feasibility of using furfural a product of the hydrolysis industry as a base monomer in the synthesis of ion-exchange resins. A methodology for obtaining new ion-exchange polymeric materials based on furfural as a secondary raw material is presented, along with the results of studies on their sorption, physicochemical, and operational characteristics. The identify cation of effective practical applications of the synthesized ion exchangers for the treatment of industrial wastewater and natural waters from chemical enterprises, including hydrometallurgical facilities, is of considerable scientific, technical, and applied significance.

1. INTRODUCTION

The scale of industrial organic synthesis has now reached such proportions that the issue of the limited availability of natural oil and gas resources required to meet its demands is becoming increasingly urgent. Under the conditions of modern scientific and technological advances, polymer composite materials formed through the combination of components of different chemical nature represent a new class of materials that, in terms of overall performance characteristics, significantly surpass the properties of their individual constituents [1-3]. Owing to their composite characteristics, such materials exhibit unique physicomechanical, magnetic, and optoelectronic properties, high chemical and thermal stability, and enhanced resistance to various types of radiation. In recent years, the development of materials and compositions with predetermined properties containing phosphate groups has gained increasing importance.

Phosphate-containing natural compounds are components of widely used medicinal pharmaceuticals. Compounds with phosphate groups constitute not only the foundation of inorganic chemistry but also the fundamental basis of vital processes in living organisms. The ability of phosphate groups to undergo facile modification with organic compounds is of both practical and theoretical significance and has generated considerable scientific interest among researchers [4-6]. Foreign literature sources devoted to the synthesis and investigation of ion-exchange materials based on furfural and its derivatives are limited to a small number of publications and are predominantly of a patent nature [7-9]. One of the earliest studies aimed at the synthesis of ion exchangers focused on the production of carboxyl and sulfo-cationites through the polycondensation of furfural with β-furylacrylic acid, benzenesulfonic acid, and *n*-phenolsulfonic acid. These cationites contain carboxyl, sulfo, and phenolic hydroxyl groups. Although sulfo-cationites are produced from relatively inexpensive raw materials, such as lignin, the sulfation process is random in nature, resulting in ion exchangers with a disordered structure. Simultaneously, both ion-exchange and electro-exchange properties were observed in the polymer obtained through the polycondensation of polyhydric phenols with furfural [9-11]. This polymer is characterized by reducing properties, with a capacity to reduce trivalent iron to divalent iron of 6.5 mg-eq/g. To improve the kinetic characteristics during the synthesis of electro-ion-exchange polymers, pre-sulfonated phenols were used, which led to a slight increase in the reducing capacity up to 7.5 mg-eq/g. The use of furfural as a crosslinking agent in the production of ion-exchange materials and the analysis of the structure of these polymers will be considered in greater detail, as the results obtained can be applied in further studies on the synthesis of nitrogen-containing anion exchangers. Among the earliest works devoted to the synthesis of ion exchangers are studies on the production of carboxyl and sulfo-cationites through the polycondensation of furfural with *p*-furylacrylic acid, benzenesulfonic acid, and *n*-phenolsulfonic acid [12-14]. Moreover, one of the most dynamically developing areas of modern organic chemistry is the synthesis of highly reactive compounds through the introduction of unsaturated groups into the structure of organic molecules. The incorporation of a vinyl group opens virtually unlimited possibilities for the use of divinylfurfuryl ethers in the targeted organic synthesis of multifunctional furan compounds [15-17]. However, the widespread application of divinylfurfuryl ethers is limited by the lack of simple and technologically convenient methods for their synthesis. In contrast to alkyl vinyl ethers, they have been studied to a much lesser extent; their chemical properties are distinguished by specificity due to the presence of additional functional groups, which makes them prone to electrophilic and radical reactions. In this context, the synthesis of silsesquioxanes and (oligo)polymers, which enhance the mechanical strength and thermal stability of compositions, as well as the study of their properties and the development of technologies for producing ion exchangers based on them, becomes particularly important [18].

2. EXPERIMENTAL PART

In this study, the synthesis based on furan derivatives was carried out as follows. A reaction flask was charged with 50 mg of vinylfurfuryl ether, 0.1 mol of thiourea, 50 mg of sodium tripolyphosphate, 50 mg of polysilicic acid, and 1% (by monomer mass) of the initiator dinitrile-azobisiminodiacetic acid (DAA). The flask was equipped with a thermometer and placed on a magnetic stirrer, then heated at 85–120 °C for 2 hours. After the reaction was complete, the viscous, yellowish, and solidifying polymer Polyphos 1 was washed three times, purified, and dried to constant weight.

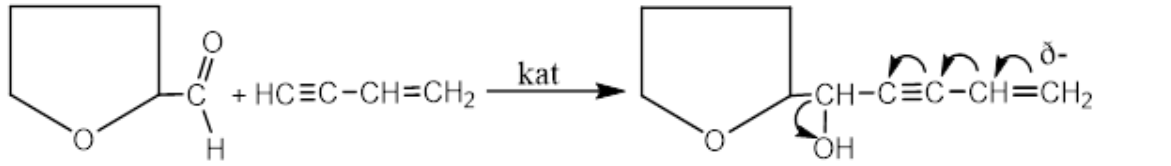

1-(tetrahydrofuran-2-yl)pent-4-en-2-yn-1-ol

Data on the direct vinylation of furfuryl alcohols with vinylacetylene are extremely limited. Considering the potential of furfural to undergo the Cannizzaro reaction in an alkaline medium, furfuryl alcohol was chosen. The reaction to produce divinylfurfuryl ether was carried out using furfuryl alcohol and vinylacetylene in an alkaline system at room temperature and atmospheric pressure, resulting in the formation of 1-(tetrahydrofuran-2-yl)pent-4-en-2-yn-1-ol.

The resulting intermediate compound possesses broad potential for modification with various substances. In particular, the introduction of compounds containing a non-bonded electron pair enables the synthesis of highly reactive compounds. Accordingly, the intermediate was modified with thiourea, sodium tripolyphosphate, and polysilicic acid to obtain an inorganic-organic ion exchanger. The reaction was carried out in the following sequence.

First, thiourea reacts with the hydroxyl group of the intermediate compound according to the following scheme.

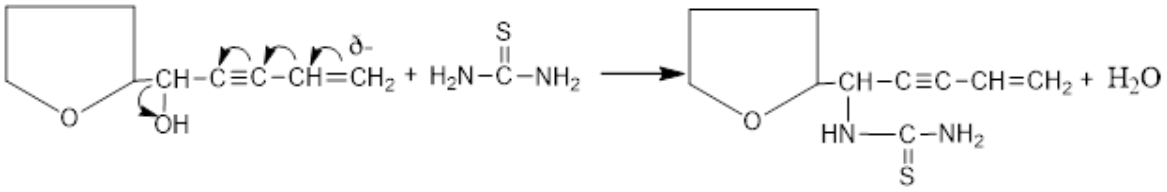

The resulting intermediate compound undergoes polymerization. The reaction proceeds in a single system following a specific sequence.

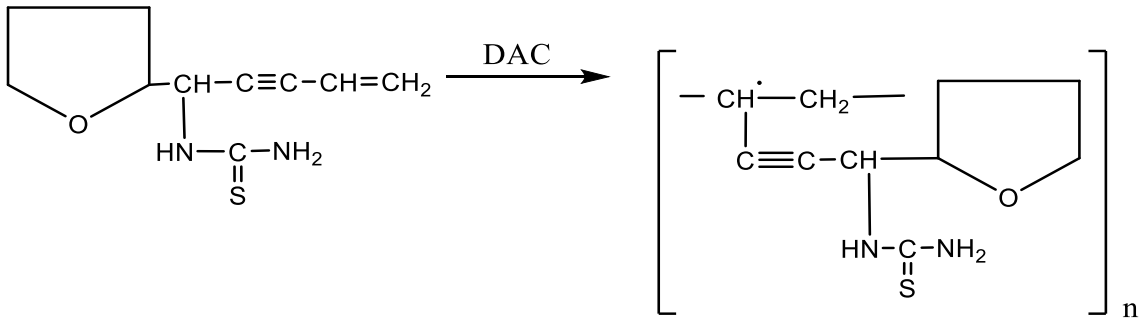

To purify the obtained ion exchanger, an extraction method using various solvents was employed. The separation method, based on the differing solubilities of the starting, intermediate, and final products in various solvents, ensures a high level of substance purity. Accordingly, a solvent was selected that does not dissolve the final product but is capable of dissolving the starting and intermediate compounds. The extraction results are presented in the following table (table 1).

To purify the obtained ion exchanger, an extraction method using various solvents was employed. This separation technique, based on the differing solubilities of the starting, intermediate, and final products in various solvents, ensures a high level of substance purity.

Accordingly, a solvent was selected that does not dissolve the final product but is capable of dissolving the starting and intermediate compounds. The extraction results are presented in the following table (table 1).

Table 1. *Solubility of reagents and reaction products in various solvents*

Solvents	**Isopropyl alcohol**	**Octane**	**Isobutyl alcohol**	**Heptane**	**Toluene**	**Hexane**	**Amyl alcohol**	**Decane**	**Ethyl alcohol**	**Dimethylformamide (**
Substances										
Furfural	+	+	+	+	-	-	-	-	-	-
Vinylacetylene	+	+	+	-	+	-	-	-	+	-
Sodium tripolyphosphate	+	+	+	+	+	+	+	+	+	-
Product										
Polifos-1	+	+	+	-	+	-	-	-	-	+

When selecting a solvent for the extraction method, the solubility of the reagents and reaction products in various solvents was taken into account. Dimethylformamide proved to be the most suitable extractant for this reaction system due to its dipole moment and selective dissolving ability compared to other solvents. Moreover, the insolubility of the intermediate and starting compounds allowed the substance to be isolated in a pure form.

In the first layer of the extraction mixture, unreacted substances and ether-soluble components (KOH + DMSO + furfural) were identified, while in the second layer, the ether-insoluble synthesis product was found, which was 1-(1-(tetrahydrofuran-2-yl)pent-4-en-2-yn-1-yl)thiourea.

In dimethylformamide, the pure polymer was isolated using the extraction method, and its physical properties were studied. The viscosity of polydivinylfurfuryl sodium tripolyphosphate (before the addition of polysilicic acid) was measured using a HAAKE Viscotester 2 Plus viscometer and can be represented in the following graph.

3. Conclusion

The conducted studies confirm that the synthesis of ion-exchange polymeric materials based on furfural and its derivatives is both scientifically and practically justified and represents a promising direction. In the context of limited oil and gas resources, the use of furfural a product of the hydrolysis industry as a valuable monomer provides a resource-saving and economically efficient solution. The inorganic-organic ion exchangers obtained with the involvement of phosphate groups, thiourea, and polysilicic acid exhibit high reactivity. The presence of functional phosphate, thiocarbamide, and silicon-containing fragments in their structure enhances their sorption properties and complex-forming ability. It has been established that the intermediate compounds formed during the synthesis of divinylfurfuryl ether and its subsequent modification create an ordered structure during polymerization. The high efficiency of dimethylformamide as a selective solvent in the purification of the product by extraction has been demonstrated, allowing the isolation of a polymer with a high degree of purity. The obtained polymer, Polifos-1, exhibits favorable physicochemical characteristics, including

viscosity and stability. The incorporation of polysilicic acid contributes to increased mechanical strength and thermal resistance of the composite material. The results of the study indicate that the furfural-based phosphorus- and sulfur-containing ion-exchange polymers can be effectively used as sorbents for the treatment of wastewater from hydrometallurgical and chemical industry enterprises. They provide efficient removal of heavy metal ions through complexation and ion-exchange mechanisms.

REFERENCE

1. Firuz O., Vohid A. Synthesis of ionites based on cremnisole //Universum. – 2022. – №. 4-13 (97). – С. 19-21.
2. Abror o'g'li, A. A. (2023). Improving the physico-chemical properties of urea furfural resin. *American Journal of Pedagogical and Educational Research*, *12*, 268-271.
3. Davron o'g'li, N. D. (2023). Application of urea-formaldehyde and urea-furfural resins in different solvents. *American Journal of Pedagogical and Educational Research*, *12*, 265-267.
4. Firuz O., Vokhid A. Synthesis and properties of complex forming ionites //Universum: технические науки. – 2023. – №. 2-6 (107). – С. 38-40.
5. Ostonov F., Akhmedov V., Olimov B. Preparation of hybrid composites by sol-gel method and analysis of its properties //Scientific Collection «InterConf». – 2022. – №. 123. – С. 256-259.
6. Zuhriddin, R., & Niginabonu, J. (2022). Production of polyethylene terephthalate. Universum (5-11 (98)), 58-62.
7. O'G'Li, R. Z. K., & Qizi, J. N. Q. (2022). Analysis of importance and methods of production of block sopolymers based on polyetylenterephtalate. International Journal of Advanced Technology and Natural Sciences, 3(1), 51-55.
8. Zuhriddin, R., Niginabonu, J., Aminjon, V., & Temurbek, D. (2022). Mechanisms of eterification of tereftalic acid with etylenglycol. Universum: технические науки, (5-11 (98)), 63-67.
9. Nigina J., Mizrob Z. Production of vinyl ethers of furfuryl alcohol //Universum: химия и биология. – 2023. – №. 9-2 (111). – С. 57-62.
10. Bobir, O., Vokhid, A., Gulnoz, G., & Sherzod, R. (2022). Synthesis and properties of nitrogen-retaining corrosion inhibitors. Universum: химия и биология, (4-2 (94)), 43-46.
11. **Ostonov, F.** (2020). Synthesis of acrylic compounds modified with organosilicon compounds. *Center of Scientific Publications (Bukhara State University)*, 1(1).
12. Olimov, B. B., & Rakhmatov, S. (2022). Synthesis and use of corrosion inhibitors on the basis of diatomic phenols in the oil and gas industry. In Kimyo va tibbiyot: nazariyadan amaliyotgacha (pp. 141-143).
13. Chavez-Sifontes, M. H., Domine, M. E., & Valencia, S. (2015). Synthesis of furan derivatives via cascade-type reactions catalyzed by solid acids. *Catalysis Today*, *257*, 305-317.
14. Gaboriaud, F., Nonat, A., Chaumont, D., & Craievich, A. (2005). Structural model of gelation processes of a sodium silicate sol destabilized by calcium ions: combination of SAXS and rheological measurements. *Journal of Non-Crystalline Solids*, *351*(4), 351-354.
15. Yang, Z., Chou, X., Kan, H., Xiao, Z., & Ding, Y. (2022). Nanoporous copper catalysts for the fluidized electrocatalytic hydrogenation of furfural to furfuryl alcohol. *ACS Sustainable Chemistry & Engineering*, *10*(22), 7418-7425.
16. Venegas-García, D. J., Mir, M., Steiger, B. G., & Wilson, L. D. (2024). Furfuryl-pyridinium-functionalization of flaxseed gum for effective methylene blue removal from aqueous solution. *Canadian Journal of Chemistry*.
17. Tanaka, K., Ohta, K., Haddad, P. R., Fritz, J. S., Miyanaga, A., Hu, W., ... & Sarzanini, C. (2001). High-performance ion-exclusion/cation-exchange chromatography of anions and cations in acid rain waters on a weakly acidic cation-exchange resin. *Journal of Chromatography A*, *920*(1-2), 239-245.
18. Jiang, H., Yuan, J., Lin, L., Wang, H., Gao, R., Chen, Y., ... & Wang, X. (2025). Electro-deionization with zirconium phosphate cation exchange resins for treating radioactive wastewater. *Separation and Purification Technology*, 134055.

2025. Volume 9, Number 2 Pages 86-98

UDC: 665.637
DOI: https://doi.org/10.30546/2521-6317.2025.02.505

DESULFURIZATION TECHNIQUES OF HEAVY OIL FRACTIONS. REVIEW

Khamis ABIYEV[1*], Elvira GUSEINOVA[1]

[1]*Azerbaijan State Oil and industry University, Baku, Azerbaijan*

ARTICLE INFO

Article history:
Received:2025-05-22
Received in revised form:2025-06-11
Accepted:2025-07-08
Available online:2025-12-25

Keywords:
sulfur removal, hydrodesulfurization, oxidative desulfurization, biodesulfurization, ionic liquid extraction

ABSTRACT

Strategies for desulfurization of heavy oil have been investigated through scrutinizing the practicality of differing heavy oil procedures along with reviewing literature regarding the topic. These methodologies include hydrodesulfurization, extractive desulfurization, oxidative desulfurization, and biodesulfurization. Each possesses its iterations along with modified versions through repeated performance for improved results. Nevertheless, these techniques do not function properly. They particularly strive to desulfurize viscous oil. This constraint exists mainly since heavy oil possesses intrinsic attributes like elevated sulfur concentration, viscosity, boiling point, and the elastic character of sulfur compounds. Since fuels must exhibit maximal environmental compatibility, ever more restrictive statutes now oversee the sulfur constituent of these fuels. Additionally, crude oil grade and its byproducts diminished and a need for remaining fuels persists, revealing the importance of sulfur removal, notably in viscous oils. The existence of detailed thiophenic compounds imparts important quantities of sulfur to these oils rendering elimination via typical high-pressure hydrodesulfurization methods arduous.

[*]Corresponding author.

E-mail address: xamisabiyev123@gmail.com (Khamis Abiyev Chingiz).

1. INTRODUCTION

Desulfurization constitutes an obligatory process during crude oil refinement to yield coveted end products (2,3). Rules concerning the levels of sulfur within transport fuels have progressively tightened over time, also a collection of petrochemical compounds get produced virtually sulfur-free currently. Thus, sulfur extraction out from oil is among the vital transformation necessities within many refineries (2). This extraction substantially influences the value and handling expenditures of unrefined petroleum.

The global demand for cleaner fuels is augmenting because progressively strict environmental statutes superintend the sulfur content of transportation fuels, notably marine fuels. Additionally, crude oil along with its components diminishes in caliber because the requirement persists regarding leftover fuels, therefore eliminating sulfur turns important, notably within viscous oils. Considering these commodities include substantial quantities of sulfur predomi-

nantly within detailed thiophenic configurations, established high-pressure desulfurization techniques battle for its extraction.

Furthermore, unprocessed substances should be immaculate. This immaculateness is paramount for the petrochemical industry. The durability of equipment, the efficiency of processing, and the quality of products in this industry directly hinge on the purity of raw materials.

Petrochemical products like plastics, polymers, fertilizers, together with other chemicals require raw materials. Superior raw materials are requisite to product quality. Absent pristine base components, the resultant item degrades, thus curtailing worth and utility.

Refining progressions become more efficient when the petrochemical sector employs pure feedstocks. Elevated levels of sulfur, nitrogen, and additional pollutants may impair catalysts given their propensity for diminishing reaction velocity and efficacy (11). Conversely, pristine feedstock eases superior equipment performance while concurrently diminishing energy expenditure.

Equipment safeguard is paramount: Raw materials occasionally harbor pollutants. Sulfur along with metal compounds, for instance, result in corrosion in addition to wear. This elevates repair expenditures and induces premature equipment failure. Conversely, should we utilize pure raw materials, this will lengthen equipment life coupled with diminished maintenance requirements.

Conservation of the environment remains quite important. Employing purified raw material consequently aids in diminishing environmental repercussions. Sulfur along with noxious materials discharged copiously augment emissions to the ecosphere, which taints the atmosphere inducing diverse ecological predicaments. Clean feedstocks ease cleaner production processes as well as a decline in these emissions.

Accordingly, feedstocks should exhibit high purity within the petrochemical sector since that remains important for economic efficiency plus product quality, together with environmental protection and regulatory compliance.

Some scholars observed that hydrodesulfurization (HDS) coupled with carbon rejection methodologies are principal industrial techniques (3,11). Coking and fluid catalytic cracking (FCC) represent instances involving these carbon rejection techniques for desulfurization of heavy oil. Although efficacious regarding sulfur reduction, these methodologies possess a prominent carbon impact.

Furthermore, high-temperature processes, which produce hydrogen for HDS, engender elevated processing costs financially along with environmentally, especially when they process heavier and sulfur-rich crude oils. Consequently, alternate desulfurization pathways are undergoing investigation amid growing consideration (5,12).

Several reviews concerning this topic have been composed. Desulfurization publications typically have concentrated mainly on sulfur extraction from refining portions such as naphtha, distillate, and light vacuum gas oil. However, the aim of this review is to comprehensively survey the processes for converting heavy fractions. Here, we will scrutinize each desulfurization method. We shall ascertain its capability regarding viscous crude oil. The desulfurization methods documented in the literature are adapted for lighter fractions, also as we examine the discussions that have taken place, it becomes clear that they are unsuitable regarding heavy oil. Therefore, this evaluation shall rest upon the degree to which such processes can desulfurize heavy oil.

2. OBJECTIVE

The main objective of this review is to provide a comprehensive and critical analysis of existing desulfurization methods applied to vacuum gas oil, with particular emphasis on the transformation and removal of sulfur-containing aromatic compounds such as dibenzothiophene, benzonaphthothiophene, and their alkylated derivatives.

This study aims to evaluate the effectiveness of various desulfurization approaches, including oxidative, hydrodesulfurization, and emerging alternative techniques, in terms of sulfur removal efficiency, reaction mechanisms, and operational conditions.

Furthermore, the review seeks to examine how different process parameters—such as oxidizing systems, temperature, reaction time, and reagent ratios—influence the reactivity, stability, and conversion pathways of sulfur compounds. Special attention is given to the structural changes in sulfur-containing aromatics during treatment processes and their impact on downstream thermal conversion, such as cracking.

Within this framework, the review will:

- summarize and compare different desulfurization technologies reported in the literature;
- analyze the transformation behavior of sulfur-containing aromatic compounds under various treatment methods;
- evaluate the influence of process conditions on desulfurization efficiency;
- review reported kinetic studies related to sulfur compound decomposition and transformation;
- identify current challenges, research gaps, and future directions in the field of deep desulfurization of heavy petroleum fractions.

3. SULFUR IN CRUDE OIL

Following carbon and hydrogen, sulfur constitutes petroleum's third most copious element (1,4). Unrefined petroleum commonly shows sulfur densities that extend in scope from 0.03 to 7.89% via mass (4) . Sulfur constituents within petroleum are generally categorized. The two categories include inorganic and organic (1). Inorganic sulfur including elemental sulfur, hydrogen sulfide (H2S), and pyrite may occur dissolved within as well as suspended. Concurrently, organic sulfur compounds represent the principal sulfur-containing components within crude oil. These include thiols, sulfides, and thiophenic constituents.

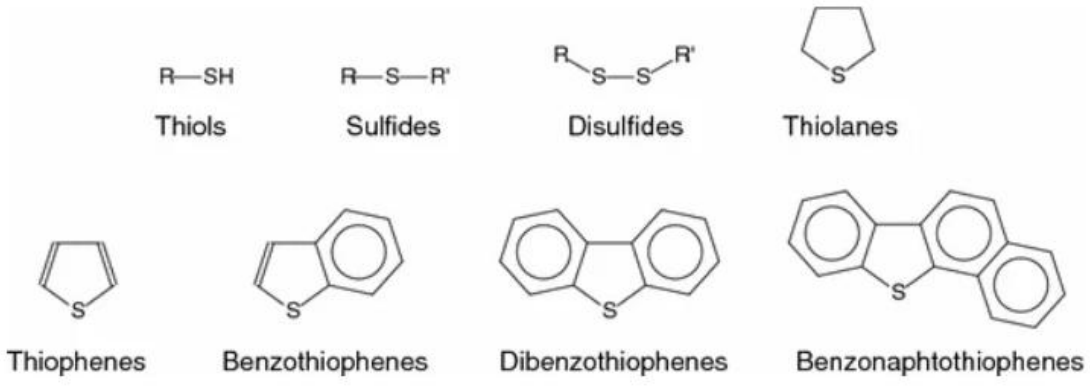

Figure 1. *Some prominent classes of organosulfur compounds*

Fluctuations are obvious in the density and constitution of sulfurous elements across the distillation spectrum. Per Table 1, sulfur quantity within the distillation portion rises alongside greater boiling temperatures because the densest portion exhibits maximum sulfur quantity. Per Table 2, sulfur compounds gain stability as the boiling point elevates, including thiols, sulfides, also thiophene among naphtha to benzothiophene compounds displaced during distillation. In vacuum gasoil as well as vacuum residues, dibenzothiophene compounds represent the foremost route of sulfur presence. Sulfur's chemical makeup immediately impacts its removal process for aliphatic sulfur-bearing compounds like thiols and sulfides are simpler to desulfurize than aromatic sulfur compounds like thiophenes (3,11).

Table 1. *Distribution of sulfur compounds across the distillation range of crude oil with a total sulfur content of 1.2%*

Distillation range(°C)	Sulfur content	Distribution of sulfur compounds (%)			
		Thiols	Sulfides	Thiophenes	Other[a]
70-180(naphta)	0.02	50	50	Trace	-
160-240(kerosene)	0.2	25	25	35	15
230-350(distillate)	0.9	15	15	35	35
350-550(vacuum gasoil)	1.8	5	5	30	60
>550(vacuum residue)	2.9	Trace	Trace	10	90

[a]*Benzothiophenes, dibenzothiophenes and heavy sulfides*

Table 2. *Physical properties of selected sulfur-containing compounds*

Compounds	Normal boiling point (°C)	Melting temperature(°C)	Density at 20°C(kg/m^3)
1-Ethanethiol (ethyl mercaptan)	35	-144.4	839.1
Dimethyl sulfide	37.3	-98.3	848.3
1-Propanethiol (propyl mercaptan)	67	-113.3	841.1
Thiophene	84.2	-38.2	1064.9
Diethyl sulfide	92.1	-103.8	836.2
1-Butanethiol (butyl mercaptan)	98.4	-115.7	833.7
Dimethyl disulfide	109.7	-84.7	1062.5
Tetrahydrothiophene(thiolane)	121.1	-96.2	998.7
Dipropyl sulfide	142.4	-102.5	837.7
Thiophenol	168.7	14.8	1076.6
Dibutyl sulfide	185	-79.7	838.6
Benzthiophene (thianaphthene)	221	32	1148.4
Dibutyl disulfide	226	-[a]	938.3
Dibenzthiophene	332	99	-[a]

[a]*No information is provided in the reference.*

Detailed sulfur constituents typically exhibit elevated concentrations in unrefined oils displaying heightened viscosities and densities. Hydrodesulfurization procedures or thermal manipulation may eliminate unbranched aliphatic sulfides (thioethers). The identical procedures or remedy may readily eliminate cyclic sulfides (thiolanes). Conversely, sulfur integrates within aromatic cycles including thiophene and relevant analogs like benzothiophene, dibenzothiophene, also benzonaphthothiophene. Hydrodesulfurization or thermal conversion methods possess increased impediments regarding its removal.

3.1 Sulfur in heavy oil cuts

Sulfur is present within dense oil fractions while its effects form a petroleum industry concern. Petroleum refinement and refining operations engender elevated-ebullition viscous oil

constituents. Oil quality as well as refining processes, along with final products' properties, are considerably affected via the sulfur amount within these fractions.

Detrimental ecological consequences from sulfur's existence within fuel commodities and petroleum derivatives are possible. Furthermore, sulfur may impair catalysts throughout oil refining and diminish their efficacy, and this degrades the procedure's efficiency and economics.

Viscous oil constituents are subjected to differing processes for sulfur reduction. Every method contains intrinsic merits and deficiencies. The oil's composition in conjunction with the refining process requirements determine their choice. In this scientific work, various methods for removing sulfur as well as sulfur-containing compounds in heavy oil fractions will be studied also each's positive and negative aspects will be listed. Fundamentally, sulfur regulation of dense oil constituents affects sustainable advancement for the petroleum sector. Therefore, researchers must consistently cultivate applicable technologies.

4. DESULPHURIZATION TECHNOLOGIES

4.1 Hydrodesulfurization (HDS)

Hydrodesulfurization represents the foremost technique toward decreasing crude oil's sulfur content within the petroleum sector (3,11). HDS commonly entails introducing oil as well as H2 into a fixed bed reactor. The reactor embraces a fitting HDS catalyst, and the induction exists concurrently. NiMo/Al2O3 and CoMo/Al2O3 represent some of the most frequently utilized HDS catalysts (3). Nevertheless, further possibilities do exist. H2S arises when the sulfur of organic sulfur compounds is transformed throughout HDS.

Selecting a specific catalyst variant hinges upon the present application. NiMo catalysts, according to, excel at hydrogenation while CoMo catalysts are better regarding hydrogenolysis. As a consequence, CoMo catalysts exist as the favored choice for HDS processes when such processes include unsaturated hydrocarbon streams, like streams derived from fluid catalytic cracking (FCC), while NiMo catalysts exist as the favored choice for fractions that do require intensive hydrogenation. Substances like NiMo have been observed to be more efficacious in the HDS of constituents like DMDBT. NiMo catalysts are favored where hydrogen flux is uninhibited yet exposure duration is constrained, characteristic of flow reactors, although CoMo catalysts can be more productive in batch reactors. Hydrotreating conditions commonly span from 200 to 425 °C and 1 to 18 MPa, and particular parameters are adjusted for the intended level of desulfurization and the proportion of sulfur compounds inside the feedstock.

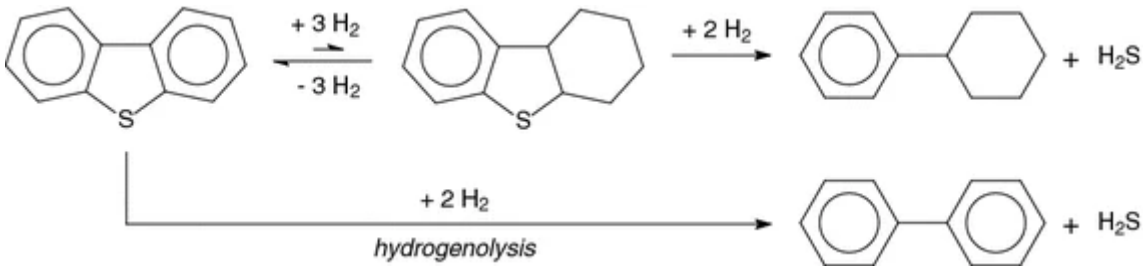

Figure 2. *Desulfurization mechanisms*

Thiophene rings pose increased difficulties regarding sulfur removal. The π-electron constitution for the conjoined C=C framework features restricted skill. Sulfur's singular electron pair is the

entirety which it includes. Despite stabilization via resonance of roughly 120–130 kJ mol-1, less than benzene's stabilization of 160–170 kJ mol-1, it markedly impedes HDS. Two discrete pathways elicit desulfurization (Figure 2). Hydrogenolysis constitutes the mechanism with less hydrogen. Nonetheless, the resonance stabilization involving sulfur inside the thiophene ring impedes straightforward hydrogenolysis. This equilibration begets the primary HDS route where the ring saturates prior to desulfurization. Nonetheless, strong dehydrogenation to aromatize compels the hydrogenated product's equilibrium concentration to persist minimally.

Due to thiophene's resonance stabilization, scission is likewise impeded, which elucidates why thiophene-bearing sulfur compounds predominantly generate coke during fluid catalytic cracking. Hydrocracking improves aromatic hydrogenation, which permits sulfur removal via cracking as well as hydrogenation. For improving distillate quality, achieving selective ring opening is the primary goal via hydrocracking heavy oil rather than increasing HDS. HDS is routinely employed for the enhancement of heavy oils. The efficacy of HDS is impeded by the attributes of viscous oils:

(a) High metal content engenders catalyst deactivation as well as precipitate formation.

(b) Coking as well as fouling stem from particular predispositions. Consequently, catalyst inactivation occurs.

(c) Minute catalyst pores constrain approach toward molecular size.

(d) HDS adsorption proves arduous because steric impedance impacts thiophene sulfur.

4.2. Extractive desulfurization

Extractive desulfurization skillfully eliminates organosulfur constituents from sulfur (6,7). Particular solvents will dissolve compounds, easing the process for removal. Within this process, liquid-liquid extraction requires that the two liquid phases remain immiscible. Elements for extractive desulfurization are represented in Figure 3.

The raw material and the dissolving agent initially merge inside some blending reservoir easing assimilation of organosulfur constituents into the dissolving agent with their great solubility. A separator divides the hydrocarbon and solvent phases thereafter. Subsequently, the refined hydrocarbon exhibiting diminished sulfur content undergoes additional treatment. The organosulfur compounds are segregated from the solvent during distillation allowing solvent reclamation. Following retrieval, it is returned into the mixing tank.

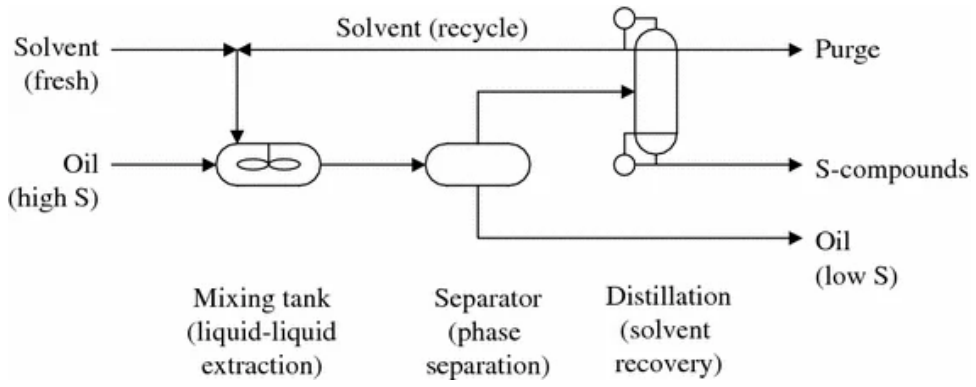

Figure 3. *General process of extractive desulfurization, using low-boiling solvent extraction as an example*

This method presents several benefits, including its facile application, the lack of hydrogen, and the capacity for performance below near-ambient conditions (6). The feedstock remains chemically unaltered, it should be noted, also extraction is physical. Nevertheless, by utilizing this procedure, diverse impediments exist that warrant resolution:

(a) Desulfurization via extraction exhibits natural efficacy when the organic sulfur constituents are soluble in the specified solvent. Thus, solvent selection must be performed with large care. Maximum desulfurization efficacy can be attained thus. An abundance of solvents like acetone, ethanol, and polyethylene glycols were scrutinized, with scrutiny revealing desulfurization rates from 50% to 90%, contingent on extraction cycles employed during the process.

(b) Physically isolating the solvent and oil phases efficiently is vital if the separation process triumphs. Furthermore, the solvent needs diminished stable solubility within the oil. This keeps the process solvent from undergoing depletion.

(c) Augmenting mixing along with extraction efficiency requires diminishing oil viscosity. Diminishing solvent viscosity remains important too. Nevertheless, heavy oil confronts obstacles herein, generally requiring its fractionation amid heightened temperatures to diminish viscosity. This constraint might require operators extracting under duress, which additionally confounds the procedure.

(d) It is imperative that the solvent possesses a disparate boiling point from the sulfur compounds extracted from the oil. While an individual favors selecting a dispersant possessing an elevated boiling point compared to the sulfur constituents since the dispersant's magnitude is generally greater with respect to what they derive from the sulfur constituents, heavy oil procurement commonly mandates utilizing a dispersant exhibiting a diminished boiling point. The expenditures linked to solvent retrieval escalate markedly as a result.

(e) The resultant solvent from extraction could possibly still contain particular constituents. These constituents had been isolated out of the oil yet still cannot undergo efficacious separation via distillation. As routine sanitation diminishes such accumulation, the density of those constituents steadily accrues throughout solvent reclamation.

The utilization of less dense solvents in extractive desulfurization processes regarding viscous oil introduces predicaments concerning the fiscal efficacy of those processes, notably the peril of solvent depletion and dissolution inside the viscous oil's detailed framework.

Sulfur compounds like S-compounds, (as shown in Figure 1) in products like gasoline and diesel fuel, act as contributors regarding sulfur oxides (SOX) emission throughout combustion. These discharges diminish combustion efficacy, neutralize three-way converters, and escalate releases regarding carbon monoxide (CO) and particulates. Thus, desulfurization of feedstocks is of paramount importance in the oil refining process.

Hydrodesulfurization (HDS) is at this moment prevalently employed within industry. It mainly includes the interaction of S compounds within petroleum via hydrogen utilizing Co-Mo/Al2O3 and Ni-Mo/Al2O3 catalysts. HDS faces predicaments, though, particularly since certain nations aim for sulfur thresholds in petroleum to possess zero sulfur content with elevated rigor. Originally, the European directive concerning transport fuels constrained sulfur content to 150 ppm for gasoline and 350 ppm for diesel in 1998, then diminished it to 50 ppm within five years, and currently promotes levels below 10 ppm. The United States along with Japan have likewise levied taxes on transport fuels. Those fuels' sulfur concentration exceeds 10 ppm.

HDS is efficacious because it mainly eliminates aliphatic S-compounds like thiols, thioethers, and disulfides, along with thiophene (TS), benzothiophene (BT), dibenzothiophene (DBT), and their derivatives, given that steric hindrance arises during adsorption onto the catalyst surface. Achieving lower sulfur content levels through HDS requires more stringent conditions, including high temperatures (approximately 400°C), high pressures (approximately 20 MPa) and more active noble catalysts, and that results in increased costs and potential oil losses, especially in the form of alkenes.

Scientists explored alternate avenues for confronting these matters. They employed extraction, oxidation, adsorption, and biodesulfurization. Extractive desulfurization (EDS) materializes as a feasible procedure among these methodologies since it is able to function under amenable and plain circumstances without modifying the fuel oils' compounds' chemical constitution. Furthermore, extracted sulfur compounds also can become feedstock that is recycled.

For use in EDS, dimethylsulfoxide, pyrimidinone, imidazolidinone as well as polyalkylene glycol, like several molecular solvents, have been assessed. Nevertheless, the capricious disposition of such molecular dissolvents coupled alongside the constraint that appropriate extractors exist scantily has deterred individuals from wide-ranging EDS utilization throughout industrial functions. Solvent differs, extractants reconstitute with complexity, also these processes considerably impede EDS's commercial implementation.

4.3. Ionic-liquid extraction method

Ionic liquids, when employed for sulfur extraction from fuels such as diesel, represent a compelling substitute to organic solvents because they have the potential to yield ultra-clean diesel fuels (5,12). Numerous investigations have underscored the efficacy of imidazolium, pyridinium, or quinolinium-based ionic liquids. They have depicted as well their propitious extraction attributes for anions like alkyl sulfates, alkyl phosphates, or halogen-containing anions.

Ideally, ionic liquids would pull sulfur out of fuel, barely touch the hydrocarbons, flow easily through pipes, and snap back into two clean layers when the job was done. Yet in the messy reality of working plants, they usually fall short of that laundry list.

They look promising in lab tests that mix pure dibenzothiophene with decane, but when the feed comes straight from the distillation column, the gain shrinks fast. It turns out that ionic liquids behave like many other solvents: they excel on model fluids yet falter with the dirty, complex blends found in everyday refining. The problem grows heavier still when dealing with vacuum gas oils or other high-viscosity cuts.

One way to nudge the system in the right direction is to first oxidize the sulfur compounds into sulfoxides and sulfones. These by-products grab onto the ionic liquid much more tightly, so the same volume of solvent strips a bigger slice of sulfur from the feed.

Despite the tuning, the high boiling points of most ionic liquids still make life harder during solvent regeneration. Pulling off the solvent to recover the sulfur is trickier than with many organic extractants, and any energy penalty cuts straight into the plants bottom line. Several investigators have suggested different strategies to address the difficulties encountered in the use of ionic liquids for desulfurization.

(a) One option is to extract sulfur species directly by vacuum distillation. While distillation works well in principle, the very high boiling points of heavier organo-sulfur compounds-such as alkylated dibenzothiophenes, which exceed 340 C-mandate the use of vacuum technology. Consequently, this pathway is usually limited to light petroleum cuts, where compound volatility is more manageable.

(b) An alternative method employs a low-boiling solvent to re-extract sulfur after the ionic liquid has been loaded. In this process, the ionic liquid is first withdrawn for recycling, then purified with the auxiliary solvent. A second distillation step subsequently separates the sulfur from the solvent used in the earlier extraction.

(c) A third separation route simply adds water to the sulfur-rich ionic liquid. When sufficient water is introduced, the partition coefficient of many sulfur compounds drops close to zero. As a result, sulfur either dissolves with light hydrocarbons, forms a separate aqueous phase, or, in some formulations, precipitates out entirely. This approach works best when the sulfur species are fully oxidized, allowing them to form stable, herbicidal ions that interact with the melt. Before the ionic liquids can be recovered and reused, however, nearly all the water must be stripped from the mixture. Water removal by simple boiling uses far more energy than most practical processes can afford, so a four-stage evaporative scheme, operating at gradually lower pressures and higher temperatures, has been proposed to trim heat overhead. When implemented carefully, this multi-stage strategy can bring the thermal burden down to levels comparable to those seen in standard hydrodesulfurization.

In short, extractive desulfurization with ionic melts inherits the same strengths that solvent extraction offers: high selectivity, mild temperatures, and compatibility with fuel hydrocarbons. Yet technical route is still held back by the steep raw-material costs and pronounced humidity-sensitivity of some ionic melts, which box plants into specially sealed, expensive infrastructure and prevent large-scale adoption.

To the authors knowledge, extractive desulfurization has never yet been tried on heavy fuels, a finding that matches expectations; many researchers have struggled even to treat straight-run distillate with the same chemistry. Consequently, ionic-liquid extraction cannot now be viewed as a practical option for cleaning heavy oil.

4.4. Adsorptıve desulfurızatıon

Adsorptive desulfurization relies on stationary solids that selectively snag organic sulfur species when a fuel passes through their bed (3,17). The overall success of any adsorptive method rests on the design of the sorbent. Key characteristics include its ability to distinguish organic sulfur from hydrocarbons, the maximum amount of sulfur it can hold, its mechanical stability over multiple cycles, and how easily it can be refreshed for further use.

Two broad strategies exist within adsorptive desulfurization:

(a) Physical adsorption relies on weak van der Waals forces, so the sulfur compounds remain chemically intact as they cling to the material. The energy penalty for regeneration in this case scales mostly with how much sulfur is loaded, yet because the bond is weak physisorption itself can be regarded as almost energy-neutral.

(b) Reactive adsorption proceeds via a genuine chemical interaction, usually converting the incoming sulfurs to metal sulfides fixed on the sorbent surface. Cleaning the material can then be

done either by heating or by flushing it with a suitable solvent. Depending on contaminants and operating conditions, released species may appear as H2S, SOx, or pure elemental sulphur.

Many candidate materials, from metal-organic frameworks to tailored zeolites, have gone through testing to gauge their promise in real-life desulfurization.

Extensive research has assessed the use of solid adsorbents such as activated carbon, zeolites, amorphous silica-alumina, and metal-organic frameworks (MOFs) for removing sulfur from model oils, fluid-catalytic-cracking (FCC) feed, coker naphtha, and distillate streams. Laboratory and pilot tests show that these materials can reach regulatory sulfur targets under relatively mild conditions, yet even the best candidate still falls short when scaled up to full refinery operations. Heavy feeds remain a particular challenge, because bulky sulfur species struggle to navigate narrow pore mouths and steric crowding further limits uptake. As a result, the accessibility limitations that plague catalytic hydrodesulfurization (HDS) are echoed in adsorptive desulfurization, since both techniques depend on molecules physisorbing or chemisorbing to a solid interface.

4.5. Oxidative desulfurization (ODS)

Oxidative desulfurization (ODS) graphically denotes a sequence where an external oxidant reacts with sulfur compounds, thereby making them easier to extract from liquid fuels. The method is frequently presented as a single unified route, yet it actually contains two separate, sequential operations that must occur for successful desulfurization. Oxidative desulfurization (ODS) begins with the oxidation of sulfur species, transforming their chemical profiles. Once oxidized, these species can be selectively separated from unoxidized compounds during a downstream removal stage that exploits the new redox properties (5-8,12).

A series of recent reviews has compiled advances in ODS, revealing sustained scholarly and practical interest evidenced by a growing publication record.

In industrial practice, ODS is routinely applied to convert low-volatility thiols into more easily handled disulfides.

$$2R\text{-}SH + \tfrac{1}{2} O_2 = R\text{-}S\text{-}S\text{-}R + H_2O \quad (1)$$

Conversion occurs in weakly alkaline solution, where hydroxide enhances thiol oxidation kinetics. A moderate NaOH concentration, often supplied as aqueous caustic soda for cost-efficiency, is paired with air as the oxidant. A soluble metal catalyst further accelerates the process, which discriminates strongly between thiols and other sulfur moieties. Heavy-oil fractions typically contain only trace thiols and therefore require no secondary desulfurization step (Table 1).

In oxidative desulfurization, or ODS, the process converts sulfur in sulfide and thiophene bonds into sulfoxides (1) and sulfones (3) through mild oxidation (9,10).

$$R\text{-}S\text{-}R' + \tfrac{1}{2} O2 = R\text{-}(SO)\text{-}R' \quad (2)$$

$$R\text{-}S\text{-}R' + O2 = R\text{-}(SO2)\text{-}R' \quad (3)$$

***Table 3**. Dependence of the breaking energy of C-S bonds in sulfur-containing compounds on classification*

Compound classifications[a]	Breaking energy of C-S bonds (kJ/mol)
Unoxidized sulfur	
CH_3S-CH_3	320
PhS-CH_3	290
Oxidized sulfur	
$CH_3(SO)$-CH_3	230
$CH_3(SO_2)$-CH_3	280
$Ph(SO_2)$-CH_3	240
$Ph(SO_2)$-Ph	290

[a]Ph =Phenyl group, -C_6H_5

Oxidation transforms sulfur-containing species into sulfoxides and sulfones, and these products display two features that support desulfurization. First, the added polar bonds raise overall polarity, which improves selectivity during solvent extraction (18-23). While the redox route does not solve solvent evaporation or the energy burden of recycling, it sharpens the extraction window. Second, oxidation weakens the C-S bond, as summarized in Table 3 (10). Weaker bonds allow the oxidized fragments to be removed much more easily via thermal decomposition. Patent records on oxidative desulfurization (ODS) reveal schemes aimed specifically at upgrading heavy oils, and these schemes vary in their oxidants and reaction conditions.

(a) One popular route relies on acidic oxidation with hydrogen peroxide activated by short-chain carboxylic acids such as formic or acetic acid. Under such conditions oxidation proceeds gently at approximately 50 °C for roughly 6 hours. Subsequent thermal treatment at 350–450 °C cleaves the now-fragile C–S linkages while limiting unwanted breakdown of the hydrocarbon matrix.

(b) Sulfur removal begins with oxidation using an air stream at 80-180 °C. The reaction may be sped up by a non-acidic catalyst, typically a Group 5A metal such as vanadium and Group 8 metals such as nickel, palladium, or platinum. Following this step, an elevated heat-treatment at 200-400 °C, preferably near 300 °C, is applied to convert the sulfur mainly to SO2. Finally, the material undergoes catalytic hydrodesulfurization.

(c) In a second method, the sample is immersed in an acidic aqueous solution and treated with an oxidant until sulfur species become sulfate. The C-S linkages are then cleaved by molten alkali-metal hydroxide, yielding water-soluble polysulfides. These soluble species are easily washed away from the hydrocarbon phase, leaving cleaner organic material.

(d) The sulfur-bearing compounds are oxidized with an external oxidant, typically a hydrogen peroxide solution. The resulting oxidized materials are subsequently extracted with a light paraffinic solvent, which preferentially dissolves the lower-sulfur fraction. This final extraction resembles the classical asphaltene-depletion procedure: when the solvent is gently evaporated, the remaining asphaltenes trap most of the higher-sulfur oxidized species within their structure.

(e) Oxidation of sulfur compounds can be effected with an oxidant such as hydrogen peroxide when the system is buffered by an acidic medium, typically acetic acid, and accelerated by a titanium-containing catalyst. Although optimal yields are reported at approximately 50 °C, the method remains practical over a broader window of 20 to 90 °C. Testing has been performed with model sulfur and nitrogen species as well as with selected cuts drawn from crude oil. Isolation of solvent and target products is then accomplished through standard distillation and solvent-extraction steps.

4.6. Biodesulfurization

Biodesulfurization proceeds at mild temperature and pressure, exploiting the metabolic pathways of specially chosen microbes that can utilize organosulfur substrates as growth factors. With carefully curated microbial consortia, scientists have demonstrated the direct treatment of crude oil without prior fractionation.

Relative to conventional processes, BDS holds promise for lower capital and operating expenditures. Documentation indicates that BDS lines can demand roughly half the initial investment and generate 15% lower ongoing costs when compared to hydrodesulfurization (HDS) units of equivalent capacity.

Recent improvements in reactor design have extended microbial longevity in biodesulfurization-processes from the former 1-2 days to a more viable 8-16 days, or roughly 200-400 hours. Better mass transport has eased resis-tance to flow, permitted higher volumetric rates, and consequently boosted overall process efficiency. Such enhancements mean that conversions can now take place in much smaller reactors, saving space and resources. On the downside, concentrating and separating these more persistent microorganisms has proven difficult, obliging operators to invest in extra equipment for oil-water-emulsion treatment. Even with these advances, commercial biodesulfurization of crude oil remains elusive, chiefly because of logistics related to disinfect-ing, moving, storing, and introducing live cultures in field or refinery settings.

5. RESULTS

A variety of strategies has been proposed to desulfurize heavy-oil fractions, including hydrodesulfurization, extrac-tive desulfurization, oxidative desulfurization, and biodesulfurization (3,5,12). Yet, despite the large number of options recorded in the literature, only a handful prove genuinely workable for treating the high-sulfur content usually present in heavy oil. These difficulties stem from intrinsic characteristics of heavy crude, particularly plentiful sulfur content, high viscosity, elevated boiling range, and the refractory stability of most sulfur species (18-23).

After surveying recent studies and considering practical options for treating heavy oil, several noteworthy points become apparent:

(a) Approaches using solid phases-catalysts or adsorbents-tend to underperform because heavy oil is dense, dirty, and features large, tangled molecules.

(b) Separation routes such as selective extraction or high-temperature distillation struggle with heavy oil's steep viscosity profile and elevated boil-up, even when sulfur compounds are prereduced by alkylation, oxidation, or chlorinolysis.

(c) Although biodesulfurization seems appealing, immutable sulfur bonds, extreme fluidity, and a heterogeneous feed still challenge microbial systems, underscoring the need for transport-tailored organisms with narrow sulfur selectivity.

(d) Finally, selective in-liquid methods that rely on stoichiometric reagents have yet to prove commercially viable for removing sulfur from heavy grades on a meaningful scale. Because heavy oils contain large amounts of sulfur, methods that depend on costly or hard-to-get reagents—most often hydrogen—tend to be uneconomic. As a result, techniques like alkylation,

chlorinolysis, and several oxidation-based routes are excluded from serious consideration for their desulfurization (13-16).

REFERENCE LIST

1. Patai, S., Rappoport, Z., Stirling, C. *The Chemistry of Sulphones and Sulphoxides*. Wiley; 2006.
2. Pawelec, B., Navarro, R.M., Campos-Martin, J.M., Fierro, J.L.G. Towards near zero-sulfur liquid fuels: A perspective review. *Catalysis Science & Technology*. 2011;1(1):23–42.
3. Ancheyta, J., Rana, M.S., Furimsky, E. Hydroprocessing of heavy petroleum feeds: Tutorial. *Catalysis Today*. 2005;109:3–15.
4. Agarwal, P., Sharma, D. Comparative studies on the biodesulfurization of crude oil with other desulfurization techniques. *International Journal of Environmental Science & Technology*. 2010;7(4):633–640.
5. Ali, M.F., Hamad, D.M., Albusairi, B.H., Fahim, M.A. Removal of dibenzothiophenes from fuels by oxidative desulfurization. *Energy & Fuels*. 2009;23:5986–5994.
6. Shiraishi, Y., Hirai, T. Desulfurization of vacuum gas oil by chemical oxidation and extraction. *Energy & Fuels*. 2003;17:558–564.
7. De Filippis, P., Scarsella, M. Oxidative desulfurization: Reactivity of sulfur compounds. *Energy & Fuels*. 2003;17:1452–1455.
8. Otsuki, S., Nonaka, T., Takashima, N., et al. Oxidative desulfurization of light gas oil. *Energy & Fuels*. 2000;14:1232–1239.
9. Ashworth, M.R.F. Detection and determination of sulphones and sulphoxides. *Analytical Chemistry*. 2006.
10. Herron, J.T. Thermochemistry of sulfoxides and sulfones. *Journal of Physical and Chemical Reference Data*. 2006.
11. Ho, T.C. Deep hydrodesulfurization of diesel fuel. *Catalysis Today*. 2004;98:3–18.
12. Campos-Martin, J.M., Capel-Sanchez, M.C., Perez-Presas, P., Fierro, J.L.G. Oxidative processes of desulfurization. *Journal of Chemical Technology and Biotechnology*. 2010;85:879–890.
13. Guseinova, E.A., Mursalova, L.A., Bagirova, N.N., et al. Computational determination of oxycracking conditions. *Petroleum Chemistry*. 2019;59:180–185.
14. Guseinova, E.A. Influence of vacuum gas oil oxycracking conditions. *Herald of the Azerbaijan Engineering Academy*. 2018;10(4):82–89.
15. Guseinova, E.A., Adzhamov, K.Y., Safarova, S.R. Kinetic parameters of oxygen-containing compounds formation. *Reaction Kinetics, Mechanisms and Catalysis*. 2020;129:925–939.
16. Guseinova, E.A., Adzhamov, K.Y., Mursalova, L.A., et al. Formation kinetics of hydrocarbons. *Reaction Kinetics, Mechanisms and Catalysis*. 2020;131:57–74.
17. Gerzeliev, I.M., Dementev, K.I., Khadzhiev, S.N. Catalytic processes in petroleum chemistry. *Petroleum Chemistry*. 2015;55:481–486.
18. Abiyev, K., Guseinova, E. Oxidative desulfurization of VGO with ozone. *Modern Approaches in Chemistry and Chemical Technology*. 2023:59–61.
19. Abiyev, K., Guseinova, E. Oxidative desulfurisation of VGO in the presence of ozone. *UFAZ Conference Proceedings*. 2025:32–33.
20. Guseinova, E.A., Mursalova, L.A., Abiyev, K. Physicochemical properties of ozonized VGO. *Science. Technology. Production*. 2023:227–229. (in Russian)
21. Abiyev, K., Guseinova, E., Serra, C.A. Sustainable desulfurization of VGO using ozone. *RISK Conference Proceedings*. 2025:99-100.
22. Abiyev, K., Guseinova, E. Comprehensive study of oxidative desulfurization and thermal conversion of VGO. *Advanced in Chemistry and Chemical Engineering*. 2026;9(1):34-40.
23. Abiyev, K., Guseinova, E., Serra, C.A. Ozone-assisted oxidative desulfurization of vacuum gas oil: A cost-effective pathway to cleaner fuels. *90th Belarusian Scientific And Technical Conference*. 2026:305-309.

2025. Volume 9, Number 2 Pages 99-106

UDC: 547.756.6
DOI: https://doi.org/10.30546/2521-6317.2025.02.527

SYNTHESIS AND STRUCTURAL STUDY OF COMPLEXES Sn(II) AND Co (II) WITH NITRODERIVATVES OF BENZOIC ACID

Q.M[1]. ALIYEVA, S. Y[1]. RAHMANOVA, M.K.[1]MUNSHIYEVA, U.M[2]. HASANOVA, S. S[2]. HASANOVA, L.N[2]. MAMMADOVA, E.M[2]. MOVSUMOV, H.F[1].MAMMADOVA, S.R[1].MAMMADOVA

[1]*Ministry of Science and Education, Institute of Chemistry Public legal entity, Baku, Azerbaijan*

[2]*Azerbaijan State Agriculture University, Ganja, Azerbaijan*

qudrataliyeva@gmail.com

ARTICLE INFO

Article history:
Received:2025-06-09
Received in revised form:2025-06-15
Accepted: 2025-07-15
Available online:2025-12-25

Keywords:
tin complex with benzoic acid derivatives, coordination number is seven, boned oxygen atoms of carboxyl group coordinated by chelating type. Cobalt complex of 5-nitro, 2- asetamidobenzoic acid, monodentate coordination, coordination number is four.

ABSTRACT

The crystal structures of a new tin complex with nitrosalisilic acid were synthesized and studied. Single crystals were obtained by X-ray diffraction analysis. Crystallochemical data were obtained on an Entrat=Nonius CAD automated diffractometer, the molecular and crystal structures were deciphered using several programs. It was found that in the crystal structure of the title compound [$Sn(C_7H_4NO_5)_2 \cdot H_2O$], the coordination sphere around the Sn atom consises of four O atoms from two chelating carboxylate groups, one water O atom and two additional O atoms belonging to a carboxyl and a hydroxyi group of neibouring molecules. So, the coordination number of Sn complements to 7. The Sn – O distances are in the range 2,419 – 3,084 Å, the shortest distance being to a water O atom. Two inframolecular and two intermolecular hydrogen bonds are also observed in the polymeric structure. A new complex compound of cobalt with 5-nitro, 2-asetamido benzoic acid with the following composition $C_{28}H_{28}CoN_6O_{12}$ was synthesized. Single crystals of the new complex were obtained using an automatic diffractometr Bruker APEX CCD and crystallochemical parametrs were obtained. Crystal structures have been deciphered using special programs. Two pyridine molecules are coordinated by the cobalt (II) atom via donor nitrogen atoms in an axial position. With the help of donor oxygen atoms, two water molecules are coordinated to the central cobalt atom and complement its coordination number to four. The distance of cobalt (II) atom and the oxygen of the carboxyl groups is Co (1) – O (1) = 2,157Å, Co – N = 2,301Å, Co – H_2O=2,181Å.

INTRODUCTION

The presence of hydrophilic groups: OH, NH_2, COOH, NO_2 leads to the formation of complexes of trace elements as well as the heavy metal ions and chelate-structured complex compounds [6, 7,8].

In our early research work Ag (1) [9], Zn (II), Co (II) [10,11] metal complexes of p-nitrosalicylic acid which was used as ligands, were synthesized by us and their molecular structures were studied. As a continuation of the research work, single crystals of the complex compound with

the Sn(II) cation were synthesized and the molecular and crystal structures were studied by X-ray structural analysis.

In this research work another nitro derivative of benzoic acid, with Co (II) cation was synthesized and its molecular and crystal structures were studied.

The substituents in the ortho position in both ligands (2-OH and 2-CH3CONH) create an "ortho effect", that mobilizes the hydrogen cation of the carboxyl group and ensures easy substitution with metals.

Early we have synthesized the complex compounds of 5-nitro, 2-acetamido benzoic acid with Ni (II), Cu (II), Mn (II), Cd (II) metals and studied their molecular and crystal structures [13, 14].

As a continuation of the research work, the complex compound of this ligand with Co (II) cation was synthesized and single crystals of its pyridine adduct were obtained and their molecular and crystal structures were studied.

Experimental

Synthesis of bis-nitrosalicylate Sn (II) –hydrate –Sn(C7H4NO5)2·H2O (complex 1): 2.05 g (10 mmol) Na 2-nitrosalicylate salt is dissolved in 50 ml of distilled water, heated to 50 –

-60 0C. An aqueous solution of 1.4985 g (5 mmol) Sn(NO3)2 salt is added to the solution and stirred for 20 minutes at 80 0C on a magnetic stirrer. The boiling solution is filtered through filter paper and stored in the dark at room temperature. After a few days, prizmatic crystals precipitate.

Synthesis of the adduct complex compound bis-(5-nitro, 2-acetamidobenzoato) – di-(pyridine) Co (II) – dihydrate (complex 2): the sodium salt of the ligand, which is well soluble in water, is obtained according to the following reaction.

$$5-NO_2-CHNOCH_3-C_6H_3COOH+NaHCO_3 \rightarrow 5-NO_2-CHNOCH_3-C_6H_3COONa+CO_2\uparrow+H_2O$$

The obtained Na salt 2.41 (10 mmol) is dissolved in 50 ml of distilled water, 1.095 g (5 mmol) of CoCI2 · 4H2O and 10 mmol of pyridine are added to it and mixed with a magnetic stirrer at 80 0C for 20 minutes. The solution is filtered and stored in the dark at room temperature. After a few days, transparent crystals precipitate.

The crystals of both complexes are washed in water, ethyl alcohol and dried in a desiccator over anhydrous CaCI2. The yield of the reactions is 78% for complex 1 and 81.65% for complex 2.

The obtained single crystals are selected under a microscope, and high-quality single crystals are sent to the Bruker APEX CCD automated diffractometer operating at Samsun University, Republic of Turkey, for X-ray structure analysis. Based on the collected crystallographic data, molecular and crystal structures are revealed with the help of special programs [14,15,16]. The crystallographic parameters of complex compounds are as follows.

For **complex 1.** Formula: $Sn(C_7H_4NO_5)_2 \cdot H_2O$, molecular weight: 581,43, Singoni Triclinic: space groupe P-1, parametrs a=4,879Å, b=12,155Å, c=14,734Å, α=68,634^0, β=86,482^0, γ=78,770^0, V=796,68^0, Z=2, d=2,457 mq m^{-3}.

Data collection Enraf-Nonius CAD diffraktometr, measured reflex, 3610, independent reflex 2822, MoK$_\alpha$ – 0,71073Å, θ=9,92 – 18,12^0, crystal size: 0,35x0,20x0,10 mm, temperature -295K, R=0,027.

For complexs 2: Empirical formula - $C_{28}H_{28}CoN_6O_{12}$, molecular weight– 695,42, temperature at the time of measurement – 100(2)K, wavelengt - $M_0K_\alpha = 0,71073$, Singoni monoklinik - space group $P2_{1/n}$, parameters – a=10,485Å, b=19,675Å, c=8,214Å, angles $\alpha = \gamma = 90^0$, $\beta = 103,456^0$, $V = 1512,5\overset{0}{A}^3$, $Z = 2$, $\alpha = 1,543 q/sm^3$, monocrystaline dimensions: 0,28x0,19x0,21 mm^3, the number of all reflexes – 18589, the number of independent reflexes – 4698, R_{factor}=0,032.

Materials and measurements

$Sn(NO_3)_2 \cdot 4H_2O$ and $CoSO_4 \cdot 6H_2O$ was commerical product highest chemical grade (Aldrich). Solvents were purified according to standart procedures. IR spectra were recorded with a Perckin – Elmer 100 FT – IR spectrometer as KBr discs, in the range of 4000 – 400 cm^{-1}. Thermal analysis was perfomed by NETZSCH STA – 409 PC/PG derivatograph. The DTA, TG and DTG curves were taken in a static air atmosphere at an increasing heating rate of 10^0C/min from 20 to 800^0C by using platinium Crucibles.

IR spectral investigation of complexes (1) and (2)

The IR – spectra of complexes (1) showed new absorption bonds in the specific regions related to the bond asymmetric $\nu_S(COO^-) = 1635\,sm^{-1}$ and symetric $\nu_S(COO^{-1}) = 1450\,sm^{-1}$. The difference between the asymmetric (ν_{as}) and symmetric (ν_{sim}) carboxylate vibrations $\Delta\nu = \nu_{as}(COO^-) - \nu_S(COO)$ is often employed for the determination of models of coordination group (17-19) (Fig.1).

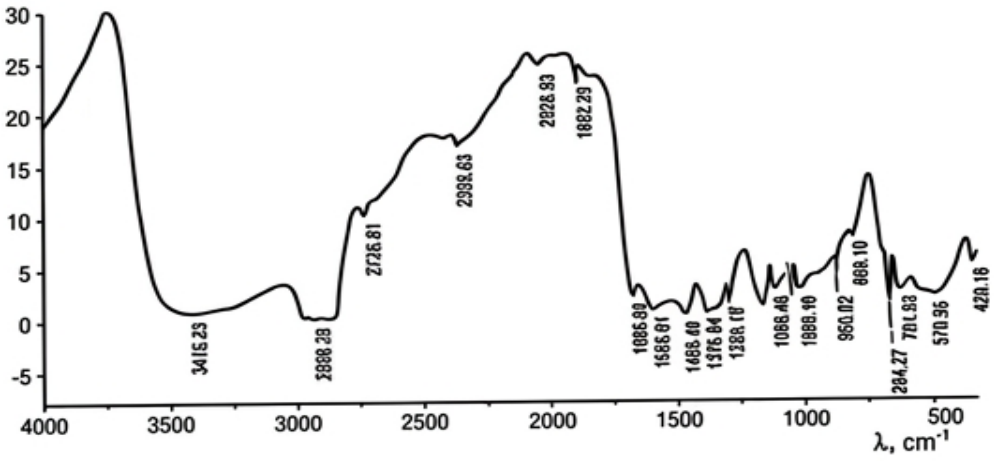

Figure 1. IR spectra of complex 2

The value of $\Delta\lambda = 185\,sm^{-1}$ is less than $200\,sm^{-1}$ in the complex (1) and indicated that the carboxylate groups participate at chelate type and bidantate-bridge manner, which is supported by the molecular structure Sn (II). $Ph - C = 1225\,sm^{-1}$, $Ph - NO_2 = 1365\,sm^{-1}$, $Sn - O(1) = 645\,sm^{-1}$, $Sn - H_2O = 825\,sm^{-1}$.

The IR-spectra of complexes (2) showed that bond of asymmetric - $\nu_S(COO^-) = 1663\,sm^{-1}$ and symmetric $\nu_S(COO^-) = 1453\,sm^{-1}$. The value of $\Delta\nu = 210\,sm^{-1}$ is more than $200\,sm^{-1}$, indicates that the carboxylate groups participate in a monodentate manner. Which is supported by the molecular structure Co(II).

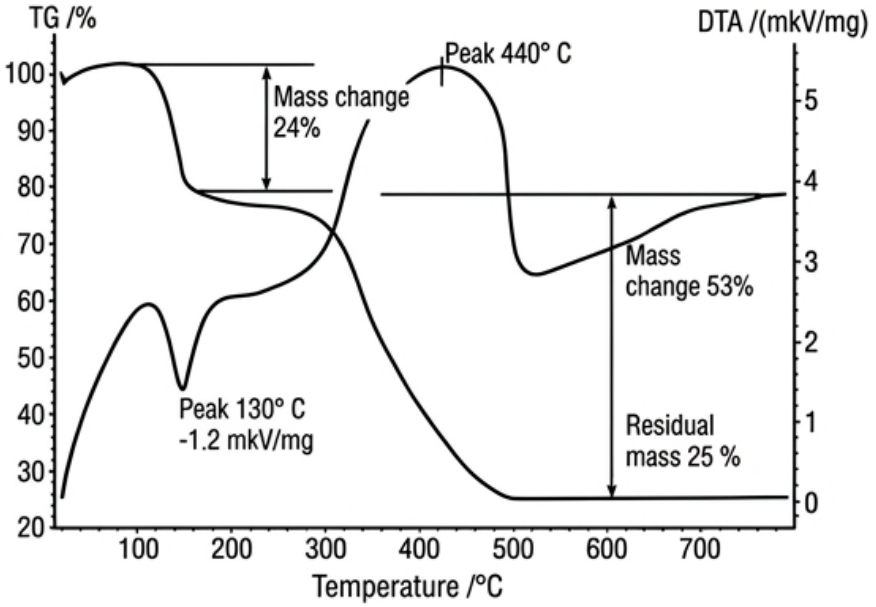

Figure 2. Termogravimetry of complex 2

Thermal analysis data for (1) showed that in both complexes thermic analyses proceeds in four stages.

In the first stage 148,8 to 205^{0}C mass loss for complex (1) equals 3,09%, for complex (2)- 24,02% (Fig. 2).

In the second stage at 220-350^{0}C, after the relase coordinated moleculs of water and pyridine, dimeric moleculas are formed that are stable. In the third stage 350-435^{0}C to the complexes the decomposition of carbon hydrate residues. In the fourth stage metal carbonates are formed (680^{0}C), that decomposes to metal oxides (750^{0}C).

Discussion of the crystal structures of complex 1 and 2.

Selected bond distances and $\left(d\ \overset{0}{A}\right)$ and angles $\left(\omega^0\right)$ for complex 1 have been shown in table 1.

Table 1. Selected bond distances (Å) and angles (^{o}) for (1).

Distanses	d, Å	Distans	d, Å
Sn – O (1)	2,452 (4)	Sn – O (11)	2,416 (4)
Sn – O (2)	2,691 (3)	O (1) – C (7)	1,269 (3)
Sn – O (5)	3,084 (4)	O (7) – C (7)	1,235 (4)
Sn – O (6)	2,428 (5)	O (6) – C (14)	1,284 (7)
Sn – O (7)	2,727 (4)	O (7) – C (14)	1,245 (8)
Sn – O (8)	2,872 (4)	C (II) – NO_2	1,436 (7)
O (1) – Sn – O (1)	50,1	O (2) – Sn – O (5)	60,7
O (1) – Sn – O (6)	89,1	O (11) – Sn – O (5)	94,5
O (1) – Sn – O (7)	75,9	O (6) – Sn – O (7)	81,3
O (1) – Sn – O (11)	74,2	O (11) – Sn – O (7)	121,2
O (2) – Sn – O (6)	133,9	Sn – O (1) – O (7)	99,2
O (2) – Sn – O (7)	120,9	Sn – O (6) – O (14)	98,5
O (2) – Sn – O (1)	74,6	O (1) – C (7) – O (2)	121,7

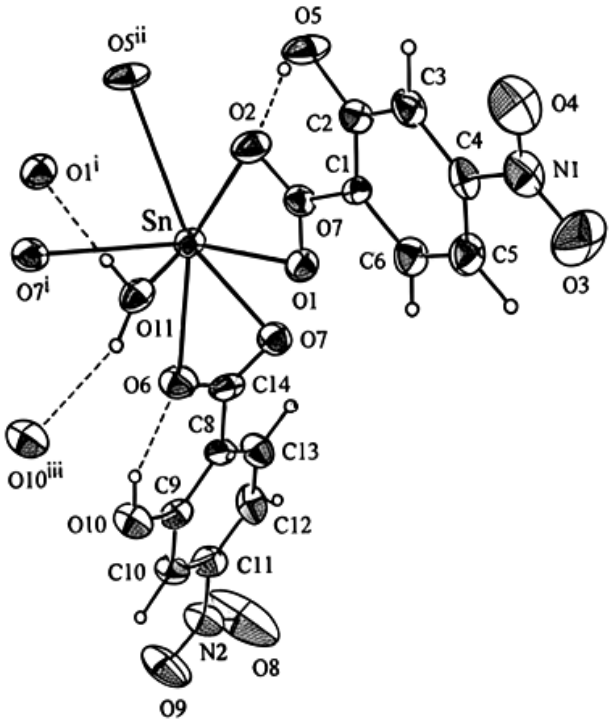

Figure 3. Molecular structure of $Sn(C_7H_4NO_5)_2 \cdot H_2O$ [complex 1]

Is can be seen brow Fig. 4 the coordination of the Sn (II) atom involves three primary bonds: carboxyl O (1) – 2,452Å, carboxyl O (6) – 2,428Å, and aqua O (11) atoms – 2,419Å, while secondary interaction with carboxyl O (2) – 2,691Å and O (7) – 2,727Å on the same molecular complex the chelate rings (Fig. 1). Two additional weaker intermolecular contacts with carboxyl O (7^1) – 2,691Å and hydroxyl O (5^1) – 3,084Å. All other O atoms are more than 3,35Å from the tin atom. The seven-coordinate geometry is highly irregular and leaves a substantial empty region on one side of the Sn atom, which can be attributed to a sterochemically-active ion pair of electrons, typical for Sn(II) [18, 19].

The two hydroxyl groups in the molecule, O (5) and O (10), are involved in inframolecular hydrogen bonds to the carboxyl O (2) and O (6) atoms, respectively. The water molecule is involved in two intermolecular hydrogen bonds to the carboxyl O (1) and hydroxy O (10) atoms.

Selected bond distances $\left(d\ \overset{0}{A}\right)$ and angles $\left(\omega^0\right)$ for complex 2 have been shown in table 2.

Table 2. Selected bond distances (Å) and angles (^{0}) for complex (2)

Distance	$\overset{0}{d}, A$	Distance	$\overset{0}{d}, A$
$Co(1)-O(1)$	2,157	$O(4)-N(2)$	1,227
$Co(1)-O(1)$	2157	$N(1)-C(8)$	1,357
$Co(1)-O(H_2O)$	1,181	$N(1)-C(3)$	1,395
$Co(1)-N(1)$	2,301	$N(2)-C(6)$	1,463
$C(1)-O(1)$	1,279	$C(1)-C(2)$	1,515
$C(1)-O(2)$	1,240	$C(3)-C(4)$	1,401
$C(8)-O(3)$	1,221	$C(2)-C(7)$	1,386

$O(1)-Co-O(2)$	180,00	$O(4)-N(2)-O(5)$	123,81
$O(1)-Co-O(H_2O)$	84,14	$O(4)-N(2)-C(6)$	118,11
$O(1)-Co-N(1)$	91,39	$O(2)-C(1)-O(2)$	125,10
$N(1)-Co-N(13)$	90,08	$C(7)-C(2)-C(1)$	117,12
$C(1)-O(1)-Co(1)$	133,86	$C(7)-C(6)-N(2)$	119,28
$C(8)-N(1)-C(3)$	129,21	$C(5)-C(6)-N(2)$	119,62

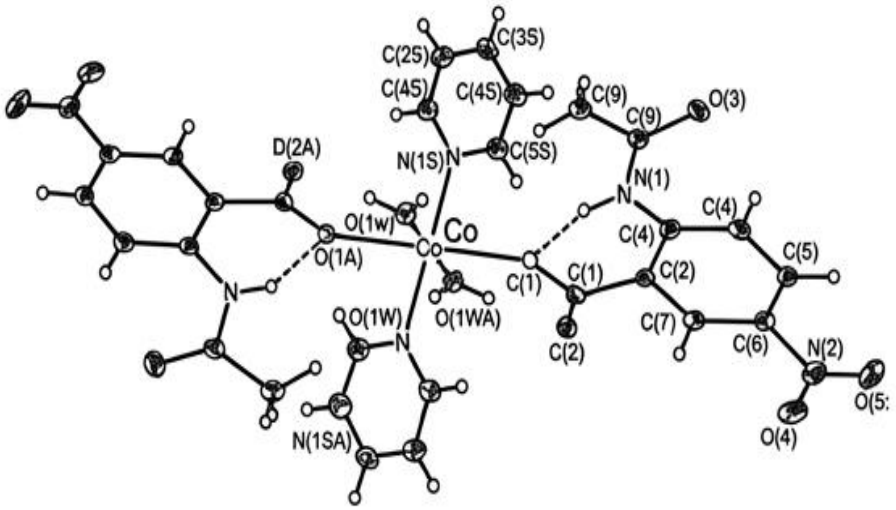

Figure 4. Molecular structure of Co (II) [complex 2]

As can be seen fig. 4, the central atom Co(II) coordinated with the oxygens atoms of the carboxyl group at monodentate bond.

The bond between the central atom and the oxygen of the carboxyl group $Co(1)-O(1)=2;157\overset{0}{A}$, it is compatible other Co(II) complexes.

The pyridin molecules enter in the structure and form the adduct which is coordinated by the donor nitrogen atoms and the central cobalt atom is coordinated throught donor-acceptor type. The length of this bond - $Co(1)-N(1)=2,301\overset{0}{A}$ and corresponds to the other cobalt-nitrogen bonds [10].

Two molecules of water from a donor oxygen atoms and a donor-acceptor bond with the cobalt atom, completing its coordination number to six. The length of this bond is $Co(1)-O(H_2O)=1,181\overset{0}{A}$ and similar to other aqua complexes of Cobalt [11].

The phenyl carbon bond $(C(2)-C(3))=1,543(6)\overset{0}{A}$ is similar to other derivatives benzoic acid .

The phenyl ring and substituents are located on a plane, which is due to the ionic structure.

The bond length between the carbons forming both the benzene and pyridine

C – C=1,385Å, the same as the bond length in other benzoic acid derivativers.

The length of the C – NO_2 bond is 1,436 Å, which is the same as in other nitrobenzoate complexes. Molecules are linked together by strong hydrogen bonds $O\cdots HO=2,89\overset{0}{A}$.

Conclusion

It has been synthesized and deciphered the molecular structure of new complex bis-(p-nitrosalysilato) Sn · H_2O. It was established that the central Sn atom is coordinated by the oxygen atoms of the carboxyl group and the oxygen atom of the hydroxyl group. The water molecule in the complex, via a donor oxygen atom, coordinates with the central atom and increases its coordination number to seven. The carboxyl oxygens form chelate bonds. It has been synthesized and deciphered molecular structure of new complex bis-(5-nitro, 2-asetamidobenzoata)-di-(pyridine) cobalt(II)-dihydrate. It was established that the central cobalt atom is coordinated by the oxygen atoms of the carboxylic group by monodentate type. Two molecules forming the adduct are coordinated by donor nitrogen atoms of pyridine to the central atom via a donor-acceptor bond. The water molecule in the complexes, via a donor oxygen atom, coordinates the central atom and increases its coordination number to four.

REFERENCES

1. Hesenova S. S., Mamedova L. N., Ashfaq M., Navaz T., Movsumov E. M. Synthesis, crystal structure polymers of cobalt and manqanes with nitrobenzene and pyrazine. Journal of Molecular Structure (2022), p. 131851 – 1311864.

2. Hesenova S. S. Synthesis, physico-chemical analysis and crystal structure of bis-(p-nitrobenzoate)-di(pyrazine) Ni (II) dihidrate. Chemical problems (2022), №1, p. 95-101.

3. Hesenova S. S., Yolcuyeva E. A., Aliyeva Q. M., Movsumov E. V. Synthesis, crystal structure of Copper nitrotereftalik. A. Ch. S. Omega (2023), p. 8530 – 8540.

4. Ali KS, Ashfaq M, Tahir M. N, Movsumov E. M, Munawar KS. Synthesis, crystal structure, Hirshfeld surface and void analysis of bis (μ2- 4-aminobenzoato-O: O′) bis [bis (4-aminobenzoato-κ2O, O′) diaquathulium (III)] dehydrate Acta. Cryst. Structure Reports 2022, 78 (3), 282-286.

5. Tahir MN, Movsumov E.M, Ülkü D. Poly [bis (3, 5-dinitrobenzoato-O1: O2) disilver (I)-O2: Ag; Ag': O2'] Crystal Structure Communications 1996, 52 (11), 2678-2680.

6. Dzhafarov NK, Amiraslanov IR, Nadzhafov GN, Movsumov EM. Crystal and molecular structure of monoaquo-bis-(p-hydroxybenzoato) lead (II) monohydrate, journal of Structural Chemistry 1981, 22 (2), 245-248.

7. Amiraslanov IR., Dzhapharov N.K., Nadzhaphov G. N., Mamedov R. S., Movsumov E. M. Crystal and molecular structure of nitrato – (p-aminobenzoato) lead (II). Journal of Structural Chemistry, (1980), 21, p-109 – 113.

8. Amiraslanov, NK Dzhafarov, GN Nadzhafov, KS Mamedov. An X-ray structural study of the complexes of p-aminobenzoic acid with metals VI the crystals and molecular structure of nitrato-(p-aminobenzoato) lead (II) IR. Journal of Structure Chemistry 21 (1), 109-443.

9. Tahir M. N, Ülkü D, Movsumov E. M. Poly [bis (p-nitrosalicylato-O:O`) disilver (I)-O3: Ag`; Ag: O3`] Crystal Structure Communications 52 (3), 593-595.

10. Tahir M.N, Ülkü D, Movsumov E M, Hökelek T. Tetraaquabis (p-nitrosalicylato) Complexes of Zinc (II) and Cobalt (II) Crystal Structure Communications 53 (2), 176-179.

11. М.Ф.Рзаева, Э.М.Мовсумов, В.С.Сергиенко, А.Б.Илюхин. Кристаллическая структура комплексов двухвалентных Co, Ni, Cd с анионами бензойной и 2-(ацетиламино)-5-нитробензойной кислоты //Кристаллография, - Россия: -2012, т.57, №2, -с. 256-260.

12. Рзаева М.Ф., Мовсумов Э.М., Лысенко К.А. Синтез и структурное исследование 5-нитро, 2-ацетамидобензоато Cu(II) и его пиридиного аддукта XXV Международная Чугаевская Конференция по координационный химии, - Суздаль, Россия, -2011, -с. 347.

13. Рзаева М.Ф. Сафарова Л.Н., Мовсумов Э.М. Синтез и исследование 5-аквакомплексов и пиразиновых аддуктов 5-нитро, 2-ацетамидобензоатов металлов Zn(II), Cd(II) // Менделеев 2013, VII Всероссийская конференция молодых ученых и аспиранты, Санкт-Петербург, 2-5 апреля 2013, -с.112-113.

14. Bruker,A. Saint and SADABS, Bruker AXS inc., Madiston üisconsin, USA. 2019, -p.426-431.

15. Dolomonov, Oleq.V., Bourthis Luc.J.? Gildea Richard J., Howard A.K. OLEX2: A complete structure solution, retiniment and analiz proqram // j.Applead Crystalloqr., -2015, V.427, №2, -p.p.339-341.

16. Sheldrick, G.M., SHELXT: Integrating space group determination and structure solution // Acta Crystallogr, Sect. A: Found, -2014, Adv 70.C –C.-pp1437-1445.

17, M. Navaz Tahir, Dinçer Ülkü, Elman Movsumov. Tetra-aqua-bis(p-nitrosalysilato) Co (II), Zn (II). Akta Crystallographica (1996), C52, p. 176 – 180.

18. Tian L. Zho, X. L. Zheng, J. Dong, Ling-Lan Tu. Catena (3,5-dinitro-2-oxibenzoato)-di Tin (II). Chin J. İnorg. Chem. (2018), 26, 2165 – 2170.

19. Накомото В.Т. Инфракрасные спектры неорганической и соединений. Москва [Н. КВ],1994,587 стр.

UDC:631.445.5:504.5
DOI: *https://doi.org/10.30546/2521-6317.2025.02.542*

THE IMPACT OF OIL CONTAMINATION ON THE MORPHOGENETIC INDICATORS AND ECOLOGICAL CHARACTERISTICS OF GRAY-BROWN SOILS IN THE ABSHERON PENINSULA

Ali IBRAHIMOV[1*], Gunay VALIYEVA[1], Azade ALIYEVA[2]

[1] *Baku Engineering University, Hasan Aliyev Street, House 120, Khirdalan city, Absheron district, AZ0102, Azerbaijan*

[2] *Sumgait State University, 43rd district, Sumgait city, AZ5008, Azerbaijan*

ARTICLE INFO

Article history:
Received:2025-07-11
Received in revised form :2025-07-19
Accepted:2025-08-17
Available online:2025-12-25

Keywords:
Soil, oil, contamination, ecological characteristics, morphological features

ABSTRACT

During the exploitation of oil fields, the fertile topsoil layer has undergone significant degradation. As a result, mechanical disturbance of the soil surface and the loss of vegetation cover on productive lands are widely observed. These soils have been contaminated to varying degrees by oil-derived wastes.

A portion of the oil mass remains on the soil surface, forming a persistent coating, while another fraction infiltrates the soil profile to different depths. Addressing the stress imposed on the soil–plant system of the Absheron Peninsula requires, first and foremost, the identification and assessment of technogenically induced disturbances, as well as the determination of the genetic characteristics and the physical, physicochemical, and sanitary–hygienic parameters of these soils.

The morphogenetic characteristics of oil-contaminated soils in the peninsula have been investigated at different times. Based on studies conducted in the territories of Binagadi, Sabunchu, Surakhani, and Azizbayov districts, a soil fertility model has been developed for heavily, moderately, and slightly contaminated soils. The proportion of oil-derived pollutants causing contamination constitutes 26.0–20.0% in heavily contaminated areas, 18.0–16.4% in moderately contaminated areas, and 13.0–10.6% in slightly contaminated soils.

The Absheron Peninsula is one of the most industrially developed and highly urbanized regions of the Republic of Azerbaijan. Over many years, waste generated from the oil industry and related sectors has led to critical levels of contamination in several areas of the peninsula. The remediation and restoration of contaminated soils and water bodies are among the urgent priorities for the Republic of Azerbaijan. These measures are essential for reducing risks to public health, supporting the sustainable development of Baku and its surrounding settlements, and reintegrating rehabilitated lands into the national economic circulation.

INTRODUCTION

The Absheron Peninsula is an oil-producing region with a history of nearly 200 years. The former lack of advanced oil extraction technologies and the failure to comply even with the most basic requirements of environmental protection led to the formation of land areas contaminated with oil and petroleum products across the peninsula.

As is well known, out of the 200 thousand hectares comprising the Absheron Peninsula, 21.3 thousand hectares are lands requiring recultivation, of which 10.1 thousand hectares are soils contaminated with oil and oil-polluted wastewater.

In the Republic of Azerbaijan, the total area of oil-contaminated lands subject to recultivation is 24,156 hectares. Of this, 13,805 hectares are located on the Absheron Peninsula (including 6,788 hectares under the jurisdiction of Azneft), while 10,351 hectares are situated in other regions. According to SOCAR regions, the distribution is as follows: Khazar district – 302 ha, Sabail district – 526 ha, Garadagh district – 1,277 ha, Surakhani district – 533 ha, Sabunchu district – 410 ha, and Binagadi district – 183 ha [2, 11].

The areas of the Absheron Peninsula located under formation waters (saline, oil-contaminated, and radioactive lakes) amount to 1,190 hectares. Approximately 6–8% of the peninsula's territory is extremely (deeply) contaminated.

The history of soil contamination by crude oil in the Absheron Peninsula is relatively long. Industrial-scale oil contamination of soils began in the late 19 th century (around 1870). During that period, oil was extracted from hand-dug wells in low-relief and gently elevated areas where oil-bearing layers were close to the surface (in locations such as Balakhani, Fatmai, Binagadi, and Sulutepe). Starting from the first quarter of the 20th century, the mechanical drilling of oil wells accelerated oil extraction, transportation, processing, as well as environmental pollution [3,7].

It should be noted that soil contamination in the Absheron Peninsula is patchy, affecting areas ranging from 2–3 ares to several hectares (5–10 hectares or more). Crude oil spilled onto soil negatively affects its morphology, as well as its water-related, physical, physicochemical, chemical, and biological properties. It destroys and alters vegetation cover, soil fauna, microorganisms, enzymes, and bacteria. The light fractions of oil infiltrate into deeper soil layers in soils with lighter granulometric composition, reach groundwater, and partially evaporate upon release. In contrast, the heavy fractions accumulate on the soil surface, blocking aeration [9,11]. As a result, the soil completely loses its fertility and ceases to function as soil. Therefore, there is a need to restore the aforementioned properties of oil-contaminated soils and, accordingly, to determine permissible limits of oil content in soils for agricultural crops.

The Absheron Peninsula is the area most exposed to environmental pollution in the Republic. Approximately 75–85% of the country's industrial potential and about one-third of its population are concentrated in this economic region. Up to 30% of the peninsula's territory has been allocated for oil fields and has been contaminated by their waste, as well as by domestic, construction, wastewater, and technical discharges. Oil and gas extraction, transportation, and processing have led to pollution and degradation of the environment, particularly soils; gas emissions have caused atmospheric contamination with various harmful substances; and water bodies and groundwater have been polluted with petroleum products, radionuclides, and heavy metals [8,9]. These factors have resulted in the formation of anthropogenic landscapes across the peninsula.

It should be particularly noted that in Azerbaijan, although reclamation measures are included in project estimates for the extraction of mineral resources, construction materials, and oil, in practice such measures have often not been implemented. Formation waters, sludges, and oil gushers discharged onto the soil surface lead to salinization and contamination [1,6].

Contamination of the soil cover, especially groundwater, by formation waters can pose serious threats not only locally but also at the regional level [4, 13]. Based on the assessment of the ecological condition of the Absheron Peninsula, the following four levels of landscape disturbance are observed:

- Satisfactory – the soil–vegetation cover is not disturbed;
- Moderate – the soil cover is slightly disturbed;
- Critical – the soil cover is destroyed and the landscape has changed;
- Catastrophic – all elements of the landscape are altered and all internal landscape relationships are disrupted.

There is a pressing need for conducting research on landscape restoration, as well as for the remediation of contaminated lakes, the recultivation of polluted soils, the leaching of saline soils, and the development of collector–drainage systems to lower groundwater levels.

The territory of the Binagadi Oil and Gas Production Department belongs to an old oil-field zone. It is located in the northwestern part of Baku city, at a distance of 8–10 km from the city center. The Binagadi Oil and Gas Production Department operates in the Binagadi, Sulutepe, Chakhnaglar, Kirmaki Shabandag, Silyanshor, Mahammadli, and Masazir fields. It has been functioning as an oil production zone since 1896. A total area of 2,759 hectares of the Absheron Peninsula is included within the company's production zone.

The primary objective of this research is to study, first of all, the impact of oil contamination on the morphogenetic indicators of gray-brown soils in the Absheron Peninsula, depending on the degree of contamination, and subsequently to develop reclamation methods for these soils under agricultural crops, taking into account their granulometric composition. In this regard, the following tasks have been set:

1) Investigation of the natural and oil-contaminated soil cover in the territories of the Binagadi and Sabunchu Oil and Gas Production Departments.
2) Assessment of the impact of oil on the morphogenetic properties of soils, depending on the degree of contamination and whether it is recent or aged.
3) Study of the effects of oil on the physical, chemical, and biological properties of soils.
4) Investigation of heavy metals and radioactivity in background and oil-contaminated soils.

Experimental Section

The 2nd oil field of the Binagadi Oil and Gas Production Department under SOCAR is located at the intersection of roads leading from Binagadi settlement to Mehtiabad settlement, on the right side of the highway, toward Balakhani settlement. From the central part of the field, a deep (more than 2 m) open drainage channel carrying wastewater flows toward the Binagadi-Boyukshor Lake. The central part of the field is a micro-depression. The soils in this depression are highly salinized and saline-alkalized due to both natural conditions and formation waters seeping from the oil wells, as well as to some extent from domestic wastewater [5,10]. These soils remain moist throughout the year and are dark in color. During the summer, they dry out relatively. Since the surrounding terrain is relatively elevated, the groundwater level in this area (central part) is very close to the surface (1.0–0.60 m).

Our studies were carried out on relatively steep slopes. For comparison, four soil profiles were established: one in uncontaminated soil (Profile N1) and three at different depths in oil-contaminated soils. These profiles were described in detail, and soil and groundwater samples were analyzed for total water extraction, granulometric composition, bulk density, exchangeable bases, pH in water suspension, carbonate content, humus, nutrient elements (NPK), heavy metals, absorption of radiation, and radioactive elements. The descriptions of these soils are presented below.

Profile No. 1. Established on a south-facing slope in the oil field area in uncontaminated gray-brown soil. Vegetation includes ephemeral plants, camel thorn, grassland species, sage, clover, etc.

AUVCa – Depth 0–10 cm; granulometric composition: light loamy; color: light gray-brown; structureless granular; consistency: soft; roots and rootlets present; moisture: dry; boundary clear; reaction in 10% HCl: vigorous effervescence.

AUV_{Ca} – Depth 10–35 cm; medium loamy; color: light gray-brown; structure: fine cloddy; consistency: firm; roots, rootlets, and new growth (small fishbone-like roots) present; moisture: dry; boundary clear; reaction in 10% HCl: vigorous.

B_{Ca} – Depth 35–67 cm; loamy; color: light gray-brown; fine cloddy; consistency: firm; roots, rootlets, white nodules (salt, gypsum) present; slightly moist; boundary gradual; reaction in 10% HCl: vigorous.

B/C_{Ca} – Depth 67–100 cm; loamy; color: light gray-brown; structure: fine cloddy; consistency: firm; very few weak roots and rootlets; numerous white nodules; compact, moist; boundary gradual; reaction in 10% HCl: vigorous.

C_1 – Depth 100–124 cm; light loamy; color: light gray-brown; structureless; consistency: firm; sparse weak rootlets; dry; boundary gradual; reaction in 10% HCl: vigorous.

C_2 – Depth 124–165 cm; light loamy; color: light gray; structureless; consistency: firm; very weak sparse rootlets; slightly moist; boundary gradual; reaction in 10% HCl: vigorous.

C_3 – Depth 165–200 cm; light loamy; color: light gray; structureless; consistency: firm; slightly moist; boundary gradual; reaction in 10% HCl: moderate.

Profile No. 2 – Located 100 m to the southeast of Profile No. 1 along the right side of the Binagadi-Balakhani highway. Microrelief is smooth, south-facing slope; soil: gray-brown; granulometric composition: upper loamy; parent material: loess, fishbone gravel, small stones, sand, various marine sediments; vegetation: ephemeral plants, camel thorn, grass, clover, sage; groundwater: absent; waterlogging: absent; erosion: absent; reaction in 10% HCl: vigorous.

X – Depth 0–25 cm; hardened oil residue (bitumen); color: black; structureless layer; consistency: firm; moisture: absent; boundary sharp; reaction in 10% HCl: none (due to oil effect).

B – Depth 25–64 cm; loamy; color: light-dark gray (oil sediment observed); structure: cloddy; consistency: firm; slightly moist; boundary gradual; roots/rootlets absent; new formation: oil deposit; reaction in 10% HCl: none.

C1 – Depth 64–100 cm; medium loamy; color: light gray-brown; structureless; consistency: firm; new formations absent; white nodules present; moisture: moist; boundary clear; reaction in 10% HCl: vigorous.

C_2 – Depth 100–150 cm; granulometric composition: sandy; color: light gray; structureless; loose; new formations absent; rootlets absent; slightly moist; boundary gradual; reaction in 10% HCl: moderate.

C_3 – Depth 150–200 cm; sandy; color: light gray; structureless; loose; new formations absent; slightly moist; reaction in 10% HCl: none.

Profile No. 3 – Located within the territory of the 2nd oil field of the Binagadi Oil and Gas Production Department, 80–100 m east of the highway, on a smooth micro-depression to the right of the drainage channel flowing toward Boyukshor Lake, near an oil well, on clayey, sandy, oil-contaminated, relatively shallow-hardened ground.

X – Depth 0–60 cm; thick layer; color: black; clayey, sandy; relatively firm; oil residues present; lower part soft; boundary clear; reaction in 10% HCl: none.

X/B – Depth 60–70 cm; sandy; color: dark ash; structureless; loose; new formation: oil-infiltrated; moisture: moist; boundary clear; reaction in 10% HCl: none.

B – Depth 70–100 cm; medium sandy; color: dark ash; structureless, layered; consistency: firm-loose; new formation: oil deposited; boundary gradual; reaction in 10% HCl: none.

C – Depth 100–200 cm; granulometric composition: sandy; color: light ash; structureless; consistency: loose; new formation: light fraction of oil filtered through; reaction in 10% HCl: none; groundwater accumulation observed. On the following morning, the oil-contaminated water level was one meter below the surface.

Table 1. Some Physicochemical Characteristics of Oil-Contaminated Gray-Brown Soils in the Territory of the Binagadi Oil and Gas Production Department

Profile No.	Depth (cm)	Hygroscopic Moisture, %	Bulk Density, g/cm³	Humus, %	Total Nitrogen, mg/kg	Phosphorus, mg/kg	Potassium, mg/kg	pH (water suspension)	$CaCO_3$, %
1	0–10	4.021	1.34	3.02	12.07	21.11	126.52	7.69	5.75
	10–35	4.019	1.56	2.38	6.04	17.78	117.47	8.25	4.61
	35–67	5.066	1.63	0.52	9.48	18.89	84.35	8.94	8.63
	67–100	3.947	1.66	0.41	5.17	32.50	78.32	9.05	7.90
	100–124	4.165	1.72	–	–	–	–	9.00	10.06
	124–165	5.905	1.73	–	–	–	–	8.59	11.49
	165–200	3.643	1.64	–	–	–	–	8.68	12.95
	0–25 Oil-contaminated	1.77	–	–	–	–	–	–	–
2	25–64	3.786	1.75	7.71	6.90	26.67	24.10	8.12	–
	64–100	4.632	1.48	0.90	5.17	27.78	102.42	8.23	0.72
	100–150	2.179	1.44	–	–	–	–	8.10	2.88
	150–200	–	1.49	–	–	–	–	8.04	1.43
	0–40 Oil-contaminated	1.80	–	–	–	–	–	–	–
3	40–59	2.296	1.73	2.38	6.04	32.50	90.37	8.20	0.43
	59–80	3.081	1.70	0.77	12.07	24.44	108.45	8.44	0.27
	80–103	3.474	1.72	–	–	–	–	8.73	4.89
	103–130	1.638	1.63	–	–	–	–	8.90	8.63

	0–60 Oil-contaminated	1.70	–	–	–	–	–	–	–
4	60–70	0.902	1.65	2.15	–	–	–	9.61	3.60
	70–100	2.451	1.62	0.96	–	–	–	9.74	4.74
	100–200	1.439	1.61	–	–	–	–	9.91	2.87
Binagadi Loamy	Experimental soil	1.763	1.40	1.74	9.48	35.00	12.05	7.52	4.75

Table 2. Results of Heavy Metals in Oil-Contaminated Gray-Brown Soils in the Territory of the Binagadi Oil and Gas Production Department, $\frac{\%}{mg/kg}$

Profile No.	Depth, cm	Cu	Pb	Zn	V	Sr	Ba
1	Background 0–10	$\frac{0,0012}{12}$	$\frac{0,0008}{8}$	$\frac{0,0094}{94}$	$\frac{0,0126}{126}$	$\frac{0,160}{1600}$	$\frac{0,0024}{24}$
3	0–40 Bitumen 40–59	$\frac{0,0017}{17}$	$\frac{0,0021}{21}$	$\frac{0,0084}{84}$	$\frac{0,0117}{117}$	$\frac{0,084}{840}$	$\frac{0,0054}{54}$
4	0–60 Bitumen	$\frac{0,0024}{24}$	$\frac{0,0011}{11}$	$\frac{0,0118}{118}$	$\frac{0,0096}{96}$	$\frac{0,192}{1920}$	$\frac{0,0086}{86}$
	60–70	$\frac{0,0011}{11}$	$\frac{0,0016}{16}$	$\frac{0,0112}{112}$	$\frac{0,0142}{142}$	$\frac{0,096}{960}$	$\frac{0,0042}{42}$
Clark values (mg/kg)		20 mg/kg	10 mg/kg	50 mg/kg	100 mg/kg	300 mg/kg	500 mg/kg.

The operational area of the Balakhani Oil and Gas Production Department (OGPD) encompasses the mining zones of oil and gas fields around the settlements of Balakhani, Zabrat, Sabunchu, and Ramana. Throughout the entire operational period of the Balakhani OGPD, primary attention was focused on oil extraction; as a result, reclamation measures were not implemented during the drilling of oil wells. Consequently, the ecological balance of the area was completely disrupted due to the discharge of formation waters into the territory and contamination of the soil with crude oil. The OGPD occupies an area of 1,510.9 hectares. The volume of formation water produced daily exceeds the oil production by 2.5 times. As a result, "Ramanagolu" Lake (with an area of 110 ha) has formed in the area. This lake was created from formation waters and the accumulation of rain and domestic waters in a micro-depression. It is oil-contaminated, saline, and radioactive.

The fifth oil field investigated in this study is located in the northern and northwestern parts of the Balakhani settlement. Topographically, it is slightly inclined to the west and east, i.e., it is situated on a gentle slope. The eastern end of the area connects to the Zabrat main road, and as a result of the discharge of formation waters along the slope, the groundwater (oil-contaminated) level is observed at approximately 1 meter.

Soil contamination with oil exerts irreversible effects on its morphological, physical, chemical, biological properties, and fertility. The direct impact of crude oil on soil morphology is evident in the genetic horizons of the soil profiles established in the oil-contaminated soils of Balakhani. Contamination of soils with oil and its products can induce significant changes in soil composition, properties, and structure. Oil contamination affects soil morphology, causing changes in the color of natural genetic horizons throughout the profile—from gray and dark shades to light brown—and also leads to deterioration of soil structure. Ultimately, this results in

the formation of a soil type modified by technogenic impact, derived from the original zonal soils [2,12].The lack of oxygen in the soil is caused by liquid oil compressing the air and covering the surface with a bituminized layer, which also prevents water infiltration and causes soil particles to adhere to each other. As a result, anaerobic conditions develop, the oxidation–reduction potential slows down, and soil alkalinity increases. Oil forms a coating around soil particles, which prevents water penetration and reduces moisture retention. The amounts of hygroscopic moisture, water infiltration, water-holding capacity, and evaporation from the upper soil layer decrease. During oil contamination, the humus content in the soil increases, but its quality changes: humic and fulvic acids decrease, and hydrolyzed residues increase Table 1 and 3. The soil's absorption capacity decreases because the oil film envelops the soil particles [14].

In addition to the strong effect of oil on the soil, saline oil formation waters cause chlorinated-sodium salinization and sodification. As a result, the soil horizon is completely altered. This type of contamination is even more hazardous than oil contamination alone [5,8].

Soil contamination with oil and its products significantly affects the number and composition of microorganisms. Bacteria that fix ammonia and nitrogen increase, whereas denitrifying bacteria, sulfate-fixing bacteria, mycromycetes, nitrifying bacteria, cellulose-degrading bacteria, and actinomycetes are completely altered. However, when the oil content in the soil is low—within permissible limits—all types of soil microorganisms remain active, positively influencing soil biota [2, 6, 13].

Profile No. 5. This profile was established on the northern side of Balakhani settlement, in the second section of Balakhani Oil Company No. 5, on a gently sloped smooth area contaminated with oil, along the roadside.

X. Depth 0–116 cm: Bitumen-contaminated sandy-loam mixture, recent oil contamination, color black with intermediate sand layers. Structure – layered, surface dry, lower part loose, moist, soft, bituminous, sandy-loam, slightly moist, transition sharp, boiling test – none .

X_1. Depth 116–124 cm: Sandy, dark brown, structureless, dense, light fraction of oil, sandy, moist, clear transition, weak to moderate boiling.

X/C. Depth 124–143 cm: Sand, sandy, whitish-gray, relatively dull, structureless, rust-colored spots, slightly moist, clear transition, moderate to high boiling.

C_{Ca}. Depth 143–200 cm: Sand, sandy, light brown, structureless, dense, rust spots, slightly moist, gradual transition, intense boiling.

Profile No. 6. Uncontaminated clean soil (background). This profile was established in the northwestern part of Balakhani settlement, on undulating gentle terrain, 25–30 m from the roadside within the area of Oil Field No. 5, on a raw, relatively elevated site. The vegetation is ephemeral, including *Qanqal*, camel thorn, willow in garden areas, and fig, which are characteristic for the entire area.

$АУV_{Ca}$. Depth 0–10 cm: Granulometric composition sandy, color light gray-brown, structureless, density loose, new formations – roots, rootlets, small stones, occasional snail shells, moisture very dry, transition gradual, boiling test intense.

АУCa. Depth 10–17 cm: Sandy, light gray-brown, weakly topsoil-like, loose, roots and rootlets present, occasional snail shells, very small stones, moisture dry, transition gradual, boiling test moderate.

AУ$_{Ca}$. Depth 17–48 cm: Granulometric composition sandy, light gray-brown, structureless, loose, smooth with occasional small stones, white snail shells, dry, occasional white rootlets, transition gradual, boiling test moderate.

B/C$_{Ca}$. Depth 48–70 cm: Sand-sandy, light gray-brown, small black-bitumen lumps, dense, clay lumps, sparse thin rootlets, sparse white nodules, transition gradual, boiling test moderate.

C$_{Ca}$. Depth 70–111 cm: Sand, whitish-gray to yellowish-brown, structureless, loose, weak rust spots, nodules present, dry, transition gradual, boiling test intense.

Depth 111–200 cm: Sand, whitish-gray, structureless, loose, no new formations, dry, transition gradual, boiling test weak.

Table 3. Selected physico-chemical properties of oil-contaminated gray-brown soils in the Balakhani section of Sabunchu Oil-Gas Production Department (OGPD)

Profile No.	Depth (cm)	Hygroscopic moisture, %	Bulk density, g/cm³	Humus, %	Total nitrogen, mg/kg	Phosphorus, mg/kg	Potassium, mg/kg	pH in water suspension	$CaCO_3$, %
5	0–116	Oil-contaminated	–	–	–	–	–	–	–
	116–124	1.006	1.63	–	–	–	–	7.00	2.02
	124–143	1.010	1.51	–	–	–	–	9.60	1.59
	143–200	1.014	1.48	–	–	–	–	9.64	6.48
6 (background)	0–10	1.010	1.32	2.17	6.04	24.44	24.10	8.00	9.05
	10–17	1.010	1.41	2.09	5.17	15.56	24.10	8.07	4.59
	17–48	1.017	1.49	0.85	4.31	15.56	24.10	7.95	6.48
	48–70	1.013	1.43	0.72	–	–	–	7.90	5.75
	70–111	1.012	1.41	Not determined	–	–	–	8.05	6.61
	111–200	1.012	1.49	–	–	–	–	8.05	2.16
7 (old contamination)	0–10	1.015	1.32	5.82	6.90	17.78	72.30	7.48	6.32
	10–40	1.031	1.30	4.96	7.76	12.22	219.31	9.39	1.60
	40–85	1.0009	1.59	2.71	3.45	23.33	24.10	9.38	5.75
	85–145	1.012	1.66	–	–	–	–	9.69	7.48
	145–210	1.012	1.63	–	–	–	–	9.50	10.80
8	0–52	–	1.71	Oil-contaminated	–	–	–	–	–
	52–70	1.018	1.53	0.62	3.45	15.56	24.10	8.50	8.33
	70–100	1.016	1.56	0.41	2.59	13.33	24.10	8.55	8.63
	100–140	1.017	1.47	–	–	–	–	8.56	8.47
	140–200	1.025	1.48	–	–	–	–	8.57	7.91
Rataxani sandy clean soil	0–25	1.018	1.03	46.56	17.78	48.20	7.73	4.75	–

Table 4. Heavy metal content in oil-contaminated soils in the Balakhani area of Sabunchu Oil-Gas Production Department (OGPD)

Profile No.	Depth (cm)	Cu	Pb	Zn	V	Sr	Ba
5	0–116 Oil-contaminated	0,0018 18	0,0009 9	0,0136 136	0,0112 112	0,0136 136	0,0114 114
	116–124	0,026 26	0,0008 8	0,0174 174	0,0136 136	0,0112 112	0,0081 81
8	Lower contamination layer	0,0014 14	0,0019 19	0,0092 92	0,0120 120	0,078 780	0,0036 36
Clarke values, mg/kg	------	20	10	50	100	300	500

In the northeastern part of the Absheron Peninsula (30 km east of Sumqayit city), the content of heavy metals in the topsoil is as follows: Ni – 75; Co – 26; Pb – 46; Mn – 3266; Cr – 127; Zn – 42; Cu – 49; Se – 36; Mo – 7.1; Ca – 4.2; V – 120; F – 31 mg/kg [9,11].

In the Sabunchu oil area, Balakhani section (near Zabrat settlement), the content of heavy metals in the oil-contaminated soils at a depth of 0–153 cm, from the upper layer downward, is as follows: Ti – 600–105; Cr – 420–160; Mn – 1200–1680–600; Ni – 3.2–3.0; Pb – 3.0–4.8–0.6; Cu – 3.4–1.0; Zn – 16.0–4.5; Co – 4.0–2.6; Sr – 200–48 mg/kg.

CONCLUSION

1. Based on the conducted comparative-geographical studies, the morphogenetic characteristics of sandy and loamy gray-brown soils in the Absheron Peninsula, in their natural-raw and oil-contaminated variants, have been determined.
2. The depth of soil contamination by oil, the physical and chemical properties of the soils, the composition of the oil, and the nutrient elements (NPK) have been studied; it was established that in contamination, the color of the morphogenetic layers' changes (deeper in sandy soils), and the water, physical, and p**hysicochemical** properties deteriorate.
3. The study shows that in soils contaminated with crude oil, the content of heavy metals and radioactive elements does not exceed the permissible limits compared to raw soil. At the same time, in natural gray-brown soils and in vegetation experiments with clover, accumulation of heavy metals and toxic elements is not observed.

REFERENCE LIST

1. Alizade V.M., Shirvani T.S., Alirzayeva E.G. Plant resistance to toxicity of metals and petroleum hydrocarbons approaches to phytoremediation. Baku: Elm, 2011, p. 276.
2. Ahmedov. V. (2011) Methods of invention and reclamation of technogenically degraded and oil-contaminated soils. // Department of Biological Sciences of ANAS. "News". Baku: Nauka Publ., volume 66, No. 2. p. 49-56
3. Aliyeva Azade, Guliyev Alovsat, Babayeva Tunzala (2024) İmpact of petroleum contamination on soil properties in Absheron Peninsula, Azerbaijan Eurasian Journal of Soil Science, Turkey Volume 13, İssue 2, p. 145-152.
4. Babyev M.P., Azizov G.Z., Mustaphayev M.G., Jafarov A.M. (2012) Natural factors that can create danger for that part of the Baku-Tbilisi-Ceyhan oil pipe-line passeng through the Azerbaijan Republic and intending measures for preservation.Baku: Elm, p. 111.
5. Babayev M. P., Nadzhafova S.I, İbrahimov A.H. (2015) Application of activated sludge to purify urban soils of Baku city from oil contamination ISSN 1064-2293.Euroasian Soil Sceince, Vol 48, pp.773-779.
6. Coulon et al. (2004) Deqradation of petroleum hydrokarbons intwosub-antarctik soils: influance of an oleophilic fertilizer. // Environ. Toxsiol. Chem, 2004, V23, № 8, p. 1893-1901.
7. Ibrahimov A.H., Gurbanova K.R., S.A.Kuliyeva S.A. (2018) Investigation of morph-ogenetic properties and reclamation methods of oil polluted soils of Absheron peninsula 10 th International Congress on "The Soil Resources and Environment Conservation" Almaty, Kazakhstan, p.251-254.
8. Ibrahimov A.H. (2013) Absorbed bases, heavy metals and radioactivity in crude and oil-contaminated soils on the territory of Binagadi Oil Company Soil Science and agrochemistry Volume 21, №3, Baku-"Science", p. 445-448.
9. Ibrahimov A.H. (2012) İnvestigation and restoration of soil polluting Soils of the Absheron Peninsula by the agromeliorative method Department of Biological Sciences of ANAS. "News". Baku: Nauka Publ., volume 67 (1), p. 128-132.
10. Mirzayev A.B., Mirzayev F.B. (2012) ecological problems of oil fields in Absheron Peninsula and Azerbaijan sector of Caspian Sea and ways of their elimination.Baku: Science, etc. 367.
11. Mozhaisky Yu.A., Tobratov S.A., Dibenok N.N., Popeochin Yu.P. Agroecology of technogenically polluted landscapes. / Magenta Publishing House, Smolensk, 2003, p. 382.
12. Oborin A.A., Ilarionov S.A., Nazarov A.V., Khmurchik V.T., Markarova M.Yu. Oil-contaminated biogeocenoses // Izvestiya RAS. Ural Branch, Perm, 2008, p. 501.
13. Orlov D.S.; Sukhanova, N.I.; Rozanova, M.S. (2001) Spectral Reflectivity of Soils and Their Components; MSU: Moscow, Russia, s.201.
14. Orlov D.S., Sadovnikova L.K.,Sukhanova N.I. Chemistry of soils, (2005) M. Higher School, p. 458.

UDC 66.074.3:665.6
DOI: *https://doi.org/10.30546/2521-6317.2025.02.511*

INVESTIGATION OF THERMAL AND CATALYTIC PURIFICATION OF OIL REFINING GASES

Sadagat MUSTAFAYEVA[1], Alakbar HASANOV[2]

[1]Master's Student, Azerbaijan State University of Oil and Industry (ASOIU), Azerbaijan.

sadagatmustafayeva03@gmail.com

[2]Doctor of Chemical Sciences, Professor, Azerbaijan State University of Oil and Industry (ASOIU), Department of Petrochemical Technology and Industrial Ecology, Azerbaijan.

alakbar48-48@mail.ru

Azadliq Avenue, 20, AZ1010, Baku, Azerbaijan

ARTICLE INFO

Article history:
Received:2025-04-30
Received in revised form:2025-05-21
Accepted:2025-06-14
Available online:2025-12-25

Keywords*: gases; thermal; catalytic purification; Claus process; sulfur compounds*

ABSTRACT

Oil refining and petrochemical industries are considered to be one of the most strategic sectors of the modern economy, but also one of the main sources of environmental pollution. During the processing of raw materials and the production of various products in these enterprises, large volumes of harmful gases are released into the atmosphere. Problems related to the utilization and purification of oil refining gases are very relevant in modern times. In this regard, thermal and catalytic methods are the most widely used and promising technologies for the decomposition and neutralization of harmful gases emitted into the atmosphere.

The article examines the methods of thermal and catalytic purification of gases resulting from technological processes in the oil refining and petrochemical industries. The ecological impacts of sulfur compounds, carbon oxides and nitrogen oxides contained in these gases are analyzed, and the main thermal and catalytic technologies used to minimize them are comparatively evaluated. The advantages and disadvantages of integrated purification schemes used in modern industrial practice are discussed. Based on the analysis, it was concluded that catalytic methods are relatively energy-efficient, while thermal methods are also a suitable technological solution for the purification of high-concentration gas streams.

1. INTRODUCTION

The oil refining and petrochemical industry is economically very important, but it is considered one of the industries that creates major problems from an ecological point of view. Gases of various compositions are formed in the primary and secondary oil refining processes, and their release into the atmosphere without purification leads to the emergence of ecological problems and imbalances [1]. The main polluting components of these gases are hydrogen sulfide, sulfur dioxide, carbon monoxide, carbon dioxide and nitrogen oxides. These substances accumulate in the atmosphere and thus lead to the formation of dangerous conditions for human health, the formation of acid rain, and climate change [2]. It is for this reason that the main priority in the entire world industry is currently the purification of gases to be released into the atmosphere and the creation of environmentally friendly processes.

The main purpose of the article is to analyze these methods in terms of scientific basis, application possibilities and efficiency. The object of the article is the process of refining sulfuric acid gases generated in the oil industry using a thermal gas burner, a Claus sulfur recovery unit, and a waste gas cleaning unit. The scheme of the experimental setup is given in Fig.1.

2. EXPERIMENTAL PART

Gas in oil refining processes are mainly generated in atmospheric-vacuum, catalytic cracking, hydrocracking and hydrotreating units. Their composition varies depending on the sulfur content of the feedstock and the process conditions [4]. H_2S, which is formed in the processes, is the main hazardous substance. Sulfur oxides formed from its oxidation react with water vapor in the atmosphere and cause the formation of acid rain [5].

As a result of the Claus process, H_2S is utilized in the form of harmless elemental sulfur [6].

The experimental part was carried out on the basis of modeling the operating mode of industrial facilities and technological analysis based on literature data. For calculations, a stationary operating mode and a constant raw material composition accepted in industrial practice were assumed. The main devices of the technological scheme adopted for the study are:

1. Thermal gas incinerator-partial oxidation of H_2S

2. Claus catalytic reactors-catalytic recovery of sulfur

3. Condensers-separation of the resulting sulfur in liquid form

4. Waste gas cleaning unit-capture of SO_2, COS, CS_2 and H_2S by reduction and absorption

The parameters affecting the course of the process are temperature and pressure, H_2S/O_2 stoichiometric ratio, type of catalyst, its activity, and the effectiveness of the reduction medium at the waste gas cleaning stage. If the necessary ratio between the parameters is maintained, along with high sulfur yield, less damage to the environment will be caused.

In the thermal stage, the temperature is assumed to be in the range of 1000-1300 °C. As a result of burning gases at 900–1200 °C, the effect of harmful components is reduced [7]. As in all chemical processes, the application of a catalyst in this process also creates conditions for reducing the operating temperature. In the catalytic stage, the temperature is assumed to be in the range of 200-350 °C. The operating pressure of the process is 0,1-0,25 MPa. The amount of H_2S in $1m^3$ sour gas is 60-75%. The stoichiometric ratio of oxygen is assumed to be 1:3 mol O_2:H_2S.

Thermal treatment methods are based on the oxidation of gases at high temperatures. These processes are usually carried out with thermal oxidizers or thermal reactors. The main advantage of these methods is that they do not require a catalyst and are suitable for the treatment of high-concentration gas streams, but the lack of energy savings and the formation of nitrogen oxides limit their use [8]. Catalytic purification methods are based on the oxidation of gases at low temperatures in the presence of catalysts.

The experimental study was conducted on the basis of modeling the processes of thermal and catalytic purification of petroleum refinery gases. The study was based on typical technological regimes adopted at industrial enterprises. In the model experiment, attention was paid to the processes of first thermal conversion of H_2S and then sulfur recovery at the catalytic stage [3].

Thermal stage:

$$H_2S + 3/2O_2 \rightarrow SO_2 + H_2O$$
$$CO + 1/2O_2 \rightarrow CO_2 \quad (1)$$

Catalytic stage:

$$2H_2S + SO_2 \xrightarrow{kat} 3S + 2H_2O \quad (2)$$

$$CO_2 + H_2S \rightarrow COS + H_2O \quad (3)$$

Side reactions:

After the sulfur removal process, small amounts of H_2S and SO_2 remain in the residual gases. These gases are fed to the catalytic residual gas treatment process for further purification. The main reaction at this stage is:

After that, the H_2S is sent back to the Claus unit [9]. This stage allows to increase the total sulfur

$$SO_2 + 3H_2 \rightarrow H_2S + 2H_2O \quad (4)$$

recovery efficiency to 99.9%.

Catalytic treatment is usually carried out in the temperature range of 200-350 °C, which creates the basis for reducing energy consumption [10]. Platinum, palladium and vanadium-based catalysts provide very good oxidation of sour gases [6]. Although the advantages of catalytic methods are their high selectivity, energy saving and impact on improving environmental performance, the loss of catalyst activity and the possibility of poisoning should be taken into account when applying these methods [9]. Literature studies prove that thermal methods are more suitable for gases with high concentrations and variable composition. Catalytic methods are distinguished by their high conversion rate and energy efficiency at low temperatures [11]. The advantages of both methods lead to their application in a combined version, and their integrated use in the modern oil refining industry gives optimal results from an ecological and economic point of view [12].

According to the results of the modeling, the oxidation rate of H_2S in the thermal reactor at a temperature range of 1100–1300 °C is 65–70%. At this stage, part of the hydrogen sulfide reacts with oxygen and turns into sulfur dioxide, while the rest forms the stoichiometric ratio required for the Claus reaction. Although the high temperature ensures the effective decomposition of H_2S, at the same time, the formation of by-products such as COS and CS_2 has been observed. Experiments show that increasing the temperature above 1300 °C in the thermal stage increases the intensity of side reactions, which creates the need for additional purification in subsequent stages. Therefore, the selection of the optimal temperature regime directly affects the efficiency of the process. In the catalytic stage, a decrease in temperature below normal weakens the kinetics of the Claus reaction, while high temperatures lead to sulfur re-evaporation and catalyst deactivation. This is considered undesirable in terms of process sustainability.

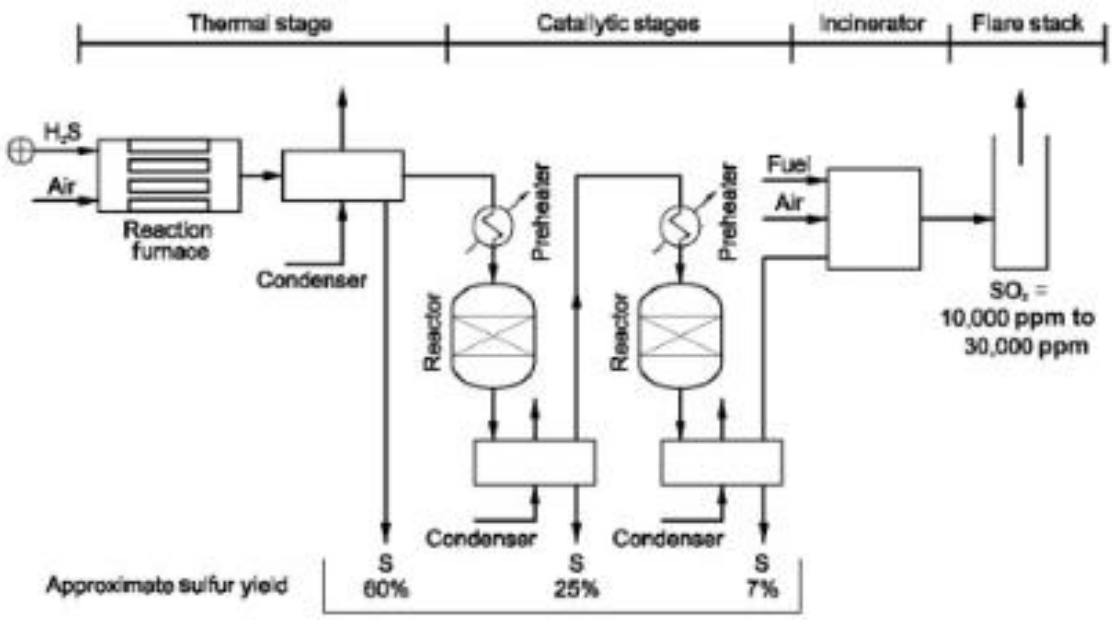

Fig. 1 Technological scheme of the plant

The modeling results of the residual gas purification unit showed that the SO_2, COS and CS_2 compounds present in the gases leaving the Claus unit are reduced with hydrogen and converted back to the H_2S form. At this stage, the converted H2S is directed to the absorption system and returned to the process.

According to the modeling results of the catalytic stage, the intensity of the Claus reaction has significantly increased with the participation of aluminum-oxide and titanium-oxide-based catalysts. As a result of the process carried out in the temperature range of 220–340 °C, an additional 25–30% sulfur recovery was ensured.

In general, as a result of the joint action of the thermal and catalytic stages, the elemental sulfur recovery efficiency varied in the range of 92–96%. This indicator corresponds to the normative limits adopted for modern industrial Claus units. As a result of the application of the residual gas purification stage, the total sulfur recovery efficiency was increased to 99,8–99,9%. The amount of sulfur compounds in the gases released into the atmosphere was below 10 ppm, which fully complies with environmental standards. Without a residual gas cleaning stage, it is impossible for the Claus unit to meet modern environmental requirements. As a result of the research conducted in the article, it was determined that the treatment of petroleum refinery gases by thermal and catalytic methods plays an important role in protecting the atmosphere.

Thermal treatment provides a reliable technological solution for highly concentrated gas streams, while catalytic methods are considered more energy-efficient and environmentally superior. The application of thermal-catalytic integrated systems allows minimizing harmful emissions in the petroleum refining industry and ensuring compliance with international environmental standards. The application of integrated thermal-catalytic treatment technologies allows reducing atmospheric emissions in the petroleum refining and petrochemical industries and ensuring compliance with international environmental standards.

3. Conclusion

- The processes of thermal and catalytic purification of petroleum refinery gases were investigated based on a model experimental approach.
- The calculations and modeling results showed that in the thermal gas combustion stage, the degree of oxidation of hydrogen sulfide in the temperature range of 1150–1300 °C varies between 66,4–70,2%, and this stage ensures the formation of the stoichiometric ratio necessary for the Claus reaction.
- As a result of the application of aluminum oxide and titanium oxide-based catalysts in the catalytic stage, additional sulfur recovery was 28,6-30,4%. As a result of the combined action of the thermal and catalytic stages, the total recovery efficiency of elemental sulfur was determined at the level of 94,7%.
- As a result of the application of the residual gas purification unit, the conversion rates of SO_2, COS and CS_2 compounds were 99,1%, 98,6% and 97,9%, respectively. After this stage, the concentration of sulfur-containing compounds in the gases released into the atmosphere was reduced to 8–9 ppm.
- Overall, the total sulfur recovery efficiency was increased to 99,85% due to the integration of the residual gas cleaning stage. The results obtained show that without this stage, the emission level is 180-220 ppm and does not meet modern environmental standards.

REFERENCE LIST

1. Gary, J. H., & Handwerk, G. E. (2018). *Petroleum refining: Technology and economics*. CRC Press, 5.
2. Speight, J. G. (2014). *The chemistry and technology of petroleum.* CRC Press, 5.
3. Abbasov, A. M. (2019). *Neft emalı proseslərinin ekoloji aspektləri.* Azərbaycan Neft Jurnalı, 3, 45-52.
4. Sadeghbeigi, R. (2012). *Fluid catalytic cracking handbook.* Gulf Publishing, 3.
5. Cooper, C. D., & Alley, F. C. (2011). *Air pollution control.* Waveland Press, 4.
6. Martin, A. (2016). *Industrial catalysis.* Wiley.
7. Fogler, H. S. (2016). *Elements of chemical reaction engineering.* Pearson, 5.
8. Rahman, M. (2018). *Thermal oxidation systems.* Energy & Fuels, 32(7), 7421-7429.
9. Jones, D. S. (2017). *Catalyst deactivation mechanisms.* Catalysis Today, 289, 176-185.
10. Bartholomew, C. H., & Farrauto, R. J. (2006). *Industrial catalytic processes.* 2, Wiley.
11. Towler, G., & Sinnott, R. *Chemical engineering design.* Elsevier, 2, (2013).
12. EPA. (2017). *Air pollution control manual.*
13. Süleymanov, N. İ. (2015). *Sənaye ekologiyası.* Bakı: Maarif.

2025. Volume 9, Number 2 Pages 122-128

UDC: 547.057+547.51+547.7/.8
DOI: https://doi.org/10.30546/2521-6317.2025.02.519

REACTIONS OF CYCLOHEXYL-SUBSTITUTED UNSATURATED MONO- AND SATURATED DICHLOROKETONES WITH ETHYLENEDIAMINE

N.Y. AHMADOVA, E.I. MAMMADOV

Azerbaijan State Pedagogical University,

AZ1000, Baku, Uzeyir Hajibayli Street. 68

mammadov.elman@rambler.ru; hasanovanur@gmail.com

ARTICLE INFO

Article history:
Received:2025-06-09
Received in revised form:2025-06-15
Accepted: 2025-07-15
Available online:2025-12-25

Keywords:
saturated dichloroketones; unsaturated chloroketones; ethylenediamine; monopyrroles; dipyrroles

ABSTRACT

Electrophilic addition of cyclohexane- and chloro-substituted cyclohexanecarboxylic acid chlorides to 3-chloro-1-propene and 2-methyl-3-chloro-1-propenes in the presence of an $AlCl_3$ catalyst at –15 ÷ –20°C yielded 1-cyclohexyl(chlorocyclohexyl)-3-H(CH_3)-3,4-dichloro-1-butanones. These were then dehydrochlorinated in a superbasic medium (DMFA + Na_2CO_3) to form 1-cyclohexyl (chlorocyclohexyl)-3-H(CH_3)-4-chloro-2-buten-1-ones. Mono- and dipyrrole compounds were synthesized by reacting cycloalkyl-substituted saturated dichloroketones and unsaturated chloroketones with ethylenediamine in an aqueous alkaline medium, depending on the ratio of the starting materials. The structures of the resulting mono- and dipyrroles were confirmed by IR and ^1H NMR spectroscopy.

INTRODUCTION

A pyrrole fragment is found in the composition of many natural and synthetic biologically active compounds, catalysts, drugs, etc. compounds [1–9]. Examples of these include vitamin B_{12}, bile pigments bilirubin and biliverdin, blood pigments heme, chlorophyll, etc. [3, 4]. Alkoxy derivatives of pyrroles have a wide range of applications as optically active compounds [10, 11]. Polymers such as polypyrrole exhibit unique electrophysical and optical properties [1, 12]. Polypyrroles are also widely used in the preparation of conventional and solar cells [13].

The wide range of applications of pyrroles has given a strong impetus to research on their synthesis by new methods.

Saturated and unsaturated chloroketones belong to a class of promising starting compounds for the synthesis of heterocyclic compounds with one or two heteroatoms [14-24]. Electrophilic addition reactions of carboxylic acid chloranhydrides to unsaturated hydrocarbons, their chlorine-substituted derivatives, and allyl chlorides are among the most favorable reactions for the synthesis of saturated and unsaturated chloroketones [15, 17–19, 21, 23–27].

It is known that pyrrole compounds are formed when the products of electrophilic addition of alkanecarboxylic acid chlorhydrides to allyl halides are reacted with monoamines [28–30]. The advantage of this new synthesis method, called the Kost-Ibrahimov-Mammadov method [31], is that, depending on the structure of the starting mono-amines, various functional groups can be introduced into the pyrrole ring, as well as one or more pyrrole rings can be formed in the molecule according to the basicity of the carbon atom taken [27–30, 32, 33].

The aim of the presented work is to synthesize compounds containing one or two pyrrole rings by reacting the products of electrophilic addition of monobasic cycloalkanocarboxylic acid chloranhydrides (CACAChA) to 3-chloropropene and 2-methyl-3-chloropropene with ethylenediamine (EDA).

EXPERIMENTAL

IR spectra were recorded on a Thermo Scientific Nicolet IS10FT-IR spectrophotometer, and NMR ^{1}H spectra were recorded on a Bruker AM-360 Spectrometer (internal standard TMS or HMDC).

Commercially available reagents such as 3-chloro-1-propene, 2-methyl-3-chloro-1-propene, and EDA were used as starting materials, and CACAChA were obtained by the reaction of the corresponding acids with PCl_3 or $SOCl_2$.

1. Synthesis of 1,2-di[2-cycloalkyl-4-H(CH_3)pyrrolyl-1]ethanes (5a-c, 6a-c). To a solution of 0.05 mol (3g) EDA and 0.2 mol (8g) NaOH in water, 0.1 mol of dichloroketones 1a-c (2a-c) is added at –5°C. The reaction mixture is heated at +60 ÷ +70°C for 4 hours, cooled and extracted with ether (3x100ml). The ether extract is washed with water, 10% Na_2CO_3 and again with water and dried over anhydrous Na_2SO_4. The solvent is removed with a water pump, and the residue is distilled under vacuum in a nitrogen atmosphere to obtain dipyrroles 5a-c (6a-c) (scheme 2). The obtained dipyrroles crystallize upon storage and are recrystallized from methanol or ethanol.

1.1. 1,2-Di(2-cyclohexylpyrrolyl-1]ethane (5a). T_m (melting temperature): 90–92^{0}C (C_2H_5OH), yield 58%. IR spectrum (cm^{-1}): 3114 (*ν*=CH, pyrrole), 1514, 1601 (*ν*C=C,C=C pyrrole). NMR ^{1}H spectrum (δ, m.h.): 1.0 – 2.1 m (22 H, cyclohexane), 4.07 s (4H, NCH_2-CH_2), 5.81-5.86 m (2H, C^3–H pyrrole), 6.02–6.07 m (2H, C^4–H pyrrole), 6.34–6.37 m (2H, C^5-H pyrrole). Found., %: C 81.56, H 9.80 8.59. $C_{22}H_{32}N_2$. Calc.,%: C 81.48, H 9.88, N 8.64.

1.2. 1,2-Di[2-(1-chlorocyclohexyl)pyrrolyl-1]ethane (5b). T_m: 101–103^{0}C (C_2H_5OH), yield 52%. IR spectrum (cm^{-1}): 3030 (*ν*=CH, pyrrole), 1504, 1605 (*ν*C=C,C=C pyrrole). Found., %: C 67.09, H 7.58, Cl 18.19, N 7.06. $C_{22}H_{30}Cl_2N_2$. Calc., %: C 67.18, H 7.63, Cl 18.07, N 7.12.

1.3. 1,2-Di[2-(4-chlorocyclohexyl) pyrrolyl-1]ethane (5c). T_m: 108–109^{0}C (C_2H_5OH), yield 54%. IR spectrum (cm^{-1}): 3025 (*ν*=CH, pyrrole), 1500, 1575 (*ν*C=C,C=C pyrrole). Found., %: C 67.26, H 7.68, Cl 17.98, N 7.08. $C_{22}H_{30}Cl_2N_2$. Calc., %: C 67.18, H 7.63, Cl 18.07, N 7.12.

1.4. 1,2-Di(2-cyclohexyl-4-methylpyrrolyl-1)ethane (6a). T_m: 152–154^{0}C (C_2H_5OH), yield 61%. IR spectrum (cm^{-1}): 3092 (*ν*=CH, pyrrole), 1505, 1585 (*ν*C=C,C=C pyrrole). NMR ^{1}H spectrum (δ, m.h.): 0.8–2.0 m (22 H, cyclohexane), 1.86 s (6H, $2CH_3$), 4.0 s (4H, NCH_2-CH_2), 5.76–5.81 m (2H, C^3-H pyrrole), 6.41–6.52 m (2H, C^5–H pyrrole). Found., %: C 81.71, H 10.16, N 8.08. $C_{24}H_{36}N_2$. Calc., %: C 81.82, H 10.23, N 7.95.

1.5. 1,2-Di[2-(1-chlorocyclohexyl)-4-methylpyrrolyl-1]ethane (6b). T_m: 142–144^{0}C (CH_3OH), yield 54%. IR spectrum (cm-1): 3120 (*ν*=CH, pyrrole), 1516, 1600 (*ν*C=C,C=C pyrrole). Found, %:

C 68.32, H 8.17, Cl 16.98. N 6.53. $C_{24}H_{34}Cl_2N_2$. Calc., %: C 68.41, H 8.08, Cl 16.86, N 6.65.

1.6. 1,2-Di[2-(4-chlorocyclohexyl)-4-methylpyrrolyl-1]ethane (6c). T_m: 146–148^{0}C (CH_3OH), yield 56%. IR spectrum (cm-1): 3020 (ν=CH, pyrrole), 1510, 1596 (νC=C,C=C pyrrole). Found, %: C 68.32, H 8.17, Cl 16.98. N 6.53. $C_{24}H_{34}Cl_2N_2$. Calc., %: C 68.41, H 8.08, Cl 16.86, N 6.65.

2. Preparation of 1-(2-aminoethyl)-2-cycloalkyl-4-H(CH_3)pyrroles (7a-c, 8a-c). Monopyrroles 7a-c (8a-c) were obtained by the reaction of 0.05 mol (3g) EDA and 0.1 mol (4g) NaOH in water with 0.1 mol of saturated dichloroketones 1a-c (2a-c) using method 1 above (scheme 2).

2.1. 1-(2-aminoethyl)-2-cyclohexylpyrrole (7a). T_b (boiling temperature): 125–126^{0}C (5), n_D^{20} 1.5295, d_4^{20} 1.0181, yield 58%. IR spectrum (cm^{-1}): 3310, 3446 (νNH_2), 3112 (ν=CH, pyrrole), 1514, 1592 (νC=C,C=C pyrrole). NMR ^{1}H spectrum (δ, m.h.): 1.0-2.2 m (11H, cyclohexane), 1.75 s (2H, NH_2), 2.55 t (2H, CH_2N, J=7), 3.42 t (2H, NCH_2 J=7), 5.51–5.59 m (1H, C^3-H pyrrole), 5.7-5.9 m (1H, C^4–H pyrrole), 6.22–6.31 m (1H, C^5–H pyrrole). Found., %: C 75.08, H 10.37, N 14.52. $C_{12}H_{20}N_2$. Calc., %: C 75.00, H 10.42, N 14.58.

2.2. 1-(2-aminoethyl)-2-(1-chlorocyclohexyl)pyrrole (7b). T_b: 148–150^{0}C (3), n_D^{20} 1.5430, d_4^{20} 1.1162, yield 49%. IR spectrum (cm^{-1}): 3350, 3450 (νNH_2), 3140 (ν=CH, pyrrole), 1510, 1605 (νC=C,C=C pyrrole). Found, %: C 63.42, H 8.27, Cl 15.81. N 12.24. $C_{12}H_{19}ClN_2$. Calc., %: C 63.58, H 8.39, Cl 15.67. N 12.36.

2.3. 1-(2-aminoethyl)-2-(4-chlorocyclohexyl)pyrrole (7c). T_b: 146–147^{0}C (4), n_D^{20} 1.5425, d_4^{20} 1.1158, yield 51%. IR spectrum (cm^{-1}): 3330, 3442 (νNH_2), 3114 (ν=CH, pyrrole), 1505, 1597 (νC=C,C=C pyrrole). Found., %: C 63.71, H 8.46, Cl 15.43. N 12.41. $C_{12}H_{19}ClN_2$. Calc., %: C 63.58, H 8.39, Cl 15.67. N 12.36.

2.4. 1-(2-aminoethyl)-2-cyclohexyl-4-methylpyrrole (8a). T_m: 141–143^{0}C (3), n_D^{20} 1.5260, d_4^{20} 0.9936, yield 56%. IR spectrum (cm^{-1}): 3305, 3440 (νNH2), 3045 (ν=CH, pyrrole), 1500, 1568 (νC=C,C=C pyrrole). NMR ^{1}H spectrum (δ, m.h.): 1.1-2.3 m (11H, cyclohexane), 1.74 s (2H, NH_2), 1.94 s (3H, CH_3), 2.54 t (2H, CH_2N, J=7), 3.44 t (2H, NCH_2, J=7), 5.60–5.65 m (1H, C^3-H pyrrole), 6.34–6.41 m (1H, C^5-H). Found., %: C 75.82, H 10.59, N 13.47. $C_{13}H_{22}N_2$. Calc., %: C 75.73, H 10.68, N 13.59.

2.5. 1-(2-aminoethyl)-2-(1-chlorocyclohexyl)-4-methylpyrrole (8b). T_b: 154–156^{0}C (2), n_D^{20} 1.5422, d_4^{20} 1.1141. IR spectrum (cm^{-1}): 3340, 3448 (νNH_2), 3120 (ν=CH, pyrrole), 1520, 1601 (νC=C,C=C pyrrole). Found., %: C 64.73, H 8.62, Cl 14.91, N 11.54. $C_{12}H_{19}ClN_2$. Calc., %: C 64.87, H 8.73, Cl 14.76, N 11.64.

2.6. 1-(2-aminoethyl)-2-(4-chlorocyclohexyl)-4-methylpyrrole (8c). T_b: 158–160^{0}C (4), n_D^{20} 1.5410, d_4^{20} 1.1126. IR spectrum (cm^{-1}): 3326, 3440 (νNH_2), 3095 (ν=CH, pyrrole), 1505, 1594 (νC=C,C=C pyrrole). Found., %: C 64.98, H 8.86, Cl 14.58, N 11.51. $C_{12}H_{19}ClN_2$. Calc., %: C 64.87, H 8.73, Cl 14.76, N 11.64.

RESULTS AND DISCUSSION

Compounds containing one or two heteroatom-containing five-membered heterocyclic rings are widely found in nature [34, 35], therefore, the synthesis of these compounds by new methods and the study of their structures are one of the most important theoretical and applied problems of modern organic chemistry.

For the synthesis of cycloalkyl-substituted mono- and dipyrroles, the reactions of the

electrophilic addition products of CACAChA to 3-chloro-1-propene and 2-methyl-3-chloro-1-propene with EDA were studied.

As a result of electrophilic coupling reactions, the corresponding 1-cycloalkyl-3-H(CH_3)-3,4-dichloro-1-butanones (1a-c, 2a-c) were obtained, and their dehydrochlorination in a super alkaline medium (DMFA+Na_2CO_3) at a temperature of +80 ÷ +85% gave 1-cycloalkyl-3-H(CH_3)-4-chloro-2-buten-1-ones (3a-c, 4a-c) (scheme 1) [15, 17, 23, 27].

Scheme 1.

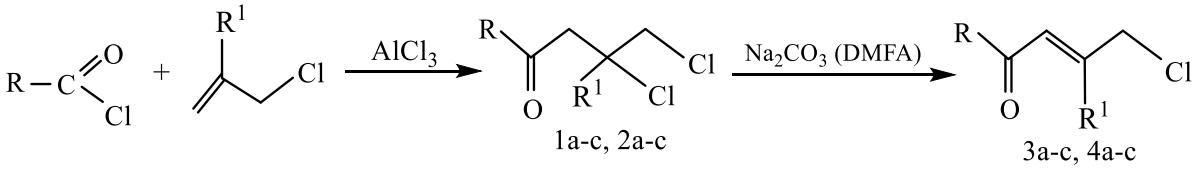

Here, R = *ts*-C_6H_{11} (a), 1-Cl-*ts*-C_6H_{10} (b), 4-Cl-*ts*-C_6H_{10} (c); R^1 = H (1a-c, 3a-c), CH_3 (2a-c, 4a-c).

During the reaction of cycloalkyl-substituted saturated dichloroketones (1a-c, 2a-c) and unsaturated chloroketones (3a-c, 4a-c) with EDA in an aqueous-alkaline medium, it was determined that, for example, dichloroketones 1a-c, 2a-c, in an aqueous solution of starting materials in a 2:1 ratio (1a-c or 2a-c : EDA - 2:1) and 4 equivalents of NaOH, mainly 1,2-di[2-cycloalkyl-4-H(CH_3)pyrrolyl-1]ethane dipyrroles (5a-c, 6a-c) are obtained, and in an aqueous solution of 1:1 ratio (1a-c or 2a-c : EDA - 1:1) and 2 equivalents of NaOH, 1-(2-aminoethyl)-2-cycloalkyl-4-H(CH_3)pyrroles (7a-c, 8a-c) are obtained (scheme 2).

Scheme 2.

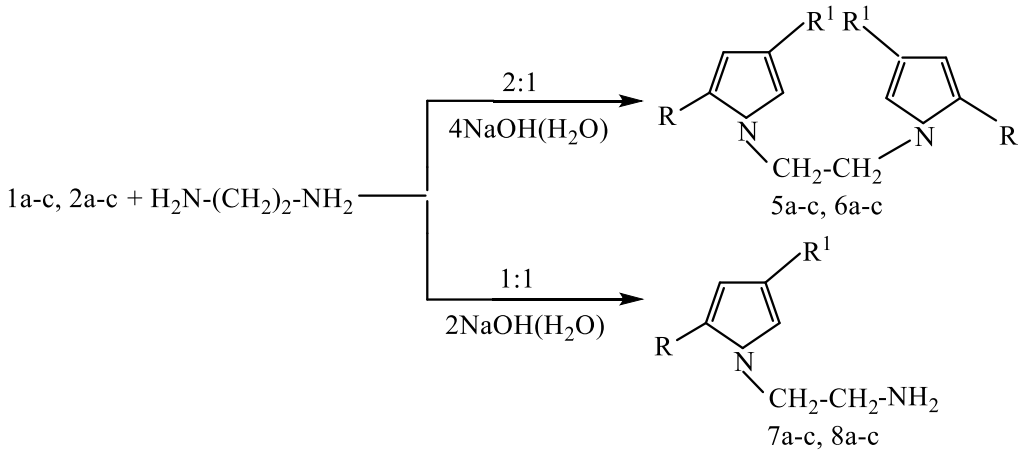

Here, R - as shown in scheme 1; R^1 = H (5a-c,7a-c), CH_3 (6a-c, 8a-c).

Unsaturated chloroketones 3a-c, 4a-c also react with EDA in aqueous medium in a 2:1 ratio of starting materials (3a-c or 4a-c : EDA - 2:1) and in the presence of 2 equivalents of NaOH, dipyrrole compounds 5a-c, 6a-c are formed, and monopyrroles 7a-c, 8a-c are formed in equimolar amounts of all reagents.

The structure of the synthesized dipyrroles and monopyrroles was confirmed by IR and NMR ^1H spectra.

In the IR spectra of pyrroles 5a-c – 8a-c, characteristic absorption bands for the pyrrole ring were determined (cm^{-1}): 3030–3140(ν=CH), 1500–1520 (νC=C), 1550–1605 (νC=C). In addition, in

monopyrroles 7a-c, 8a-c, the absorption band of the valence vibration of the amine group appears in the regions 3305–3350 and 3440–3450 cm^{-1}.

In the NMR ^1H spectra of dipyrroles (5a-c, 6a-c) and monopyrroles (7a-c, 8a-c), the protons of the pyrrole ring appear in the form of a characteristic multiplet (m) in the regions 5.50–6.52 m.h. Also, in dipyrroles 5a-c, 6a-c the protons of the substituted ethane fragment are observed as singlets (s) in the 4.0-4.07 m.h. regions, and in monopyrroles 7a-c, 8a-c these protons are observed as two triplets (t) in the 2.54–2.55 and 3.42–3.44 m.h. absorption regions.

It should be noted that the dichloroketones 1a-c, 2a-c used in the synthesis of pyrroles do not require special separation from the reaction products and additional purification, they were used as crude products. Since they are easily heterocyclized to furan compounds during distillation under vacuum [15, 36].

CONCLUSION

Cycloalkyl-substituted saturated dichloroketones 1a-c, 2a-c were obtained from electrophilic coupling reactions of CACAChA to 3-chloro-1-propene and 2-methyl-3-chloro-1-propene in the presence of $AlCl_3$ catalyst at a temperature of -15 ÷ -20°C in dichloroethane medium, and unsaturated chloroketones 3a-c, 4a-c were synthesized from their dehydrochlorination in a super-alkaline medium (DMFA+Na_2CO_3) (scheme 1). During the reaction of saturated dichloroketones 1a-c, 2a-c and unsaturated chloroketones 3a-c, 4a-c with EDA in an aqueous-alkaline (H_2O+NaOH) medium, depending on the ratio of the starting materials, 5a-c, 6a-c dipyrroles and 7a-c, 8a-c monopyrroles (scheme 2) were obtained.

The obtained experimental results contributed to the introduction of new information into the theoretical issues of organic chemistry. It was established that in the DMFA+Na_2CO_3 super alkaline medium (scheme 1), under the influence of DEA and an aqueous solution of alkali (H_2O+NaOH) (scheme 2), the chlorine atoms in the cyclohexyl ring do not undergo any chemical transformations, that is, they do not enter into nucleophilic (S_N) or dehydrochlorination reactions.

Thus, a simple and convenient method for the preparation of monopyrrole and dipyrrole compounds from the interaction of the electrophilic addition products of CACAChA to 3-chloro-1-propene and 2-methyl-3-chloro-1-propene with EDA has been proposed.

Conflicts of Interest

The authors declare no conflict of interest.

REFERENCES

1. Trofimov B.A., Mikhaleva A.L., Schmidt E.Yu. [et al.]. *Pyrrole Chemistry. New Pages*. Novosibirsk: Nauka, 2012, 383 p.
2. Mashkovsky M.D. *Medicinal Products*. Moscow: Novaya Volna, 2021, 1216 p.
3. Borah B., Dwivedi K.D., Chowhan LR. *Recent approaches in the organocatalytic synthesis of pyrroles.* RSC Advances, Vol. 11, Iss. 22, pp. 13585–13601, 2021
4. Yuselius J., Sundholm D. *The aromatic pathways of porphyrins, chlorins and bacteriochlorins.* Physical Chemistry Chemical Physics, Vol. 2, Iss. 10, pp. 2145–2151, 2000
5. Bhandari N., Gaonkar S.L. *A facile synthesis of N-substituted 2,5-dimethylpyrroles with saccharin as a green catalyst.* Chemistry of Heterocyclic Compounds, Vol. 51, No. 4, pp. 320–323, 2015
6. Bhardway V., Gumber D., Abbot V. [et al.]. *Pyrrole: a resorceful small molecule in key medicinal heteroaromatics.* RSC Advances, Vol. 5, Iss. 20, p. 15233–15266, 2015

7. Bulumulla C., Gunawardhana R., Gamade P.L. [et. al.]. *Pyrrole-containing semiconducting materials: synthesis and applications in organic photovoltaics and organic field-effect transistors.* ACS Applied Materials and Interfaces, Vol. 12 (29), pp. 32209–32232, 2020
8. Maharramov A., Kurbanova M., Taslimi [et al.]. *Synthesis, characterization, crystal structure and bioactivities of novel enamine and pyrrole derivatives endowed with acetylcholinesterase, α-glycosidase and human carbonic anhydrase inhibition effects*. Organic Communications, Vol.14 (2), pp. 144–156, 2021
9. Xu J., Green A.P., Turner N.Y. *Chemo-enzymatic synthesis of pyrazines and pyrroles.* Angewandte Chemie International Edition, Vol. 130, Iss. 51, pp. 16760–16763, 2018
10. Islam M.S., Barakat A., Al-Majid A.M. [et al.]. *Catalytic asymmetric synthesis of indole derivatives as novel α-glucosidase inhibitors in vitro.* Bioorganic Chemistry, Vol . 79, pp. 350–354, 2018
11. Akhmedov I.M., Guseinov E.Z., Safarova A.S. [et al.]. *Catalytic effect of molecular iodine in the pyrrolization of tetramethoxytetrahydrofuran with optically active amines*. Russian Journal Organic Chemistry, Vol. 52, Iss. 12, pp. 1849–1850, 2016
12. Safarova A.Sh. *Synthesis and some transformations of di-, tri- and tetrasubstituted pyrroles.* Abstract of the PhD thesis in organic chemistry. Baku, 2025
13. Michlik S., Kempe R.A. *A sustainable catalytic pyrrole synthesis.* Nature Chemistry, V. 5 (2), pp. 140–144, 2013
14. Petkevich S.K., Potkin V.I., Kaberdin R.V. *Synthesis of 3-aryl-5-dichloroethyl-N-carbonylpyrazoles based on 1-aryl-3,4,4-trichloro-3-buten-1-ones.* Russian Journal Organic Chemistry, Vol. 42, Iss. 10, pp. 1496–1499, 2006
15. Guseinova V.A., Zaidova G.A., Mammadov E.I. *Reaction of chloranhydrides of cycloalkanecarboxylic acids with some allylic chlorides.* Chemical Problems, No. 3 (19), pp. 179–185, 2021
16. Bozhenkov G.V., Savosik V.A., Klyba L.V. [et al.]. *1-Alkylpyrazoles and 1-alkyl-5-chloropyrazoles from halovinyl ketones and 1,1-dialkylhydrazones.* Russian Journal of Organic Chemistry, Vol. 44, Iss. 8, pp. 1207-1212, 2008
17. Ahmadova N.Y. *Synthesis of 1-Allyl-2-cycloalkyl-4-H(CH3)pyrroles from saturated dichloroketones and unsaturated chloroketones.* News of Pedagogical University. Mathematics and natural sciences series. Baku: ASPU, Vol. 72, No. 3, pp. 95-101, 2024
18. Ibragimov I.I., Mamedov E.I., Ismailov A.T. [et al.]. *Chemistry of allyl-type systems. II. Acylation of 3-bromo- and 2-methyl-1-propenes.* Russian Journal of Organic Chemistry, Vol. 26, Iss. 8, pp. 1648–1654, 1990
19. Ahmadova N., Mammadov E. *Synthesis of ethane compounds containing a pyrrole ring.* Abstracts of reports of the IV Republican scientific conference of doctoral students, master's students and young researchers on the topic "Chemistry and chemical technology" dedicated to the 102nd anniversary of the birth of the national leader Heydar Aliyev, Baku: BSU, 17-18 April, 2025, pp. 72-73
20. Levkovskaya G.G., Bozhenkov G.V., Larina L.I. [et al.]. *A new route for the preparation and properties of 3-alkyl-, chloroalkyl-, perfluoroalkyl-, aryl-1-methyl-5-H(Br)(Cl)pyrazoles from chloro(bromo)vinyl ketones and N,N-dimethylhydrazine.* Russian Journal of Organic Chemistry, Vol. 38, Iss. 10, pp. 1554–1559, 2002
21. Mammadov E., Mammadov A., Huseynova V. [et al.]. *Temperature Dependence of the Reaction of Electrophilic Addition of Acyl Chlorides to Allyl Chloride.* 6th International Conference: Thermophysical and Mechanical Properties of Advanced Materials (Thermam 2019), Izmir, Turkey, September 22-24, 2019, pp. 54-55
22. Bozhenkov G.V., Levkovskaya G.G., Larina L.I. [et al.]. *Synthesis, structure and properties of 1,2-dichlorovinylalkyl ketones.* Russian Journal of Organic Chemistry, Vol. 40, Iss. 11, pp. 1632–1640, 2004
23. Ahmadova N.Y., Mammadov E.I. *A new approach to the synthesis of cycloalkyl-substituted pyrroles.* Proceedings of the International Scientific Conference on "Monomers and Modern Problems of Petroleum Chemistry" dedicated to the 100th anniversary of Academician S.Mehdiyev, Baku, December 19-20, 2024, pp. 86-87
24. Mammadov E.I., Huseynova V.A., Mekhtieva S.T. [et al.]. *New synthesis of 3- and 1,3-pyrazole derivatives based on 1-cycloalkyl-2,3-dichloro-1-propanones.* Azerbaijan Chemical Journal, No. 4, pp. 89-94, 2022
25. Guseinova V.A. *Reaction of 1-R-2,3-dichlorobutan-1-ones with hydrazine and phenylhydrazine.* Scientific Notes of ATU, No. 1, pp. 169-173, 2021
26. Mammadov E., Huseynova V., Yusubov F. [et al.]. *New way for the synthesis of 1,3-pyrazole derivatives by the reaction of 1-alkyl-2,3-dichloropropanones with phenylhydrazine.* Norwegian Jornal of development of the International Science, Oslo, Nor-Norway, No 90, pp. 3–7, 2022
27. Ahmadova N.Y., Mammadov E.I. *New synthesis of 1,2- and 1,2,4-substituted pyrroles.* News of Pedagogical University. Series of Mathematics and Natural Sciences. Baku: ASPU, Vol. 71, No 3, p. 84–93, 2023

28. Ismailov A.G., Mamedov E.I., Goyushov R.D. [et al.]. *Preparation of derivatives of alkanes and cyclohexane with two heterocyclic substituents of the furan, pyrrole, and thiophene series.* Chemistry of Heterocyclic Compounds, No. 9, p. 1185–1189, 1991
29. Gadzhily R.A., Fedoseyev V.M., Nadzhafova R.A. [et al.]. *Synthesis and properties of 1-(2¹-bromoethyl)-, 1-(2¹-alkoxyethyl)- and 1-(2¹-dialkylaminoethyl-2-alkylpyrroles*. Chemistry of Heterocyclic Compounds, No. 8, pp. 1047–1049, 1990
30. Mamedov E.I., Ismailov A.G., Ibragimov V.G. [et al.]. *Synthesis of N-functionally substituted pyrroles from 1-R-3-R¹-3,4-dichlorobutanones.* Chemistry of Heterocyclic Compounds, No. 9, pp. 1181–1184, 1990
31. Sobenina L.N., Mikhaleva A.I., Trofimov B.A. *Synthesis of pyrroles from aliphatic compounds*. Russ. Usp. Chem., Vol. 58, Iss. 2, pp. 275–302, 1989
32. Mamedov E.I., Ismailov A.G., Ibragimov V.G. [et al.]. *Synthesis of 1,2-dipyrrolylethanes.* Chemistry of Heterocyclic Compounds, No. 11, p. 1561, 1983
33. Ahmadova N.Y. *A new synthesis of 1,4-dipyrrolylcyclohexanes*. The founder of the Azerbaijan Democratic Republic M.A. Dedicated to Rasilzade's 140th anniversary, "The flag that rises once will never come down again!" Proceedings of the International Scientific Symposium, Kars, Turkey, January 27, 2024, pp. 666–670
34. Joule J., Mills K. *Chemistry of heterocyclic compounds*. Moscow: Mir, 2009, 728 p.
35. Yurovskaya M.A. *Chemistry of aromatic heterocyclic compounds.* Moscow: Binom, 2015, 208 p.
36. Zaidova G.A., Ahmadova N.Y., Mammadov E.I. *A new method for the synthesis of 1,4-difurylcyclohexane compounds.* Materials of the International Scientific Conference on "Monomers and Modern Problems of Petrochemistry" dedicated to the 100th anniversary of Academician S.Mehdiyev, Baku, December 19-20, 2024, pp. 72-73
37. Ahmadova N.Y., Mammadov E.I. *Features of the synthesis of cycloalkanecarboxylic and 1,4-cyclohexanedicarboxylic acid chloranhydrides.* Materials of the II International Scientific Conference on "Education and Research Activities in the New Era: Realities and Challenges", Vol. III, Mingechevir, December 13-14, 2024, pp. 526–528

UDC: 620.193.2
DOI: https://doi.org/10.30546/2521-6317.2025.01.468

IONIC LIQUIDS AS A CORROSION INHIBITOR

Sevinc S. AYDAMIROVA

seyaqubova@beu.edu.az

Chemical Engineering department of Baku Engineering University

Baku, AZERBAIJAN

ARTICLE INFO

Article history:
Received:2025-06-11
Received in revised form:2025-06-30
Accepted:2025-07-25
Available online:2025-12-25

Keywords:
Ionic liquids, corrosion, corrosion inhibitors

ABSTRACT

Room-temperature ionic liquids (RTILs) are innovative salts characterized by low volatility, high thermal stability, and strong surface activity, making them highly effective corrosion inhibitors. Imidazolium-, ammonium-, and Brönsted acid–based RTILs provide excellent protection for metals like mild and carbon steel through mixed-type inhibition mechanisms and Langmuir-type adsorption. Their efficiency is influenced by factors such as alkyl chain length, type of anion, concentration, and operating temperature. At suitable concentrations, RTILs form dense protective layers that limit the penetration of corrosive species. Recent developments include smart inhibitor systems using chitosan microspheres and polymeric ionic liquids for controlled release and enhanced protection. Compared to conventional inhibitors, RTILs offer superior environmental compatibility, tunability, and thermal resistance. Their anticorrosive behavior is commonly analyzed by electrochemical impedance spectroscopy and potentiodynamic polarization. These liquids are emerging as sustainable and efficient solutions for corrosion mitigation in challenging environments like acidic media and CO_2 capture systems.

1. Introduction to Ionic Liquids and Their Role in Corrosion Inhibition

Room-temperature ionic liquids (RTILs) are salts that remain in the liquid state at ambient temperatures and are composed of organic cations paired with various anions. Owing to their distinctive characteristics and broad applicability, RTILs have garnered considerable interest, especially for their potential to act as corrosion inhibitors (1).

Research has shown that RTILs can effectively tackle corrosion problems in industrial environments, particularly in systems designed for CO_2 capture. Notably, imidazolium-based RTILs with ethyl groups have been examined for their corrosion-inhibiting performance in aqueous monoethanolamine solutions. Among those evaluated, [emim][acetate] emerged as the most effective in reducing corrosion within alkanolamine-based CO_2 capture processes (1). This underscores the value of RTILs as viable corrosion inhibitors in industrial contexts.

Beyond corrosion inhibition, RTILs are also employed in electrodeposition applications. For instance, RTILs derived from aluminium trichloride and benzyltrimethyl ammonium chloride enable the deposition of aluminium and aluminium/platinum alloys. These specific ionic liquids present several benefits, including reduced sensitivity to moisture, simpler purification methods,

and greater cost efficiency when compared to earlier solutions (2). This multifaceted utility of RTILs underlines their importance in materials science and engineering.

RTILs represent a promising class of corrosion inhibitors, especially for use in industrial operations like CO_2 capture. Their distinct characteristics—such as low volatility and high thermal stability—position them as strong contenders to replace traditional corrosion inhibitors. As studies in this area progress, RTILs are expected to assume a more significant role in overcoming corrosion challenges across a wide range of industries.

2. Synthesis and characterization of ionic liquids for corrosion inhibition

- Imidazolium-based ionic liquids

Imidazolium-based ionic liquids (ILs) have been widely researched as corrosion inhibitors for metals like mild steel and carbon steel, especially in acidic environments. These ILs are synthesized by combining imidazolium cations featuring various alkyl chain lengths with different anions (3)(4). Their properties are typically assessed through a combination of physicochemical and spectral analyses, along with computational studies using techniques such as B3LYP to evaluate optimized molecular structures, HOMO-LUMO distributions, and quantum chemical descriptors (4).

The inhibition performance of imidazolium-based ILs is notably affected by parameters such as the length of the alkyl chain, the nature of the anion, and the IL concentration. For example, one study reported the inhibition efficiency in the order: [PDMIM][NTf_2] > [HMIM][NTf_2] > [BMIM][NTf_2] > [PMIM][NTf_2], suggesting that longer chains and additional methyl groups on the imidazolium ring improve performance (3). Another investigation supported this trend, finding that longer alkyl chains enhanced the inhibitory effect of the ILs studied (5).

In summary, the synthesis and evaluation of imidazolium-based ILs for corrosion inhibition require strategic selection of both cation and anion components. These ILs typically demonstrate mixed-type inhibition, with their performance improving as concentration increases (5)(6). Their adsorption behavior on metal surfaces often aligns with the Langmuir adsorption isotherm, and they function primarily by forming protective layers on the substrate (7)(4). Innovative developments such as polymer-based ILs or ILs integrated into advanced delivery systems like chitosan microspheres offer promising pathways for advancing corrosion resistance (8).

- Ammonium-based ionic liquids

Ammonium-based ionic liquids (ILs) have been developed and examined in numerous studies for their effectiveness as corrosion inhibitors. In one such investigation, Cornejo Robles (9) synthesized 15 ILs derived from quaternary ammonium and carboxylate ions and tested them on API X52 steel in 0.5 M HCl. The inhibition efficiency (IE) varied based on the specific chemical structures of the anions and cations, with ILs such as [$THDA^+$][−AA], [$THDA^+$][−AI], and [$THDA^+$][−AD] achieving IE values between 56% and 84% (9).

In a related study, Olivares-Xometl et al. (2017) reported the synthesis of four novel halide-free ammonium-based ILs, which displayed inhibition efficiencies ranging from 51% to 89% when applied to API 5L X60 steel in 1 M sulfuric acid. Both investigations concluded that the ILs functioned as mixed-type inhibitors and adhered to the Langmuir adsorption isotherm model (10)(9).

Further exploration by Gabler et al. (11) focused on two ammonium-based ILs with potential lubricating properties, particularly assessing their corrosion resistance. The study evaluated (2-hydroxyethyl)-trimethyl-ammonium (choline) and butyl-trimethyl-ammonium cations, identifying the choline-based IL as exhibiting more favorable performance. Notably, the incorporation of additional corrosion inhibitors markedly enhanced the protective properties of these ILs (11).

The design and testing of ammonium-based ILs have yielded encouraging outcomes in corrosion prevention. These ILs display substantial inhibition efficiency, conform to recognized adsorption models, and can be further optimized through the addition of specialized corrosion inhibitors. Collectively, the findings affirm the promise of ammonium-based ILs as effective and environmentally responsible solutions for protecting metal surfaces in acidic environments.

- Brönsted acid ionic liquids

Brönsted acid ionic liquids (BAILs) have been developed and investigated for their effectiveness as corrosion inhibitors for carbon steel in acidic conditions. These innovative ILs, which contain multiple Brönsted acid functional groups, were synthesized with high efficiency (≥98%) and evaluated through a combination of electrochemical techniques and surface characterization methods (12). The tailored cation structure—featuring one phenyl ring and two imidazolium units—enables BAILs to act as mixed-type inhibitors by adhering to steel surfaces and mitigating both anodic and cathodic reactions (12).

Notably, BAILs exhibit excellent corrosion inhibition performance in acidic media regardless of their Brönsted acidity. This challenges the conventional expectation that acidity would hinder inhibitor performance, thereby broadening the scope of BAILs in industrial use (12). In parallel, other ILs such as protic ionic liquids (PILs) and imidazolium-based variants have also shown significant corrosion-inhibiting capabilities in environments like neutral chloride and hydrochloric acid solutions (3, 13).

The synthesis and analysis of BAILs have confirmed their effectiveness as corrosion inhibitors for carbon steel. Their distinctive structure and adsorption behavior promote the formation of protective layers on metal surfaces, consistent with the Langmuir adsorption isotherm (12). These advancements in ionic liquid design present valuable opportunities for improving corrosion resistance in harsh acidic settings, with potential benefits for industrial durability and material longevity.

3. Mechanisms of corrosion inhibition by ionic liquids

- Adsorption Behavior: Physisorption and Chemisorption

Room-temperature ionic liquids (RTILs) have proven effective in mitigating corrosion through a range of mechanisms, with adsorption onto metal surfaces being particularly significant. This adsorption can occur via both physisorption and chemisorption, depending on the nature of the ionic liquid and the metal involved. Physisorption involves relatively weak interactions, such as electrostatic forces and van der Waals attractions. For example, imidazolium-based RTILs with ethyl side chains have been shown to adsorb onto carbon steel surfaces, thereby lowering corrosion rates in aqueous monoethanolamine environments used for CO_2 capture (1). The adsorption of RTIL cations and anions forms a barrier layer on the metal, preventing contact with corrosive agents.

In contrast, chemisorption entails the formation of stronger, more stable chemical bonds between the RTIL and the metal surface. This results in more robust and enduring corrosion inhibition. A notable instance is the hydrogen evolution reaction (HER) on platinum electrodes, where the addition of [Emim]-based RTILs to alkaline media led to their pre-adsorption on the electrode. This stabilized intermediate hydrogen species and influenced both adsorption and charge transfer dynamics at the metal-electrolyte boundary (14).

The corrosion-inhibiting efficiency of RTILs is influenced by several parameters, such as the nature and concentration of the constituent ions. Among the studied options, [emim][acetate] demonstrated superior performance in reducing corrosion rates in CO_2 capture systems that utilize alkanolamines (1). Additionally, factors like alkyl chain length on the cation can affect adsorption behavior, as shown in chromatographic analyses where longer chains increased hydrophobic interactions with stationary phases (15).

- Mixed-type inhibition

Ionic liquids (ILs) have shown considerable potential as corrosion inhibitors for a range of metals exposed to different corrosive environments. Numerous studies have indicated that ILs generally function as mixed-type inhibitors, simultaneously affecting both anodic and cathodic processes on the metal surface (3).

The primary mechanism behind their corrosion inhibition is the adsorption of IL molecules onto the metal surface, leading to the formation of a protective film that blocks the penetration of corrosive agents. This adsorption can involve a combination of physical and chemical interactions between the ILs and the substrate (8). Often, this process adheres to the Langmuir adsorption isotherm model, suggesting a monolayer adsorption of ILs across the metal surface (16).

A range of factors influences the inhibition efficiency of ILs, including their molecular configuration, concentration, and the specific properties of the corrosive medium. For example, elongating the alkyl chain in imidazolium-based ILs has been found to enhance their inhibitory performance (5). Furthermore, innovative approaches—such as the use of polymeric ILs and IL-loaded microspheres—have been developed to provide advanced corrosion protection through synergistic actions and pH-sensitive release systems (8; 17).

ILs inhibit corrosion through a mixed-type mechanism involving their adsorption onto metal surfaces, which disrupts both anodic and cathodic reactions. Their overall efficiency is governed by structural and environmental factors, and continued research is focused on designing new ILs and delivery systems to optimize their protective capabilities across varied conditions.

- Protective layer formation

Ionic liquids (ILs) effectively inhibit corrosion by forming protective films on metal surfaces. The adsorption of IL species establishes a barrier that shields the metal from aggressive environments (18). This protective layer arises from several mechanisms, including electrostatic attraction, proton transfer, and electron donor-acceptor interactions (8).

The morphology and composition of these protective layers can differ based on the IL used. For example, certain ILs generate a stratified structure with a compact layer adjacent to the metal surface, a porous intermediary layer, and a flake-like outer region (19). Additionally, the creation of surface-bound metal-IL complexes contributes to enhanced corrosion resistance (20). The

adsorption behavior of both IL cations and anions is central to this process—bromide and imidazolate anions, along with vinylimidazolium cations, have been particularly effective in promoting strong surface interactions (20).

ILs offer corrosion protection primarily through film formation via adsorption and the development of complex surface compounds. Their performance is influenced by variables such as IL concentration, temperature, and the specific pairing of metal and IL. The ability to tailor ILs for specific functions by modifying anion or cation structures enables the customization of interfacial properties, making them highly adaptable and promising for corrosion control across a wide range of industrial applications (21).

4. Factors affecting inhibition efficiency

- Concentration dependence

The corrosion inhibition efficiency of ionic liquids (ILs) typically improves with increasing concentration, as evidenced by numerous studies: At elevated concentrations, ILs are more likely to form compact and uniform protective layers on metal surfaces, enhancing corrosion resistance. For instance, the performance of Quaternium-32 increased with concentration, achieving up to 94% efficiency at 20 μmol/L (22). Similarly, the polymeric IL PDBA-IL-NH_2 demonstrated a steady rise in inhibition efficiency with concentration, reaching a maximum of 94.67% at 100 ppm (8). However, this concentration-efficiency relationship is not strictly linear. In the case of imidazolium-based ILs, a notable rise in efficiency occurred below the critical micelle concentration (CMC), but further increases beyond the CMC did not yield additional improvements. This is attributed to the saturation of adsorption sites on the metal surface (23). Such behavior indicates that each IL has an optimal concentration range for peak performance.

Although increasing IL concentration generally enhances corrosion protection, phenomena like micelle formation and adsorption saturation must be considered. Identifying the optimal concentration for each IL through experimental evaluation is essential for maximizing efficiency while maintaining cost-effectiveness. This understanding plays a critical role in designing practical corrosion inhibition systems using ILs.

- Temperature effects

Temperature has a significant influence on the corrosion inhibition efficiency of ionic liquids (ILs), with most studies indicating a decline in performance as temperature increases. For example, Quaternium-32 (Q-32) showed reduced inhibition efficiency at elevated temperatures (23). Likewise, imidazolium-based ILs with varying alkyl chain lengths (R8, R10, R12) exhibited increased corrosion rates and diminished effectiveness when the temperature rose from 20°C to 50°C (5). Similar findings were reported for vinylimidazolium-based poly(ionic liquid)s, which reached their peak inhibition efficiency (75%) at 308 K, beyond which performance decreased (20). However, not all ILs follow this trend. In some cases, higher temperatures led to enhanced inhibition. For instance, 1-butyl-3-methylimidazolium trifluoromethyl sulfonate ([BMIm]TfO) displayed a progressive increase in efficiency as the temperature increased from 303 K to 333 K (24). Conversely, 1-methyl-1-propyl-piperidinium bromide (MPPB) experienced a drop in performance at elevated temperatures, with a maximum efficiency of 60% observed at 308 K (25).

Overall, temperature is a key parameter affecting the performance of IL-based corrosion inhibitors. While many ILs demonstrate decreased efficiency at higher temperatures due to desorption or accelerated corrosion kinetics, others may benefit from improved mobility or

enhanced adsorption. Careful evaluation of temperature effects is essential for selecting and optimizing ILs for use in temperature-variable environments.

- Molecular structure influence

The corrosion inhibition efficiency of ionic liquids (ILs) is heavily influenced by their molecular architecture, particularly the structure of their cationic and anionic components. One of the most critical factors is the alkyl chain length on the cation. Studies have shown that increasing the alkyl chain length in 1-alkyl-3-methylimidazolium bromide ILs enhances inhibition efficiency, likely due to stronger surface interactions and the formation of more compact adsorption layers on the metal substrate (23). Additionally, the nature of the cation plays a key role, with imidazolium-based ILs frequently outperforming other cation types in corrosion inhibition (8)(26). The identity of the anion also affects performance. For example, a comparison between 1-butyl-3-methylimidazolium chloride and bromide revealed differences in inhibition efficacy, underscoring the influence of anion chemistry on surface interactions (18). Moreover, functional groups attached to the cationic side chain can increase electron-donating capacity, enhancing adsorption onto metal surfaces (27). IL concentration is another important factor—efficiency generally improves with increasing concentration up to a threshold often associated with the critical micelle concentration (23).

In summary, the inhibition efficiency of ILs is governed by the structural characteristics of both their cations and anions, including alkyl chain length, type of functionalization, and ionic composition. Understanding these molecular-level relationships is essential for the rational design of high-performance, sustainable corrosion inhibitors based on ionic liquids.

5. Advanced applications of ionic liquids in corrosion inhibition

-Smart Corrosion Inhibitors Using Chitosan Microspheres

Ionic liquids (ILs) have opened new avenues in corrosion protection, particularly through the development of smart corrosion inhibitors. A notable example involves chitosan microspheres loaded with synthesized Gemini imidazolium-based ILs—specifically [C2(Bim)2]Cl2@CSM and [C6(Bim)2]Br2@CSM—designed for protecting N80 steel in hydrochloric acid. These systems achieved high inhibition efficiencies of 94.68% and 95.96%, respectively, at a concentration of 300 mg L^{-1} (17). What sets these microspheres apart is their pH-responsive behavior, enabled by Schiff-base C=N bonds. This feature allows the ILs to be rapidly released in acidic environments, such as corrosion sites, where they synergize with decomposed microspheres to enhance protective action (17). In comparison, room-temperature ionic liquids (RTILs) like [emim][acetate] have also shown corrosion mitigation capabilities, particularly in monoethanolamine-based CO_2 capture systems (1).

Incorporating ILs into smart delivery systems like chitosan microspheres represents a significant advancement in targeted corrosion inhibition. These responsive systems enable precise delivery and improved efficiency, highlighting the adaptability of ILs for diverse industrial applications.

-Polymeric Ionic Liquids

Polymeric ionic liquids (PILs) are gaining traction as high-performance corrosion inhibitors, offering distinct advantages over traditional and monomeric ILs. One such PIL, PDBA-IL-NH2—synthesized using short-chain imidazolium IL monomers—demonstrated excellent inhibition efficiency, reaching 94.67% at 100 ppm for mild steel (8). Notably, PDBA-IL-NH2 outperformed

its counterparts, including PDBA-IL-OH, PIL-NH2, and IL-NH2, under identical conditions (8). The corrosion protection efficiency of PILs is closely tied to their composition. For example, PILs developed from chitosan and various fatty acids exhibited differing performance, with the inhibition order being CSPTA-lauric > CSPTA-myristic > CSPTA-palmitic > CSPTA-stearic (28). This suggests that tailoring the fatty acid component can significantly influence the overall inhibition behavior.

PILs present a promising direction for developing sustainable and effective corrosion inhibitors. Their customizable structure, superior performance, and potential for smart functionality make them ideal candidates for future corrosion protection technologies. Continued research into their structural optimization and mechanism of action is likely to yield even more effective solutions.

6. Comparative studies of ionic liquids with other inhibitors

-Surfactants

Ionic liquids (ILs) share notable similarities with surfactants in their physicochemical behaviors, including self-assembly and micelle formation. However, ILs often exhibit a higher degree of self-organization, especially in long-range ordering, due to their ionic nature and tunable structures (29). Studies on the critical micelle concentration (CMC) of surfactant-IL systems highlight the crucial role of interfacial energy in surfactant aggregation, with the extent of this effect largely dependent on the structure of the IL used (30).

Some ILs, such as those based on pyrrolidinium cations, resemble surfactants in structure and behavior, forming local aggregates that can influence ion mobility and conductivity—properties important for electrochemical applications (31). In recent developments, surface-active ionic liquids (SAILs) have emerged, integrating the advantages of ILs and surfactants. These SAILs offer enhanced performance across a variety of applications, including chromatography, extraction processes, and wood protection (32)(33).

While ILs and surfactants share overlapping characteristics, ILs provide greater structural tunability. This versatility is especially evident in SAILs, which outperform conventional surfactants in several domains. Their adaptability makes them promising candidates for future applications in enhanced oil recovery, CO_2 capture, and other environmentally demanding processes (34).

- Traditional corrosion inhibitors

Comparative studies between ionic liquids (ILs) and traditional corrosion inhibitors often focus on their environmental impact, physical properties, and inhibition performance. While specific inhibition efficiencies can vary greatly depending on the metal, corrosive medium, concentration, and temperature, a general comparison of their characteristics and performance is possible. The following table summarizes the key comparative features.

Table 1. Comparative Studies of Ionic Liquids and Traditional Corrosion Inhibitors

Feature	Ionic Liquids (ILs)	Traditional Organic/Inorganic Inhibitors
Environmental Impact & Toxicity	Generally considered "**greener**" alternatives. Lower toxicity (especially new generations). **Negligible vapor pressure** (non-volatile), minimizing air pollution.	Many organic inhibitors (e.g., those containing heavy metals, volatile amines) can be **highly toxic** or environmentally damaging. Often possess **high volatility**.

Corrosion Inhibition Efficiency	Often exhibit **high and comparable, or even superior, inhibition efficiencies** (frequently \gt 90\%) at relatively low concentrations.	Efficiency is highly variable, but many conventional inhibitors also show high efficiency. Performance can degrade faster in harsh conditions.
Tunability and Versatility	**Highly tunable** and "task-specific." The cation and anion can be modified independently to optimize for a specific metal, medium, or temperature.	Limited tunability. Chemical structure is more rigid, offering less scope for fine-tuning properties for specific applications.
Physical and Chemical Stability	Exhibit **excellent thermal and chemical stability** over a wide range of temperatures and pressures, which is advantageous for high-temperature and high-pressure industrial processes.	Thermal stability is often lower, which can limit their application in harsh industrial environments.
Mechanism of Action	Typically function as **mixed-type inhibitors** (affecting both anodic and cathodic reactions). Adsorption involves **both the organic cation and the anion** on the metal surface.	Primarily form a protective barrier via adsorption of the organic molecule (often involving heteroatoms like N, S, O). Many are either anodic or cathodic-specific.
Volatility	**Non-volatile** (negligible vapor pressure).	Many are volatile, contributing to potential environmental and health hazards.
Cost and Availability	Currently, their **high synthesis cost** is a major drawback, though this is decreasing as production scales up.	Generally **less expensive** and widely commercially available.
Solubility	**High solubility and compatibility** with many organic and inorganic substances. Can be designed to be miscible or immiscible with specific solvents.	Solubility can be limited, especially for organic inhibitors in aqueous or highly polar media.

The primary motivation for using ionic liquids over traditional inhibitors stems from their superior environmental profile (non-volatility and lower toxicity) and their structural tunability, which allows for the creation of "designer" inhibitors with high thermal stability and performance tailored to specific corrosive conditions.(33)34)(35)

7. Plant Extracts and Pharmaceutical Drugs

Ionic liquids (ILs) are increasingly recognized alongside plant extracts and pharmaceutical drugs as effective organic green corrosion inhibitors (OGCIs). These inhibitors are appreciated for their eco-friendliness, biodegradability, and cost-effectiveness (35). Comparative studies indicate that ILs perform effectively in various corrosive environments, such as hydrochloric acid and brackish water (36)(37). Unlike plant extracts and pharmaceuticals, ILs exhibit multifunctional properties. Beyond corrosion inhibition, ILs have been applied in drug solubilization, targeted delivery, and even as active pharmaceutical ingredients (API-ILs) (38)(39)(40). This broader utility provides ILs with a unique advantage in multidisciplinary applications.

Nonetheless, it is important to consider the potential environmental toxicity of ILs when evaluating them against other OGCIs (41). The selection of an appropriate inhibitor should balance efficiency, cost, environmental impact, and application-specific requirements.

8. Electrochemical Techniques for Evaluating Ionic Liquids

- Electrochemical Impedance Spectroscopy (EIS)

EIS is a widely used technique to assess the corrosion inhibition performance of ionic liquids. It provides insights into the electrochemical processes at the metal-electrolyte interface and evaluates the formation and stability of protective films (12)(42). Key parameters such as charge transfer resistance (Rct) and double-layer capacitance (Cdl) are measured—an increase in Rct and decrease in Cdl typically signify improved corrosion resistance (43).

In more complex systems like concrete, EIS interpretation can be challenging due to overlapping signals from multiple phenomena. Innovative methods, such as analyzing characteristic relaxation angular frequencies and employing odd random phase EIS (ORP-EIS), have been proposed to overcome these limitations and study time-dependent behavior (44)(45). EIS offers detailed insights into inhibition mechanisms and complements other electrochemical and surface techniques for a holistic evaluation of IL-based inhibitors (28)(46)(47).

- Potentiodynamic Polarization

Potentiodynamic polarization is another essential technique for evaluating ILs as corrosion inhibitors. It helps elucidate corrosion behavior and inhibition mechanisms across various metal surfaces. For example, pyrrolidinium ILs demonstrated inhibition efficiencies up to 85% for copper in 1 M HNO_3 at a concentration of 0.05 mM (42). Imidazolium and pyridinium ILs similarly showed high efficiency in inhibiting steel corrosion in 1 M HCl, with performance increasing alongside concentration (6). Many ILs function as mixed-type inhibitors, reducing both anodic and cathodic reactions, as seen with Brönsted acid ILs on carbon steel and other imidazolium-based ILs (12)(6). However, some chloride-containing ILs failed to develop a passive region on 1018 carbon steel, as evident in anodic polarization curves (48), indicating that IL composition critically affects inhibition behavior.

- Weight Loss Method

The weight loss method remains a foundational technique for quantifying corrosion rates and evaluating inhibitor efficiency. It involves comparing the mass of a metal sample before and after exposure to a corrosive environment with and without the IL. Numerous studies have confirmed its effectiveness. Pyrrolidinium ILs provided up to 85% inhibition for copper in 1 M HNO_3, and similar results were observed for imidazolium and pyridinium ILs in acidic environments (6)(42). In carbon steel immersed in 3.5% NaCl, 1-butylpyrrolidinium chloride also demonstrated significant inhibition based on weight loss measurements (49). The weight loss method is frequently corroborated by results from polarization studies, reinforcing its reliability in assessing IL performance (6).

9. Surface Analysis Techniques for Studying Inhibition Mechanisms

- Scanning Electron Microscopy (SEM)

SEM is instrumental in analyzing the morphology and topography of metal surfaces before and after corrosion. It delivers nanometer-scale resolution, making it ideal for visualizing the physical effects of corrosion and the presence of protective inhibitor films (50)(51). Advanced SEM setups, including environmental SEM, allow imaging under moist or high-pressure conditions with minimal resolution loss (52). Coupling SEM with complementary techniques such as Auger electron spectroscopy and NMR relaxometry enables multidimensional material characterization, as seen in studies of hydrated cement and corrosion-affected metals (53).

- X-ray Photoelectron Spectroscopy (XPS)

XPS provides chemical state and compositional data for the top few nanometers of a surface. It is particularly valuable for identifying adsorbed inhibitor species, quantifying elemental content, and analyzing surface interactions relevant to inhibition (54)(55).

The technique is highly sensitive, detecting as low as 0.1 atomic % and all elements except hydrogen and helium (54). XPS can reveal the formation of new chemical bonds or interaction sites indicative of successful inhibitor adsorption (56)(57). Although traditional XPS requires ultra-high vacuum conditions, modern near-ambient pressure XPS (NAP-XPS) enables surface analysis under more realistic environmental conditions (58). Despite the challenges in sample preparation and data interpretation, XPS remains indispensable in corrosion science and surface chemistry (59)(60)(61).

10. Industrial applications and future prospects

- Electroplating

Ionic liquids (ILs) have emerged as promising alternatives to conventional electrolytes in industrial electroplating processes due to their unique physicochemical properties. Composed entirely of ions, ILs offer several advantages over aqueous electrolytes, including lower toxicity, wider electrochemical windows, higher thermal stability, and improved current efficiencies (62). These features make ILs particularly attractive for sustainable electroplating applications and corrosion protection strategies.

In electroplating, ILs have been successfully employed for the electrodeposition of metals and alloys such as zinc and zinc–nickel, which are extensively used in the automotive and aerospace sectors to protect steel components from corrosion (63). Notably, deep eutectic solvents—a subclass of ILs—have been used to deposit nanocrystalline nickel coatings with superior mechanical properties, enhanced corrosion resistance, and improved electrolyte stability (64). Moreover, the electrodeposition of aluminum and aluminum–platinum alloys from room-temperature ILs has been demonstrated, showcasing reduced water sensitivity and simplified purification, thereby enhancing process efficiency and reducing costs (2).

Looking forward, the design of task-specific ionic liquids—where the anion or cation chemistry is tailored for specific electrochemical applications—offers exciting opportunities. Such precision engineering enables better control of metal deposition, surface morphology, and interfacial interactions, which are crucial for advanced material applications (21). The inherently wide electrochemical windows of many ILs (often exceeding 5 V) further extend their usability in high-voltage electrochemical systems (65). However, despite their advantages, the industrial-scale adoption of IL-based electroplating processes remains limited due to unresolved challenges in cost, stability, and scalability (62)(63).

Challenges and Opportunities in Large-Scale Applications

In addition to electroplating, ionic liquids have garnered attention as effective corrosion inhibitors across various industries. Numerous studies have highlighted the ability of ILs to reduce corrosion rates on metals such as carbon steel and stainless steel, especially in aggressive environments like acidic or saline media (6)(10)(66). Their inhibition efficiency is strongly influenced by molecular structure and concentration, with higher concentrations often resulting in greater surface coverage and protection (8)(10).

ILs inhibit corrosion primarily through adsorption mechanisms, forming protective films on metal surfaces. This behavior often conforms to the Langmuir adsorption isotherm model, indicating monolayer adsorption with uniform energy sites (6)(10)(37). Such protective behavior is advantageous for dynamic and corrosive industrial settings. However, scaling up the application of ILs for real-world corrosion protection presents several challenges. Laboratory results may not directly translate to complex industrial environments—such as high-temperature, high-pressure, and high-salinity conditions found in oil and gas reservoirs—where inhibitor stability and persistence become critical concerns (67). Additionally, the synthesis of ILs, which often involves multi-step processes and expensive precursors, can hinder their commercial feasibility.

On the positive side, advances in green chemistry and materials science are paving the way for the development of cost-effective, biodegradable, and task-specific ILs. These innovations aim to reduce toxicity, improve environmental compatibility, and tailor properties for specific corrosion systems (68). Continued research into the structure–activity relationships and environmental behavior of ILs will be key to unlocking their full industrial potential (11)(8).

Conclusion

Ionic liquids offer transformative possibilities in both electroplating and corrosion inhibition, combining versatility with environmental and performance benefits. While challenges remain—particularly regarding scalability, cost, and complex operating conditions—ongoing research in green synthesis, tailored IL design, and hybrid applications provides a path forward. As the field of ionometallurgy matures, ILs are expected to play a central role in next-generation surface engineering technologies, especially where traditional methods fall short.

REFERENCES

1. Hasib-Ur-Rahman, M., & Larachi, F. (2013). Prospects of Using Room-Temperature Ionic Liquids as Corrosion Inhibitors in Aqueous Ethanolamine-Based CO2 Capture Solvents. Industrial & Engineering Chemistry Research, 52(49), 17682–17685.

2. Abbott, A. P., Griffith, G. A., Eardley, C. A., Farley, N. R. S., & Pratt, A. (2001). Electrodeposition of aluminium and aluminium/platinum alloys from AlCl3/benzyltrimethylammonium chloride room temperature ionic liquids. Journal of Applied Electrochemistry, 31(12), 1345–1350.

3. Murulana, L. C., Singh, A. K., Shukla, S. K., Kabanda, M. M., & Ebenso, E. E. (2012). Experimental and Quantum Chemical Studies of Some Bis(trifluoromethyl-sulfonyl) Imide Imidazolium-Based Ionic Liquids as Corrosion Inhibitors for Mild Steel in Hydrochloric Acid Solution. Industrial & Engineering Chemistry Research, 51(40), 13282–13299.

4. Rathore, A., Sharma, S., Sharma, A., & Sharma, S. K. (2023). Evaluation of structure-reactivity correlation of efficient corrosion inhibitor ionic liquids for mild steel in acidic medium. Journal of Dispersion Science and Technology, 45(6), 1107–1119.

5. El-Nagar, R. A., Khalil, N. A., Atef, Y., Nessim, M. I., & Ghanem, A. (2024). Evaluation of ionic liquids based imidazolium salts as an environmentally friendly corrosion inhibitors for carbon steel in HCl solutions. Scientific Reports, 14(1)

6. Ibrahim, M. A. M., Messali, M., Moussa, Z., Alzahrani, A. Y., Alamry, S. N., & Hammouti, B. (2011). Corrosion Inhibition of Carbon Steel by Imidazolium and Pyridinium Cations Ionic Liquids in Acidic Environment. Portugaliae Electrochimica Acta, 29(6), 375–389.

7. Al-Rashed, O., & Abdel Nazeer, A. (2022). Effectiveness of Some Novel Ionic Liquids on Mild Steel Corrosion Protection in Acidic Environment: Experimental and Theoretical Inspections. Materials, 15(6), 2326

8. Jia, H., Jia, H., Wang, Q., Xu, Y., Wang, B., Wang, Q., Li, X., Wang, Z., Lv, K., & Huang, P. (2024). Imidazolium-Based Polymeric Ionic Liquids with Short Alkyl Chains as Green Corrosion Inhibitors for Mild Steel in 1 M HCl: Experimental

and Theoretical Investigations. Langmuir : The ACS Journal of Surfaces and Colloids, 40(27), 14141–14152.

9. Cornejo Robles, E., Olivares-Xometl, O., Likhanova, N. V., Arellanes-Lozada, P., Lijanova, I. V., & Díaz-Jiménez, V. (2023). Synthesis of Ammonium-Based ILs with Different Lengths of Aliphatic Chains and Organic Halogen-Free Anions as Corrosion Inhibitors of API X52 Steel. International Journal of Molecular Sciences, 24(8), 7613.

10. Olivares-Xometl, O., Álvarez-Álvarez, E., Likhanova, N. V., Lijanova, I. V., Hernández-Ramírez, R. E., Arellanes-Lozada, P., & Varela-Caselis, J. L. (2017). Synthesis and corrosion inhibition mechanism of ammonium-based ionic liquids on API 5L X60 steel in sulfuric acid solution. Journal of Adhesion Science and Technology, 32(10), 1092–1113.

11. Gabler, C., Tomastik, C., Allmaier, G., Brenner, J., Pisarova, L., & Doerr, N. (2011). Corrosion properties of ammonium based ionic liquids evaluated by SEM-EDX, XPS and ICP-OES. Green Chemistry, 13(10), 2869.

12. Cao, S., Yang, L., Yang, P., Lu, H., Liu, D., Gui, J., & Zhang, P. (2017). Green Br\xf6nsted acid ionic liquids as novel corrosion inhibitors for carbon steel in acidic medium. Scientific Reports, 7(1).

13. Schmitzhaus, T. E., Schroeder, R., Muller, I. L., Malfatti, C. D. F., Ortega Vega, M. R., & Mattedi, S. (2020). An amino-based protic ionic liquid as a corrosion inhibitor of mild steel in aqueous chloride solutions. Materials and Corrosion, 71(7), 1175–1193.

14. Amaral, L., Sequeira, C. A. C., Cardoso, D. S. P., Šljukić, B., & Santos, D. M. F. (2017). Room Temperature Ionic Liquids as Electrolyte Additives for the HER in Alkaline Media. Journal of The Electrochemical Society, 164(4), F427–F432.

15. Berthod, A., Ruiz-Angel, M. J., & Huguet, S. (2005). Nonmolecular Solvents in Separation Methods: Dual Nature of Room Temperature Ionic Liquids. Analytical Chemistry, 77(13), 4071–4080

16. Cui, F., Ni, Y., Jiang, J., Ni, L., & Wang, Z. (2020). Experimental and theoretical studies of five imidazolium-based ionic liquids as corrosion inhibitors for mild steel in H2S and HCl solutions. Chemical Engineering Communications, 208(11), 1580–1593.

17. Wang, L., Sun, S., Li, M., Liu, Y., Wang, Z., Cui, N., Hu, S., & Li, F. (2023). pH-Responsive Chitosan Microspheres Loaded with Gemini Imidazolium-Based Ionic Liquids as Smart Corrosion Inhibitors for N80 Steel in Hydrochloric Acid Solution. Advanced Engineering Materials.

18. Scendo, M., & Uznanska, J. (2011). The Effect of Ionic Liquids on the Corrosion Inhibition of Copper in Acidic Chloride Solutions. International Journal of Corrosion, 2011(2011), 1–13.

19. Visser, P., Terryn, H., Liu, Y., & Mol, J. M. C. (2016). Lithium salts as leachable corrosion inhibitors and potential replacement for hexavalent chromium in organic coatings for the protection of aluminum alloys. Journal of Coatings Technology and Research, 13(4), 557–566.

20. Gómez-Sánchez, G., Díaz-Jiménez, V., Olivares-Xometl, O., Arriola-Morales, J., Guzmán-Lucero, D., Arellanes-Lozada, P., Lijanova, I. V., & Likhanova, N. V. (2022). Inhibition Mechanism of Some Vinylalkylimidazolium-Based Polymeric Ionic Liquids against Acid Corrosion of API 5L X60 Steel: Electrochemical and Surface Studies. ACS Omega, 7(42), 37807–37824.

21. Forsyth, M., Basile, A., Macfarlane, D. R., Somers, A. E., & Howlett, P. C. (2017). Interphase engineering of reactive metal surfaces using ionic liquids and deep eutectic solvents\u2014from corrosion control to next-generation batteries. Npj Materials Degradation, 1(1).

22. Sliem, M. H., Mohamed, F. S., Abdullah, A. M., Alnuaimi, N. A., & Radwan, A. B. (2020). An efficient green ionic liquid for the corrosion inhibition of reinforcement steel in neutral and alkaline highly saline simulated concrete pore solutions. Scientific Reports, 10(1).

23. Liu, C., Wang, X., Zhou, J., Wang, B., Liu, J., & Gao, G. (2024). Effect of Alkyl Chain Length on the Corrosion Inhibition Performance of Imidazolium-Based Ionic Liquids for Carbon Steel in 1 M HCl Solution: Experimental Evaluation and Theoretical Analysis. Langmuir, 40(17), 8806–8819.

24. Abbas, M. A., El-Shamy, A. M., Zakaria, K., El Abedin, S. Z., & Ismail, A. S. (2022). Adsorption, thermodynamic, and quantum chemical investigations of an ionic liquid that inhibits corrosion of carbon steel in chloride solutions. Scientific Reports, 12(1).

25. Kedimar, N., Rao, P., & Rao, S. A. (2023). Ionic liquid as an effective green inhibitor for acid corrosion of aluminum composite: experimental and theoretical considerations. Journal of Applied Electrochemistry, 53(7), 1473–1489.

26. Sherif, E.-S. M., Abdo, H. S., & Abedin, S. Z. E. (2015). Corrosion Inhibition of Cast Iron in Arabian Gulf Seawater by Two Different Ionic Liquids. Materials, 8(7), 3883–3895.

27. Gurjar, S., Sharma, S., Ratnani, S., & Sharma, S. K. (2023). Adsorption of Ionic Liquids on The Metal Surface: Co-

ordination Chemistry Of Ionic Liquids (pp. 77–92). bentham science.

28. Elsaeed, S. M., Ashour, H., El Tamany, E. S. H., El Nagy, H. A., Zaki, E. G., & Khamis, E. A. (2018). Corrosion and hydrogen evolution rate control for X-65 carbon steel based on chitosan polymeric ionic liquids: experimental and quantum chemical studies. RSC Advances, 8(66), 37891–37904.

29. Smirnova, N. A., & Safonova, E. A. (2010). Ionic liquids as surfactants. Russian Journal of Physical Chemistry A, 84(10), 1695–1704.

30. Chen, L. G., & Bermudez, H. (2012). Solubility and Aggregation of Charged Surfactants in Ionic Liquids. Langmuir, 28(2), 1157–1162.

31. Kunze, M., Winter, M., Passerini, S., Paillard, E., Appetecchi, G. B., Schönhoff, M., & Jeong, S. (2011). Inhibition of Self-Aggregation in Ionic Liquid Electrolytes for High-Energy Electrochemical Devices. The Journal of Physical Chemistry C, 115(39), 19431–19436.

32. Brown, P., Plana, D., Fermin, D., Eastoe, J., Richardson, R. M., Butts, C. P., Parker, D., Lee, H.-C., & Grillo, I. (2012). Anionic Surfactant Ionic Liquids with 1-Butyl-3-methyl-imidazolium Cations: Characterization and Application. Langmuir, 28(5), 2502–2509.

33. Wojcieszak, M., Syguda, A., Fojutowski, A., Kropacz, A., Lewandowska, A., Kaźmierczak, K., & Materna, K. (2024). Imidazolium surface-active ionic liquids as antifungal agents in wood protection. Journal of Molecular Liquids, 398, 124247.

34. Shao, M., Li, X., Wang, Y., Zhu, T., Liu, P., & Fu, L. (2023). Synthesis and Evaluation of Interfacial Properties and Carbon Capture Capacities of the Imidazolium-Based Ionic Liquid Surfactant. ACS Omega, 8(23), 21113–21119.

35. Popoola, L. T. (2019). Progress on pharmaceutical drugs, plant extracts and ionic liquids as corrosion inhibitors. Heliyon, 5(2), e01143.

36. Chen, L., Zhang, Y., & Lu, D. (2022). Organic Compounds as Corrosion Inhibitors for Carbon Steel in HCl Solution: A Comprehensive Review. Materials (Basel, Switzerland), 15(6), 2023.

37. Zunita, M., Bundjali, B., Wahyuningrum, D., Wenten, I. G., Buchari, B., & Boopathy, R. (2020). Corrosion Inhibition Performances of Imidazole Derivatives-Based New Ionic Liquids on Carbon Steel in Brackish Water. Applied Sciences, 10(20), 7069.

38. Curreri, A. M., Mitragotri, S., & Tanner, E. E. L. (2021). Recent Advances in Ionic Liquids in Biomedicine. Advanced Science, 8(17), 2004819.

39. Pedro, S. N., R Freire, C. S., Silvestre, A. J. D., & Freire, M. G. (2020). The Role of Ionic Liquids in the Pharmaceutical Field: An Overview of Relevant Applications. International Journal of Molecular Sciences, 21(21), 8298

40. Zandu, S. K., Singh, I., & Chopra, H. (2020). Ionic Liquids for Therapeutic and Drug Delivery Applications. Current Drug Research Reviews, 12(1), 26–41.

41. Stock, F., Ondruschka, B., Ranke, J., Störmann, R., Hoffmann, J., & Jastorff, B. (2004). Effects of ionic liquids on the acetylcholinesterase – a structure–activity relationship consideration. Green Chem., 6(6), 286–290.

42. El-Katori, E. E., & Abousalem, A. S. (2019). Impact of some pyrrolidinium ionic liquids on copper dissolution behavior in acidic environment: experimental, morphological and theoretical insights. RSC Advances, 9(36), 20760–20777.

43. Yadav, D. K., & Quraishi, M. A. (2012). Application of Some Condensed Uracils as Corrosion Inhibitors for Mild Steel: Gravimetric, Electrochemical, Surface Morphological, UV–Visible, and Theoretical Investigations. Industrial & Engineering Chemistry Research, 51(46), 14966–14979.

44. Ribeiro, D. V., Souza, C. A. C., & Abrantes, J. C. C. (2015). Use of Electrochemical Impedance Spectroscopy (EIS) to monitoring the corrosion of reinforced concrete. Revista IBRACON de Estruturas e Materiais, 8(4), 529–546.

45. Meeusen, M., Zardet, L., Homborg, A. M., Lekka, M., Andreatta, F., Fedrizzi, L., Boelen, B., Mol, J. M. C., & Terryn, H. (2020). The effect of time evolution and timing of the electrochemical data recording of corrosion inhibitor protection of hot-dip galvanized steel. Corrosion Science, 173, 108780.

46. Jadhav, N., & Gelling, V. J. (2019). Review—The Use of Localized Electrochemical Techniques for Corrosion Studies. Journal of The Electrochemical Society, 166(11), C3461–C3476.

47. Sayed, A. G., Ashmawy, A. M., Elgammal, W. E., Hassan, S. M., & Deyab, M. A. (2023). Synthesis, description, and application of novel corrosion inhibitors for CS AISI1095 in 1.0 M HCl based on benzoquinoline derivatives. Scientific Reports, 13(1).

48. Arenas, M. F., & Reddy, R. G. (2003). Corrosion of steel in ionic liquids. Journal of Mining and Metallurgy, Section B:

Metallurgy, 39(1–2), 81–91.

49. Abbas, M. A., El-Shamy, A. M., Abedin, S. Z. E., & Zakaria, K. (2019). Utilization of 1-butylpyrrolidinium Chloride Ionic Liquid as an Eco-friendly Corrosion Inhibitor and Biocide for Oilfield Equipment: Combined Weight Loss, Electrochemical and SEM Studies. Zeitschrift Für Physikalische Chemie, 235(4), 377–406.

50. Akhtar, K., Khan, S. A., Asiri, A. M., & Khan, S. B. (2018). Scanning Electron Microscopy: Principle and Applications in Nanomaterials Characterization (pp. 113–145). springer.

51. Watanabe, H., & Ichikawa, M. (1996). Development of a multifunctional surface analysis system based on a nanometer scale scanning electron beam: Combination of ultrahigh vacuum-scanning electron microscopy, scanning reflection electron microscopy, Auger electron spectroscopy, and x-ray photoelectron spectroscopy. Review of Scientific Instruments, 67(12), 4185–4190.

52. Farley, A. N., & Shah, J. S. (1990). Primary considerations for image enhancement in high-pressure scanning electron microscopy. Journal of Microscopy, 158(3), 379–388.

53. Naber, C., Nguyen-Tuan, L., Kleiner, F., Becker, F., Etzold, M. A., Rößler, C., & Neubauer, J. (2020). C-S-H Pore Size Characterization Via a Combined Nuclear Magnetic Resonance (NMR)-Scanning Electron Microscopy (SEM) Surface Relaxivity Calibration. Materials, 13(7), 1779.

54. Andrade, J. D. (1985). X-ray Photoelectron Spectroscopy (XPS) (pp. 105–195). springer us.

55. Lefebvre, J., Galli, F., Bianchi, C. L., Boffito, D. C., & Patience, G. S. (2019). Experimental methods in chemical engineering: X-ray photoelectron spectroscopy-XPS. The Canadian Journal of Chemical Engineering, 97(10), 2588–2593.

56. Di Giulio, T., De Benedetto, G. E., Malitesta, C., Ditaranto, N., & Mazzotta, E. (2024). Insights into Plastic Degradation Processes in Marine Environment by X-ray Photoelectron Spectroscopy Study. International Journal of Molecular Sciences, 25(10), 5060.

57. Matuana, L. M., Balatinecz, J. J., Sodhi, R. N. S., & Park, C. B. (2001). Surface characterization of esterified cellulosic fibers by XPS and FTIR Spectroscopy. Wood Science and Technology, 35(3), 191–201.

58. Lian, X., Ding, Y., Liu, Y., Gao, J., & Chen, W. (2022). Unraveling Catalytic Reaction Mechanism by In Situ Near Ambient Pressure X-ray Photoelectron Spectroscopy. The Journal of Physical Chemistry Letters, 13(35), 8264–8277.

59. Stevie, F. A., & Donley, C. L. (2020). Introduction to x-ray photoelectron spectroscopy. Journal of Vacuum Science & Technology A: Vacuum, Surfaces, and Films, 38(6), 063204.

60. Desimoni, E., & Brunetti, B. (2015). X-Ray Photoelectron Spectroscopic Characterization of Chemically Modified Electrodes Used as Chemical Sensors and Biosensors: A Review. Chemosensors, 3(2), 70–117.

61. Mikhlin, Y. (2020). X-ray Photoelectron Spectroscopy in Mineral Processing Studies. Applied Sciences, 10(15), 5138.

62. Abbott, A. P., Frisch, G., & Ryder, K. S. (2013). Electroplating Using Ionic Liquids. Annual Review of Materials Research, 43(1), 335–358.

63. Maniam, K. K., & Paul, S. (2020). Progress in Electrodeposition of Zinc and Zinc Nickel Alloys Using Ionic Liquids. Applied Sciences, 10(15), 5321.

64. Danilov, F. I., Kumar, U. P., Vasil'Eva, E. A., Kityk, A. A., Kennady, C. J., Shaiderov, D. A., & Protsenko, V. S. (2017). Electrodeposition of Nanocrystalline Nickel Coatings from a Deep Eutectic Solvent with Water Addition. Protection of Metals and Physical Chemistry of Surfaces, 53(6), 1131–1138.

65. Buzzeo, M. C., Evans, R. G., & Compton, R. G. (2004). Non-haloaluminate room-temperature ionic liquids in electrochemistry--a review. ChemPhysChem, 5(8), 1106–1120.

66. Atef, Y., & Ghanem, A. (2020). Ionic Liquids based on Different Chain Fatty Acids as Green Corrosion Inhibitors for C-steel in Produced Oilfield Water. IOP Conference Series: Materials Science and Engineering, 975(1), 012014.

67. Velusamy, S., Sakthivel, S., Neelakantan, L., & Sangwai, J. S. (2017). Imidazolium-based ionic liquids as an anticorrosive agent for completion fluid design. Journal of Earth Science, 28(5), 949–961.

68. Shehata, O. S., Korshed, L. A., & Attia, A. (2018). Green Corrosion Inhibitors, Past, Present, and Future. institute for new technologies.

UDC:532.5; 556.3
DOI: https://doi.org/10.30546/2521-6317.2025.02.523

STUDY OF THE DENSITY AND THERMAL COEFFICIENTS OF "PALCHIQ-OBA" THERMAL WATER IN KHACHMAZ DISTRICT OF AZERBAIJAN AT VARIOUS PRESSURES AND TEMPERATURES

MAHIR BASHIROV
Department of Mechanical Engineering
Baku Engineering University
Baku, Azerbaijan
mbashirov@beu.edu.az

NOFAL NABIYEV
Department of Mechanical Engineering
Baku Engineering University
Baku, Azerbaijan
nnabiyev@beu.edu.az

AYTAN NAMAZOVA
Technical-Humanitarian Lyceum
Baku, Azerbaijan
aytan_bashirova@yahoo.com

ARTICLE INFO
Article history:
Received:2025-05-23
Received in revised form:2025-06-11
Accepted:2025-07-16
Available online:2025-12-25

Keywords:
density,
pressure,
temperature,
thermal waters.

JEL Classification: Q25; Q48; Q32

ABSTRACT
The presented study examines the temperature and pressure-dependent variations in the density of the geothermal water known as "Palchyg-oba," located in the Khachmaz district of Azerbaijan. The experiments were conducted using a high-pressure, high-temperature DMA HPM vibrating densimeter within the temperature range of T = (278.15÷373.15) K and the pressure interval of p = (0.1÷40) MPa.
The measuring unit of the device primarily comprises a magnetic measurement system, a DMA HPM Density Meter chamber equipped with a Hastelloy C-276 vibrating tube, an interferometer, and the high-pressure, high-temperature mPDS2000V3 control system (Anton Paar, Austria).
The obtained results are presented in graphical form. The DMA HPM Density Meter registers the oscillation period and temperature, transmitting these data to the IBM PC–based computing system, where the parameters can be monitored continuously. Simultaneously, the signals from the P-10 pressure gauge are transferred to the mPDS2000V3 control system and subsequently forwarded to the IBM PC computing unit. During the experiments, the temperature in the measuring cell was maintained with an accuracy of 0.01 K using an F32-ME thermostat (Julabo, Germany). Temperature measurements were performed using calibrated Pt100 platinum resistance thermometers (ITS-90) with an uncertainty of ±3 mK.

INTRODUCTION

The depletion of traditional energy sources, global climate change, and environmental pollution are among the main environmental problems of today. Various measures are being taken to address these problems, the most significant of which is the utilization of renewable and alternative energy sources. Taking these into account, environmentally friendly alternative energy sources (solar and wind energy, small hydroelectric power plants, thermal waters, biomass energy) are widely used in developed countries of the world.

Azerbaijan, due to its geographical location and climatic conditions, is among the countries with highly favorable potential for utilizing alternative energy sources. Across the territory of the

Republic of Azerbaijan, there are more than 200 underground thermal, mineral, and potable spring water resources enriched with various mineral substances, with a total daily productivity exceeding 100 million liters. These waters have more than 1,000 natural outlets [1]. According to their chemical composition, the mineral waters of Azerbaijan are classified into ten groups: hydrocarbonate, hydrocarbonate–chloride, hydrocarbonate–chloride–sulfate, chloride–hydrocarbonate, chloride, chloride–sulfate, sulfate–chloride, sulfate–hydrocarbonate, and bluestone.

Following the Decree of the President of the Republic of Azerbaijan dated October 21, 2004, on the approval of the "State Program on the Use of Alternative and Renewable Energy Sources in the Republic of Azerbaijan", large-scale initiatives have been implemented in this field across the country [2]. In the present study, the density of the "Palchig-oba" geothermal water, located in the northern part of Azerbaijan (Khachmaz region), was investigated under high temperature and pressure conditions. The primary objective of this research is to assess the potential of alternative energy resources in the northern regions of Azerbaijan. The waters in this area contain gaseous compounds such as H_2S and sulfate ions and are characterized by a high degree of mineralization. The geothermal waters discharge at surface temperatures that are relatively close to each other. The outlet temperature of the "Palchig-oba" geothermal water is T=317.15 K. These geothermal waters in the Khachmaz region are mainly utilized for therapeutic purposes and as a source of hot water [3].

The DMA HPM Density Meter measuring system determines the oscillation period and temperature and transmits these data to the IBM PC computer-based computing system, where the parameters are continuously monitored. Simultaneously, the signals from the P-10 pressure gauge are transmitted to the mPDS2000V3 control system and subsequently to the IBM PC computing unit. During the experiment, the temperature in the measuring chamber is maintained with an accuracy of 0.01 K using an F32-ME thermostat (Julabo, Germany). Temperature measurements are performed using calibrated Pt100 platinum thermometers, with an error of ±3 mK (ITS-90) [4].

The sample was collected directly from the source, filtered, and degassed, as the presence of air and gas bubbles in geothermal water negatively affects density measurements. First, a chemical analysis of the "Palchig-oba" geothermal water was performed using an IRIS II optical emission spectrometer with a dual argon plasma source [5]. Subsequently, the density was experimentally analyzed over a wide range of temperatures and pressures. The obtained results are presented in Table 1 and Figures 2–3.

Table 1. Experimental pressure p, density ρ, temperature T, isothermal compressibility k_T, isobaric thermal expansion coefficient α_p, and the difference between isobaric and isochoric heat capacities c_p-c_v. of the "Palchig-oba" geothermal water.

$\frac{p}{MPa}$	$\frac{T}{K}$	$\frac{k_T \cdot 10^6}{MPa^{-1}}$	$\frac{\alpha_p \cdot 10^6}{K^{-1}}$	$\frac{c_p - c_\upsilon}{C \cdot кq^{-1} \cdot K^{-1}}$	$\frac{\gamma}{MPa \cdot K^{-1}}$	$\frac{p_{int}}{MPa}$
0.786	278.21	500.3	41.3	0.9	0.0825	22.2
5.073	278.22	489.6	57.8	1.9	0.1181	27.8
9.995	278.23	478.8	75.1	3.2	0.1568	33.6
15.101	278.22	467.0	94.3	5.2	0.2019	41.1
20.015	278.22	456.7	111.5	7.4	0.2441	47.9

25.229	278.22	446.4	129.2	10.2	0.2895	55.3
30.097	278.21	436.9	145.9	13.3	0.3338	62.8
34.985	278.21	428.1	161.8	16.6	0.3778	70.1
40.100	278.20	418.8	179.0	20.7	0.4273	78.8
0.958	288.24	470.2	169.9	17.6	0.3612	103.2
5.188	288.25	459.1	181.1	20.4	0.3944	108.5
10.057	288.24	448.9	191.5	23.3	0.4267	112.9
15.089	288.23	438.8	202.1	26.5	0.4606	117.7
19.951	288.21	429.5	212.0	29.7	0.4937	122.3
24.990	288.20	419.7	222.7	33.5	0.5306	127.9
30.037	288.18	410.5	233.0	37.4	0.5676	133.5
35.041	288.17	402.1	242.5	41.3	0.6031	138.8
40.010	288.15	393.6	252.4	45.6	0.6413	144.8
1.035	298.24	452.5	271.7	48.4	0.6005	178.0
5.147	298.24	442.9	277.0	51.4	0.6255	181.4
10.054	298.23	433.2	282.5	54.5	0.6520	184.4
14.991	298.23	423.3	288.3	57.9	0.6810	188.1
20.021	298.22	413.6	293.9	61.5	0.7105	191.9
25.061	298.21	404.9	299.1	64.9	0.7387	195.2
30.128	298.21	396.4	304.2	68.4	0.7673	198.7
35.104	298.20	388.2	309.2	72.1	0.7966	202.4
40.035	298.17	380.1	314.1	75.8	0.8263	206.3
0.845	313.15	442.5	397.6	111.9	0.8986	280.6
5.021	313.16	433.8	398.1	114.2	0.9177	282.4
10.002	313.14	423.9	398.3	116.8	0.9396	284.2
15.203	313.15	413.9	398.7	119.5	0.9631	286.4
19.996	313.15	405.3	398.9	122.0	0.9842	288.2
25.025	313.16	396.5	399.1	124.6	1.0064	290.1
29.994	313.14	388.3	399.0	126.9	1.0275	291.8
35.024	313.15	380.4	399.1	129.4	1.0493	293.6
39.995	313.15	372.9	399.0	131.7	1.0702	295.1
0.870	327.11	446.4	500.3	184.6	1.1207	365.7
5.123	327.12	437.5	497.7	186.1	1.1377	367.1
10.042	327.13	428.2	494.9	187.7	1.1560	368.1
15.187	327.14	418.3	491.8	189.2	1.1755	369.4
19.978	327.15	410.2	489.0	190.5	1.1922	370.0
25.227	327.16	401.0	485.7	191.8	1.2111	371.0
30.096	327.16	392.8	482.5	192.8	1.2282	371.7
35.090	327.17	385.1	479.4	193.8	1.2449	372.2
40.068	327.18	378.1	476.4	194.6	1.2600	372.2
0.924	343.14	459.8	602.4	275.1	1.3102	448.7
5.001	343.15	451.5	598.5	276.0	1.3256	449.9
10.005	343.16	441.9	593.7	276.9	1.3435	451.0
15.203	343.15	432.4	588.4	277.4	1.3610	451.8
19.997	343.15	424.0	583.6	277.7	1.3765	452.4
25.004	343.15	415.6	578.5	277.8	1.3920	452.7
29.989	343.16	407.6	573.4	277.7	1.4066	452.7
35.207	343.15	399.7	568.0	277.2	1.4209	452.4
39.992	343.15	392.8	563.0	276.7	1.4333	451.9
1.012	358.15	473.2	672.1	350.7	1.4206	507.8
5.065	358.16	465.4	668.7	352.2	1.4369	509.6
10.025	358.15	456.4	664.3	353.7	1.4556	511.3

15.047	358.14	447.5	659.6	354.7	1.4738	512.8
20.035	358.15	439.1	654.7	355.4	1.4909	513.9
25.621	358.15	430.2	649.1	355.7	1.5089	514.8
30.058	358.16	423.3	644.4	355.7	1.5225	515.2
35.106	358.15	415.8	639.0	355.2	1.5367	515.2
39.985	358.15	408.9	633.6	354.4	1.5496	515.0
1.326	373.12	481.7	701.4	394.8	1.4561	542.0
5.108	373.12	474.7	700.1	398.4	1.4750	545.2
10.166	373.15	466.5	698.3	402.4	1.4968	548.4
15.004	373.18	459.0	696.2	405.6	1.5167	551.0
20.071	373.18	451.3	693.6	408.5	1.5368	553.4
25.167	373.18	443.8	690.6	411.0	1.5560	555.5
30.106	373.16	436.7	687.4	412.7	1.5738	557.2
35.011	373.17	430.3	684.1	414.0	1.5896	558.2
40.022	373.16	423.8	680.2	414.8	1.6052	559.0

The obtained results were analyzed using the equation of state [6]:

$$p = A(T)\,\rho^2 + B(T)\,\rho^8 + C(T)\,\rho^{12}, \tag{1}$$

here: the coefficients *A(T), B(T)* and *C(T)* of equation (1) depend on temperature:

$$A(T) = \sum_{i=1}^{3} a_i T^i,\ B(T) = \sum_{i=0}^{2} b_i T^i,\ C(T) = \sum_{i=0}^{2} c_i T^i, \tag{2}$$

The values of the coefficients *ai, bi* and *ci* are presented in Table 2.

Table 2: Coefficients *ai, bi* and *ci* of the equation of state of the "Palchig-oba" geothermal water.

a_i	b_i	c_i
a1= -5.96906137647	b0= 7660.5225241	c0= -5397.473667514
a2= 0.03060188658	b1= -49.491673	c1= 35.409651677
a3= -0.4800227471·10-4	b2= 0.0829263	c2= -0.0575229913

Equation of state (1) allows the experimental density values to be expressed with an average relative error of $\Delta\varrho/\varrho$ = 0.010 %, and this error for each experimental value is shown in Figure 3.

Using the equation of state, various thermodynamic parameters were determined: the isothermal compressibility, k_T/MPa^{-1} which describes the relative volume change under a pressure change at constant temperature, is computed as follows:

$$k_T = (1/\rho)(\partial p/\partial \rho)_T^{-1}, \tag{3}$$

Equation of state (1) can be expressed in the following form using Equation (3):

$$k_T = 1/(2A\rho^2 + 8B\rho^8 + 12C\rho^{12}). \tag{4}$$

The calculated values of the isothermal compressibility, k_T/MPa^{-1} are presented in Table 1 and illustrated in Figure 4.

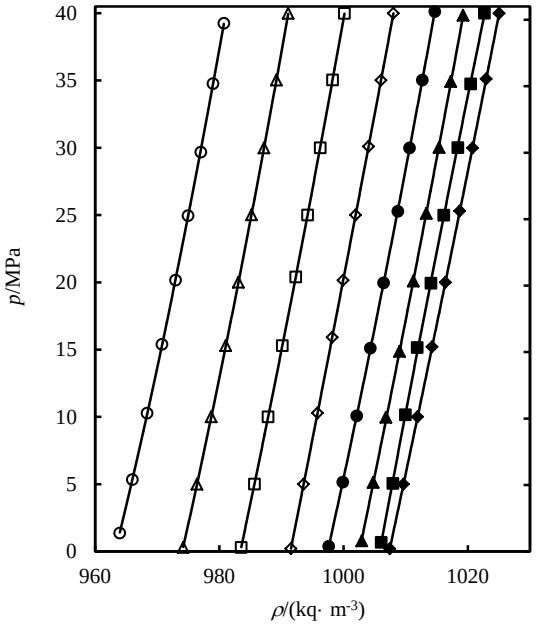

Figure 1. Dependence of the pressure ρ of the "Palchig-oba"geothermal water on density ρ : ◆, 278.15 K; ■, 288.12 K; ▲, 298.15 K; ●, 312.95 K; ◇, 328.15 K; □, 343.16 K; Δ, 358.15 K; ○, 373.09 K; ___ result calculated using the equation of state.

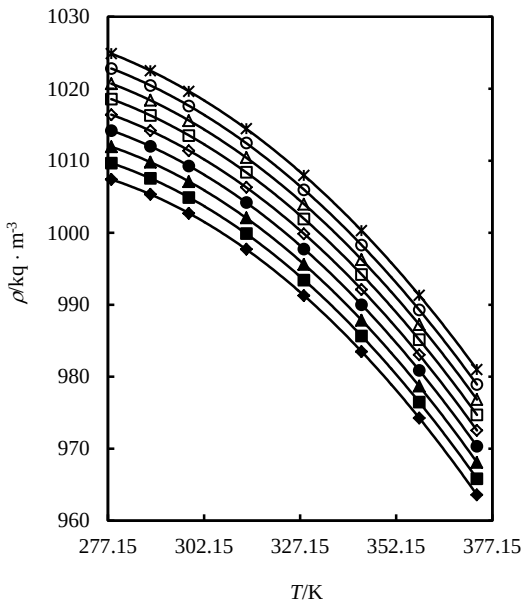

Figure 2. Dependence of the density ρ of the "Palchig-oba"geothermal water on temperature *(T)* : ◆, 0.101 MPa; ■, 5 MPa; ▲, 10 MPa; ●, 15 MPa; ◇, 20 MPa; □, 25 MPa; Δ, 30 MPa; ○, 35 MPa; *, 40 MPa.

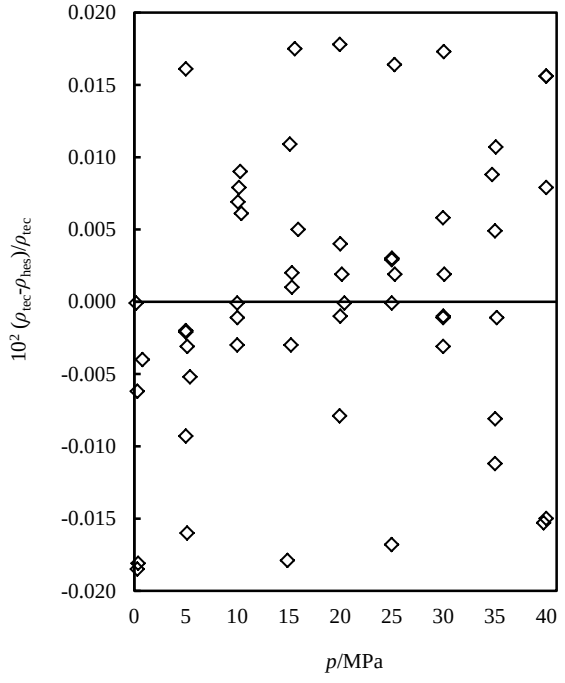

Figure 3. Percent difference between the experimental density (ϱ_exp) and the density calculated using the equation of state (ϱ_calc).

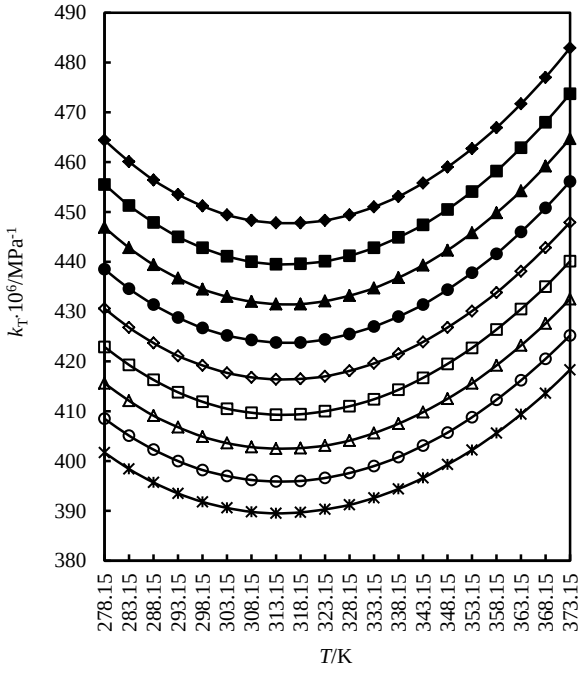

Figure 4. Dependence of the isothermal compressibility $k_T \cdot 10^6/MPa^{-1}$ of the "Palchig-oba" geotermal water on temperature T ◆, 0.101 MPa; ■, 5 MPa; ▲, 10 MPa; •, 15 MPa; ◇, 20 MPa; □, 25 MPa; Δ, 30 MPa; ○, 35 MPa; *, 40 MPa.

The isobaric thermal expansion coefficient α_p/K^{-1} for the "Palchig-oba" geothermal water was determined using the following relation.

(5)

$$\alpha_p = [A'(T) + B'(T)\rho^6 + C'(T)\rho^{10}]/[2A(T) + 8B(T)\rho^6 + 12C(T)\rho^{10}], \quad (6)$$

here: *A'(T), B'(T),* and *C'(T)* denote the temperature derivatives of the coefficients *A(T), B(T),* and *C(T),* respectively, and are determined as follows:

$$A'(T) = \sum_{i=1}^{3} ia_i T^{i-1},\ B'(T) = \sum_{i=1}^{2} ib_i T^{i-1},\ C'(T) = \sum_{i=1}^{2} ic_i T^{i-1}\ . \qquad (7)$$

Calculated values of the isobaric thermal expansion coefficient α_p/K^{-1} are given in Table 1.

The difference in specific heat capacities at constant pressure and constant volume $(c_p\text{-}c_v)$ / $Jkq^{-1}K^{-1}$ is calculated as follows:

$$c_p = c_v + T\frac{(\partial p/\partial T)_\rho^2}{\rho^2(\partial p/\partial \rho)_T}, \qquad (8)$$

here: c_p and c_v are the specific heat capacities at constant pressure and constant volume. Using equations (3) and (5), the following dependence can be obtained:

$$c_p - c_v = \frac{\alpha_p^2 T}{\rho k_T}, \qquad (9)$$

Calculated values of $(c_p\text{-}c_v)$/$Jkq^{-1}K^{-1}$ the difference in specific heat capacities at constant pressure and volume, are presented in Table 1.

As a result of the experimental analysis, anomalies were observed in the dependence of density and the calculated thermal properties of the "Palchig-oba" geothermal water. Specifically, the isothermal compressibility initially decreases with increasing temperature, as is typical for water, but begins to increase again at approximately T = (313.15–318.15) K. These anomalies are primarily attributed to the high water content of the geothermal fluid, which constitutes (96–97%) of its composition. Thus, at low temperatures, the molecular network of water adopts an expanded, open structure, which facilitates higher compressibility. As the temperature increases, the molecular structure becomes more compact, resulting in reduced compressibility.

REFERENCES

1. Babayev, A. M. Mineral waters of the mountainous folded regions of Azerbaijan. Baku, 2000, Chashiogly, 384 pp.
2. State Program for the Use of Alternative and Renewable Energy Sources in the Republic of Azerbaijan (2004, October 21). Approved by Decree No. 462 of the President of the Republic of Azerbaijan.
3. Nabiyev, N. D., Bashirov, M. M., Safarov, C. T., Shahverdiyev, A. N. Chemical analysis of the composition of geothermal waters of the Khachmaz region of Azerbaijan. *Scientific Works of AzTU*, 2008, 7,2, 10–13.
4. Nabiyev, N. D. Temperature dependence of the density of geothermal energy sources in the Khachmaz region of Azerbaijan. *Problems of Energy*, 2009, 1, 119–122.
5. Nabiyev N., Bashirov M., Safarov J., Shahverdiyev A., Hassel E. Thermodynamic Properties of the Geothermal Resources (Khachmaz and Sabir-oba) of Azerbaijan, *J. Chem. Eng. Data* 2009, 54, 1799-1806.
6. Nabiyev, N. D. "Study of thermal-physical properties of geothermal energy resources of the Khachmaz region of Azerbaijan". Dissertation submitted for the degree of Doctor of Philosophy in Engineering, Baku, 2011, 177 pp.

UDC: 004.94:544.77
DOI: https://doi.org/10.30546/2521-6317.2025.01.452

DIGITAL SIMULATION AND COMPUTATIONAL MODELLING OF SURFACE-ACTIVE COMPLEXES BASED ON QUATERNIZED ETHYL PIPERAZINE

Elgun E. HASANOV*, Gulnara A. AHMADOVA

Institute of Petrochemical Processes of the Ministry of Science and Education of Azerbaijan,
Hojaly ave. 30, AZ 1025,
Baku, Azerbaijan

ARTICLE INFO

Article history:
Received:2025-07-08
Received in revised form:2025-07-19
Accepted:2025-08-05
Available online:2025-12-25

Keywords:
Computational;
Molecular simulation;
Dissipative Particle Dynamics;
Surface-active;
Quaternized

ABSTRACT

Modelling and simulation of real-life phenomena in virtual environment is gradually becoming an integral part of science and technology. One crucial benefit of computer modelling in science and engineering is the opportunity to extract useful information about the nature of the subject system that would otherwise be available only through tedious experimental procedures. The other advantage of computer simulation is the ability to analyze the system from a new perspective and identify new information which would not be available via experimental methodologies. Future development and improvement on the accuracy of computer modelling techniques depend on how simulation results are successfully verified against experimental findings. This work presents the outcome of a molecular simulation performed on a novel surface-active complex alongside the relevant experimental findings to verify that the identified simulation methodology is robust enough to predict the behavior of the molecular system under specified real-life conditions.

1. INTRODUCTION

The age of fast digitalization and diminishing resources oversees the rapid development of computational models and simulation techniques in chemistry and chemical engineering. Computational methods are being utilized successfully for prediction of structures and properties of various chemical and biological systems and processes [1]. Simulation of molecular systems in virtual environment using computational tools helps to minimize the usage of resources such as material, energy and time while evaluating various alternatives during chemical product development process. It is predicted that with the future progress of computational methods in chemistry, automated generation of reaction paths will be possible [2]. In addition, application of machine learning to molecular simulations and computational chemistry is another promising idea that can unlock the potential of this field for future product development [3].

However, development of various computational tools depends on their successful benchmarking against experimental data. Several works have been dedicated to linking experimental findings with computer simulations of various molecular systems and processes [4]-[7].

Surface and interfacial science is one of the most important fields in need of progressive computational modelling work for its future development. Combining computational input with novel experimental findings in surface and interfacial science can lead to revolutionary inventions with great application potential. Considering this, our work reports the computer modelling of self-assembly and micellization behavior of a novel surface-active complex. The suggested coarse graining and parametrization scheme can be successfully extrapolated to similar molecular structures.

2. EXPERIMENTAL WORKS

2.1 Synthesis

Synthesis of the surface-active complexes was done as described in Fig. 1 below. In the first step of reaction sequence ethyl piperazine reacted with propylene oxide to produce alkanolamine. In the next step the alkanolamine was protonated with hydrogen chloride to obtain di-ammonium dichloride salt. The third step was the total quaternization of the diammonium salt by reacting it with propylene oxide in 1:2 molar ratio. In the final step surface-active complexes were obtained by mixing the quaternized product with long chain carboxylic acids or their sodium salts.

For the purposes of this study, the surface-active complex with stearic acid fragments (named as [C_{18}-EPPO_3-C_{18} + 2 NaCl]) has been chosen and both experimental and computational evaluation of the product has been performed.

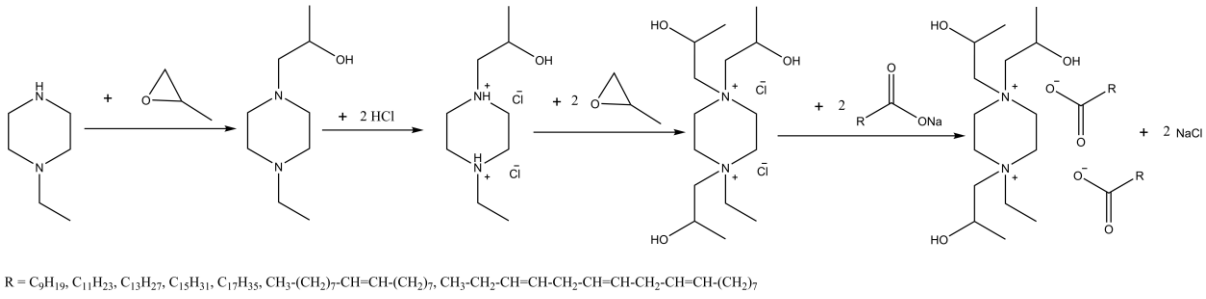

Fig. 1 Synthesis of the surface-active complexes from ethyl piperazine

2.2 Self-assembly Properties

Critical Micelle Concentration (CMC) of the obtained surface-active complex [C_{18}-EPPO_3-C_{18} + 2 NaCl] has been measured via conductometric method and was recorded as ? mM. Its high surface activity and self-assembly properties were also verified by tensiometric measurements. Fig. 2 and Fig. 3 below present the conductivity and surface tension of aqueous [C_{18}-EPPO_3-C_{18} + 2 NaCl] solutions as a function of their concentration.

The conductometry and tensiometry analyzes indicate that [C_{18}-EPPO_3-C_{18} + 2 NaCl] possess surface activity and is able to form molecule clusters called "micelles" in aqueous solution. The characteristic break point on Fig. 2 corresponds to the minimum concentration that allows formation of micellar clusters and is denoted as CMC point.

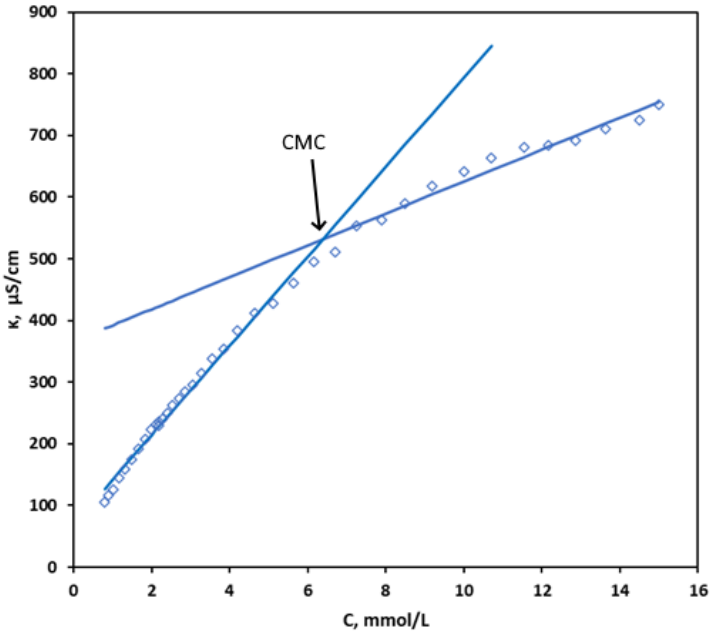

Fig. 2 *Conductivity vs concentration graph of [C_{18}-EPPO_3-C_{18}+ 2 NaCl]*

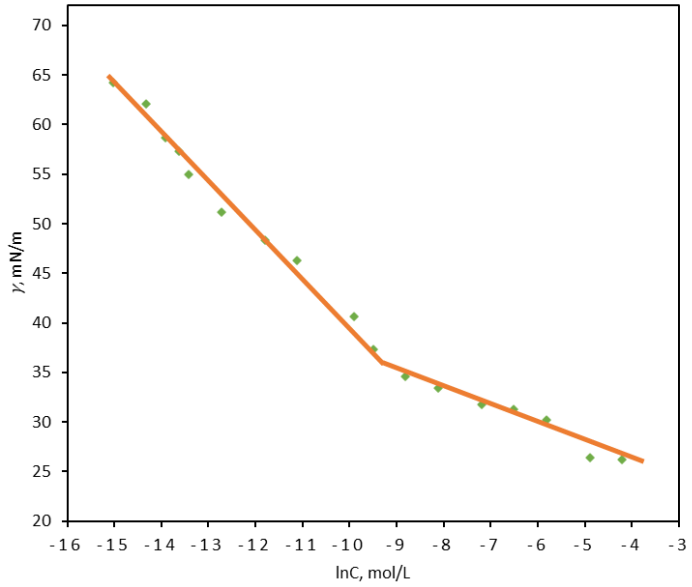

Fig. 3 *Surface tension vs ln of concentration graph of [C_{18}-EPPO_3-C_{18}+ 2 NaCl]*

3. DPD METHODOLOGY

Dissipative Particle Dynamics (DPD) technique is a computational scheme designed to simulate the mesoscopic particles' motion in fluid environment by utilizing Newton's classical motion theory [7]. This method is regarded as one of the most useful molecular simulation tools to model and study the behavior of self-assembling systems such as surfactant solutions.

The basis of DPD methodology is computation of two types of forces acting on the particles of interest in the finite simulation volume. The two types of forces are categorized as bonded and non-bonded forces, whereas the particles of interest are generally named as "beads".

3.1 Non-bonded Forces

The non-bonded DPD forces consist of the following:

- The conservative force F_{ij}^C
- The dissipative force F_{ij}^D
- The random force F_{ij}^R
- The electrostatic force F_{ij}^E

The conservative force F_{ij}^C accounts for the repulsive interactions between bead particles and the soft harmonic form of conservative force (1) is utilized for the simulation:

$$F_{ij}^C=\begin{cases} a_{ij}\left(1-\frac{r_{ij}}{r_C}\right) & r_{ij}<r_C \\ 0 & r_{ij}\geq r_C \end{cases} \qquad (1)$$

Where a_{ij} is called the repulsive interaction parameter between beads i and j, r_C is called the cut-off radius and r_{ij} is the distance separating beads i and j. The repulsive interactions take effect only within the cut-off radius r_C.

The frictional forces between the beads in the fluid medium is represented by the dissipative force F_{ij}^D (2):

$$F_{ij}^D=-\gamma_{ij}\omega^D(r_{ij})(v_{ij}) \qquad (2)$$

Where γ_{ij} is the friction coefficient and $\gamma_{ij}=\gamma_{ji}>0$. $v_{ij}=v_i-v_j$ is the velocity difference between the bead particles. ω^D is called the distance dependent weight function is calculated by (3):

$$\omega^D=\begin{cases} \left(1-\frac{r_{ij}}{r_C}\right)^2 & r_{ij}<r_C \\ 0 & r_{ij}\geq r_C \end{cases} \qquad (3)$$

The random motion of the particles in the fluid medium is represented by the random force F_{ij}^R (4):

$$F_{ij}^R=\sigma_{ij}\omega^R(r_{ij})\xi_{ij}\frac{1}{\sqrt{\Delta t}} \qquad (4)$$

Where σ_{ij} is the noise amplitude ($\sigma_{ij}=\sigma_{ji}>0$). $\xi_{ij}=\xi_{ji}>0$ is a randomly fluctuating Gaussian variable with a zero mean and a unit variance, Δt represents the time step utilized in DPD simulations. ω^R is the distance dependent weight function (5):

$$\omega^R=\begin{cases} 1-\frac{r_{ij}}{r_C} & r_{ij}<r_C \\ 0 & r_{ij}\geq r_C \end{cases} \qquad (5)$$

The noise amplitude σ_{ij} and the friction coefficient γ_{ij} are related:

$$\sigma_{ij}^2=2\gamma_{ij}k_BT \qquad (6)$$

In (6) above k_B is the Boltzmann constant ($k_B=1.380649\times10^{-23}\ J\cdot K^{-1}$) and T is the absolute temperature in K (Kelvin).

Finally, the electrostatic force F_{ij}^E is represented by the Coulomb's Law (7):

$$F_{ij}^E=k_e\frac{q_iq_j}{\varepsilon_r r_{ij}^2} \qquad (7)$$

Where k_e is the Coulomb's constant (k_e=8.99 × 10^9 $N \cdot m^2 \cdot C^{-2}$), q_i and q_j are the electrostatic charges of the beads *i* and *j*, and ε_r is the relative permittivity.

3.2 Bonded Forces

The spring force F_{ij}^S and the angle force F_{ijk}^A are the bonded forces taking effect when two or more bead particles are sharing a bond in a manner similar to covalent bonds in chemistry.

The strength of bonds connecting the bead particles is simulated by the spring force F_{ij}^S. The spring force F_{ij}^S (8) and its potential U^S (9) are:

$$F_{ij}^S = -\frac{\delta U^S}{\delta r_{ij}} \qquad (8)$$

$$U^S = \sum_j \frac{1}{2} C^b \left(r_{ij} - r_0\right)^2 \qquad (9)$$

Where C^b is the spring constant and r_0 is the equilibrium length of the bond connecting beads *i* and *j*.

The stiffness of the angle between two bonds is simulated by the angle force F_{ijk}^A. The cosine harmonic functional form the angle force F_{ijk}^A is used as expressed by (10) and (11):

$$F_{ijk}^A = -\frac{\delta U^A}{\delta r_{ij}} \qquad (10)$$

$$U^A = \sum_j \frac{1}{2} C^a \left(cos\theta_{ijk} - cos\theta_0\right)^2 \qquad (11)$$

Where C^a is the angle constant, θ_{ijk} is the actual bond angle, θ_0 is the equilibrium bond angle between *i-j* and *j-k* bonds.

4. SIMULATION SET-UP

The simulation was performed using Materials Studio v23 molecular modelling software. The simulation was performed in a box with dimensions of 200 Å × 200 Å × 200 Å with NVT ensemble for 100000 time steps.

4.1 Coarse Graining

Coarse graining in molecular simulation is the process of modelling the actual molecular structure for computational process via the specified scheme. Water molecules and molecules of surface-active complex [C_{18}-EPPO_3-C_{18} + 2 NaCl] have been coarse grained in accordance with the schematic described in Fig. 4 below.

4.2 Parametrization

The repulsive interaction parameters a_{ij} used in Materials Studio v23 are presented in Table 1 below.

In addition, all other DPD parameters from (1) to (11) that are required by the software to converge are defined below:

- The cut-off radius r_C=6.46 Å
- The friction coefficient γ_{ij}=4.5

- Time step $\Delta t=0.05$
- The bond spring constant $C^b=150$
- The bond angle constant $C^a=5$
- The equilibrium bond angle $\theta_0=180°$

For electrostatic effects the charges of +1, +1 and -1 were assigned to NH, eNH and CO beads, respectively. The relative permittivity ε_r of water at 25°C ($\varepsilon_r=78.2$) was selected to simulate aqueous environment.

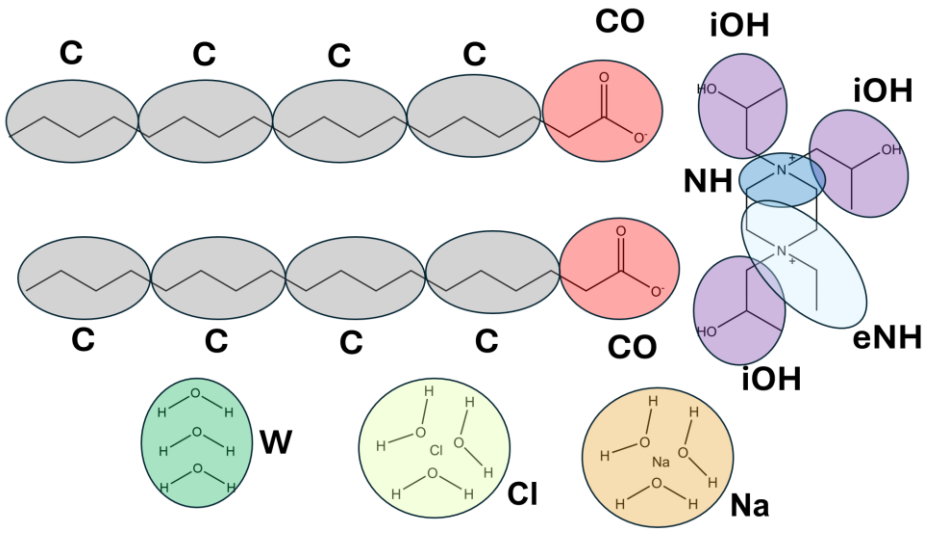

Fig. 4 Coarse graining schematic of [C_{18}-EPPO_3-C_{18}+ 2 NaCl]

Table 1. DPD repulsive interaction parameters

Bead type	C	CO	iOH	NH	eNH	W	Na	Cl
C	78.33							
CO	134.22	78.33						
iOH	89.25	93.35	78.33					
NH	82.32	80.68	73.97	78.33				
eNH	79.38	77.98	74.75	78.18	78.33			
W	118.79	80.77	75.50	74.24	72.69	78.33		
Na	118.79	80.77	75.50	74.24	72.69	78.33	78.33	
Cl	118.79	80.77	75.50	74.24	72.69	78.33	78.33	78.33

4.3 Simulation Outcomes

The molecular simulation converged successfully, and the equilibrated simulation trajectories were obtained (see Fig. 5). Water molecules have been hidden in the final simulation box frames to clearly indicate the structure of surface-active molecules. The final state of the simulation box shows distinctive clustering of the surfactant molecules. The ionic moieties, on the other hand, are randomly distributed within solution phase. These findings agree with the experimental

findings, indicating self-assembly and micellization tendencies of [C_{18}-$EPPO_3$-C_{18} + 2 NaCl].

Therefore, it is established that DPD simulation performed in Materials Studio could successfully predict system behavior provided that correct parametrization is done.

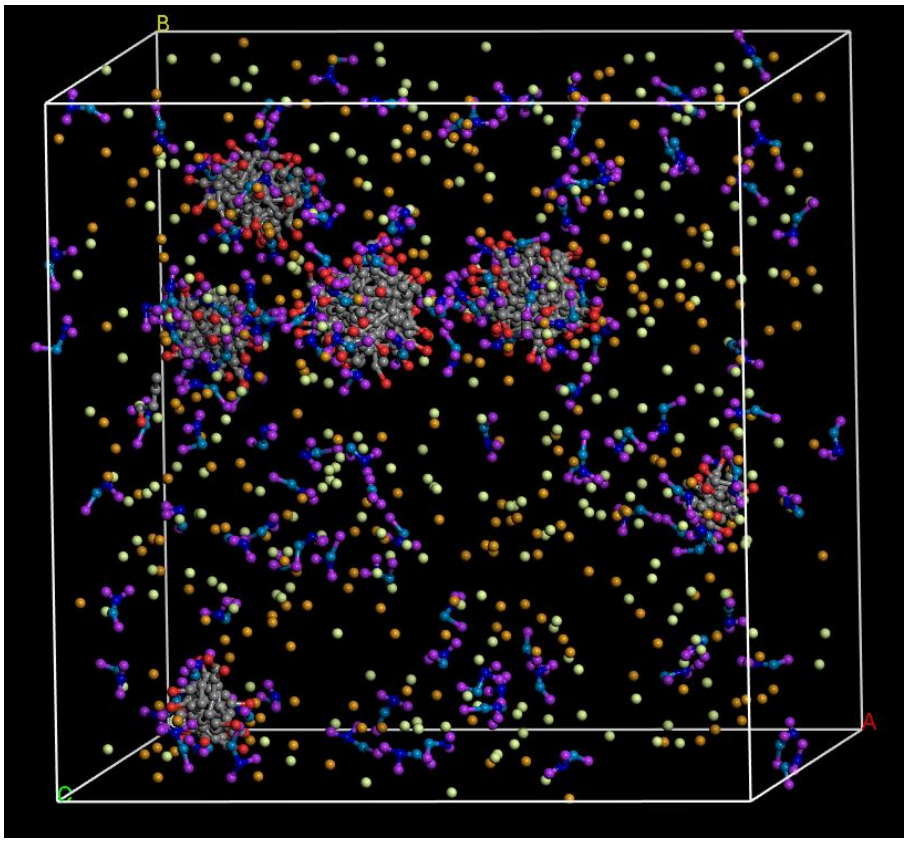

Fig. 5 Equilibrated simulation box depicting micelle formation

5. CONCLUSION

The synthesis of a completely new surface-active complex and its successful computer modelling have been done. The simulation results agree with the experimental findings. The methodology utilized for computational modelling of the novel surface-active complexes can be further applied to similarly constructed molecular systems for deeper and more rigorous study of self-assembly and micellization behavior.

REFERENCES

[1] Leszczynski, J., & Shukla, M. K. (2022) Practical Aspects of Computational Chemistry V. *Springer International Publishing*, https://doi.org/10.1007/978-3-030-83244-5

[2] Grimme, S., & Schreiner, P. R. (2018). Computational Chemistry: The Fate of Current Methods and Future Challenges. *Angewandte Chemie - International Edition*, *57*(16), 4170–4176. https://doi.org/10.1002/anie.201709943

[3] Ciccotti, G., Dellago, C., Ferrario, M., Hernández, E. R., & Tuckerman, M. E. (2022). Molecular simulations: past, present, and future (a Topical Issue in EPJB). *European Physical Journal B*, *95*(1). https://doi.org/10.1140/epjb/s10051-021-00249-x

[4] Shah, D., & Mjalli, F. S. (2014). Effect of water on the thermo-physical properties of Reline: An experimental and molecular simulation based approach. *Physical Chemistry Chemical Physics*, *16*(43), 23900–23907. https://doi.org/10.1039/c4cp02600d

[5] Firouzi, M., Rupp, E. C., Liu, C. W., & Wilcox, J. (2014). Molecular simulation and experimental characterization of the nanoporous structures of coal and gas shale. *International Journal of Coal Geology*, *121*, 123–128. https://doi.org/10.1016/j.coal.2013.11.003

[6] Cao, P., Short, M. P., & Yip, S. (2017). Understanding the mechanisms of amorphous creep through molecular simulation. *Proceedings of the National Academy of Sciences of the United States of America*, *114*(52), 13631–13636. https://doi.org/10.1073/pnas.1708618114

[7] Hu, C., You, G., Liu, J., Du, S., Zhao, X., & Wu, S. (2021). Study on the mechanisms of the lubricating oil antioxidants: Experimental and molecular simulation. *Journal of Molecular Liquids*, *324*, 115099. https://doi.org/10.1016/j.molliq.2020.115099

[8] Español, P., & Warren, P. B. (2017). Perspective: Dissipative particle dynamics. *Journal of Chemical Physics*, *146*(15). https://doi.org/10.1063/1.4979514

2025. Volume 9, Number 2 Pages 157-160

UDC: 614.842.61:674.048
DOI: https://doi.org/10.30546/2521-6317.2025.02.534

SYNTHESIS OF A FIRE-RETARDANT EUF MODIFIER FOR WOODEN STRUCTURAL CONSTRUCTIONS AND INVESTIGATION OF THE PROPERTIES OF A LIQUID GLASS-BASED COMPOSITION

KAMOLOVA Zaynura M

Bukhara State Technical University,

Bukhara, Uzbekistan

ARTICLE INFO

Article history:
Received: 2025-06-13
Received in revised form:2025-06-21
Accepted: 2025-07-19
Available online:2025-12-25

Keywords:
organic modifier, liquid glass, extraction, composition, oligo(poly)mer, DMSO, modification, diurethane, formaldehyde.

ABSTRACT

This article presents the analytical results of a scientific study devoted to one of the most relevant current problems, namely the fire protection of wooden building structures and the synthesis of compositions based on organic modifiers for this purpose. The modification of liquid glass, which makes it possible to significantly change its main properties, was studied in accordance with the SST standard, based on the modifier extraction method and the results of testing its thermal properties, which demonstrated a decrease in mass.

1. INTRODUCTION

The global construction industry is developing rapidly, primarily due to the growing demand for modern building and structural systems, which stimulates the improvement of their fire protection efficiency. Fire statistics clearly show that fires on a global scale have a negative impact not only on the economy but also on human life. Therefore, preventing the ignition of building structures, especially wooden materials, is of great importance. The use of local raw materials in the development of thermal insulation compositions leads to the creation of new products capable of replacing imported materials. The selection of liquid glass as a base material and the utilization of its properties as a coating make it possible to obtain coatings with localized thermal insulation properties.

To regulate the properties of liquid glass, it is modified using specific additives employed in the synthesis of its components. The modification of liquid glass, that is, the introduction of new organic bonds and changes in the composition of Na2SiO3, makes it possible to significantly expand its field of application. All additives used for the modification of liquid glass are divided into six types: acidic, precipitating, saline, hydrophilic, binding, and organic modifiers. Acidic additives reduce the alkalinity of the system and promote the formation of polysilicate ions, which increases the elastic modulus of liquid glass. Their advantage lies in the fact that, in addition to binding alkali, they release silicic acid during decomposition, which significantly densifies the hardening system [2].

The selection of an organic modifier in the system primarily leads to a significant increase in the adhesion of liquid glass to various surfaces, which is considerably higher than that achieved with inorganic modifiers, thereby expanding its range of applications. In general, without compromising the operational characteristics of the material, this makes it possible to improve not only

thermal properties but also adhesion, elasticity, plasticity, and viscosity. However, organic modifiers are not without disadvantages, namely their tendency toward coagulation, and this problem is resolved through the use of an emulsifier.

2. EXPERIMENTAL PART

During the synthesis process, appropriate reagents were selected, and the resulting product was synthesized under specified temperature and time conditions. The correct selection of reaction conditions is essential for the formation of an oligo(poly)mer with the desired thermal properties.

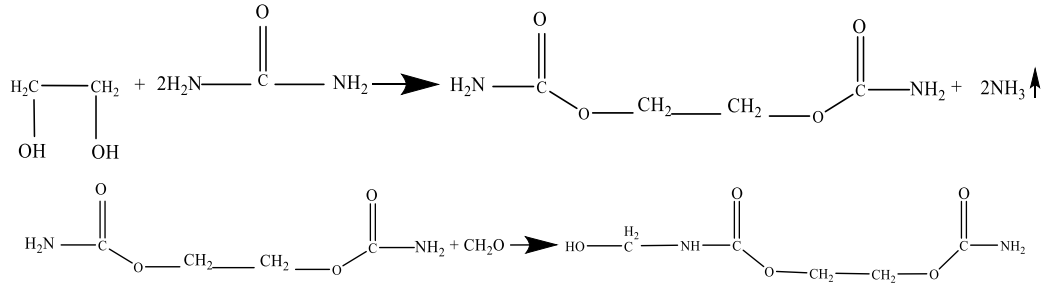

The formed diurethane reacts with formaldehyde to produce an oligo(poly)mer in accordance with the following reaction equation. Depending on the amount of formaldehyde, mono-, di-, or highly methylolated derivatives are formed. The ratio of the components is selected based on the intended application of the resulting derivative.

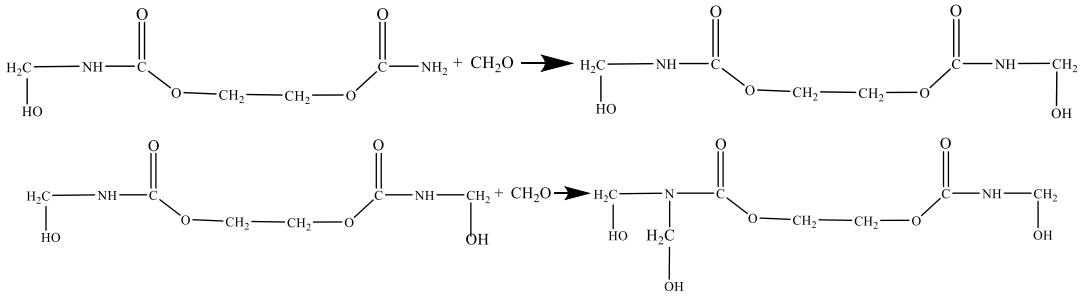

At the end of the process, a ready-to-use EUF modifier with a white–brown color and viscous consistency was obtained. The isolation of the synthesized compounds was carried out using the conventional extraction method. The resulting oligo(poly)mer was purified by extraction using various solvents. In particular, when dissolving the reagent and the synthesis product in alcohol, ethylene glycol and formaldehyde were dissolved, urea dissolved in small amounts, while the EUF modifier remained insoluble. A similar procedure was performed using other solvents. The extraction results are presented in the following table (Table 1).

Table 1. Solubility of Reagents and Products in Solvents

Solvents	Reagents and Products			
	Ethylene glycol	Urea	Formaldehyde	EUF
Water	dissolved	dissolved	dissolved	dissolved at 70-80 ^{0}C
Ethanol (Alcohol)	dissolved	partially dissolved	dissolved	partially dissolved
Benzene	insoluble	insoluble	insoluble	insoluble
Hexane	dissolved	insoluble	dissolved	partially dissolved
Dimethylformamide (DMF)	dissolved	insoluble	dissolved	partially dissolved
Decane	dissolved	insoluble	dissolved	dissolved
Octane	dissolved	insoluble	dissolved	insoluble
Acetone	dissolved	dissolved	dissolved	partially dissolved
Diethyl ether	dissolved	dissolved	dissolved	dissolved

DMSO	dissolved	dissolved	dissolved	insoluble
Isopropyl alcohol	dissolved	insoluble	dissolved	partially dissolved
Tetrahydrofuran (THF)	dissolved	dissolved	dissolved	dissolved
Benzene + DMSO	insoluble	insoluble	insoluble	partially dissolved
4 ml acetic acid + 4 ml ethanol + 2 ml butanol	dissolved	dissolved	dissolved	dissolved

Based on the obtained data, it can be concluded that the insolubility of the EUF substance in DMSO makes it possible to use this solvent in the extraction process to isolate the required synthesized compound. Particular attention should be paid to the purity of DMSO. Based on the determination of the solubility of the substance in various solvents and the results of the conducted experiments, it can be confidently stated that DMSO is used as the solvent after the extraction process.

It was established that one layer of the extraction mixture contains unreacted substances and compounds dissolved in the solvent (ethylene glycol, urea, and formaldehyde), while the second layer contains the synthesized reaction product, EUF, which is insoluble in the solvent. By applying the solvent replacement method, the oligo(poly)mer was isolated in a pure form, after which its structure, morphology, and composition were investigated using modern analytical methods.

3. Results and Discussion

To investigate the thermal properties of the oligo(poly)mer synthesized from the selected reagents, samples were prepared in a modified form using liquid glass solutions of varying concentrations. Wooden samples were treated by impregnation with the prepared liquid glass-based composition. According to fire safety regulations, the critical temperature for metallic structures, at which they lose strength, is 500 ^{0}C.

Aqueous solutions of the synthesized compounds with concentrations ranging from 1 to 10 % were prepared, and pine wood samples were impregnated in a specialized bath at 40–50 ^{0}C for 1–1.5 hours. As a result, it was established that the fire resistance of the treated wooden materials increased significantly. These findings were analyzed in accordance with SST 16363-98 (Table 2)

Table 2. Test results obtained for evaluating the thermal performance of liquid glass-based coatings (6 % modified composition).

№	Sample Mass, g		Temperature, ^{0}C		mass loss, g		Note
	Before	Before	T Start	T End	g	%	
1% Na_2SiO_3 solution	155,2	153,8	220	380	1,4	0,9	no complete destruction observed
2% Na_2SiO_3 solution	155,4	153,9	220	380	1.5	0,96	no complete destruction observed
3% Na_2SiO_3 solution	157,3	155.6	220	380	1,7	1,08	no complete destruction observed.
4% Na_2SiO_3solution	156,2	155.8	220	380	0,4	0,26	no complete destruction observed.
5% Na_2SiO_3solution	155,2	154,4	220	380	0,8	0,52	charring
6% Na_2SiO_3solution	155,5	154,5	220	380	1	0,64	charring
7% Na_2SiO_3solution	157,7	156,5	220	380	1,2	0,76	charring
8% Na_2SiO_3 solution	157,9	156,4	220	380	1,5	0,95	charring
9% Na_2SiO_3solution	157,9	156	220	380	1,9	1,2	charring
10% Na_2SiO_3solution	156,7	154,5	220	380	2,2	1,4	charring

Based on the results presented in Table 2, it can be concluded that, according to the requirements of SST 16363-98, as the concentration of the modified liquid glass increases, its degree of penetration into the wood decreases. Consequently, the thermal stability initially increases and then decreases, with the maximum value observed for the 4 % solution.

4. CONCLUSION

In conclusion, it can be noted that an EUF modifier with the desired properties was successfully synthesized using the selected reagents. To isolate this compound in a pure and individual form, a suitable solvent for extraction was selected, ensuring the purity of the obtained modifier.

The next key step in achieving the study objectives involved preparing solutions of modified liquid glass, testing them on wood samples, and conducting experiments in accordance with SST standards to evaluate the significant improvement in the fire resistance of the treated wooden materials. According to Table 2, the best performance for the selected 6 % modified composition and its corresponding Na_2SiO_3 was observed at a concentration of 4 %. This is primarily due to the low mass loss of 0.4 % and the absence of complete destruction, which supports the conclusion that the study's objectives have been successfully achieved.

REFERENCE

1. Akhmedov V.N., Kamolova Z.M., Olimov B.B. "Modification Method of Sodium Silicate." *Universum: Technical Sciences*, 2024, No. 3(120), pp. 45–48.
2. Kamolova Z.M., Beshimov I.A. "Structural and Thermal Characterization of a GMK Thermostable Coating via Chromatographic-Mass Spectrometry Analysis." *Universum: Technical Sciences*, April 2025, No. 4(133), pp. 33–36.
3. Kamolova Z.M. "Change in Viscosity of Modified Liquid Glass Depending on Concentration." *Development of Science. Scientific Journal*, 2025, Vol. 4, pp. 137–143.
4. Korneev V.I., Danilov V.V. "Soluble and Liquid Glass." Saint Petersburg: Stroyizdat, 1996.
5. Bobrov Yu.L., Ovcharenko E.G., Shoikhet B.M., Petukhova E.Yu. "Thermal Insulation Materials and Structures: Textbook." Moscow: Infra-M, 2003, 268 p.
6. Zin Min Htet, Tikhomirova I.N. "Thermal Insulation Material Based on Expanded Perlite and Foamed Mineral Binder." *Construction Materials*, 2019, No. 1–2, pp. 107–112.
7. Senkov S.A. "Special-Purpose Dry Construction Mixtures Based on Alkali-Silicate Binders."
8. Karnaukhov Yu.P., Sharova V.V. "Liquid Glass from Silicon Industry Waste for Slag-Alkali and Ash-Alkali Binders." *Construction Materials*, 1994, No. 11, pp. 14–15.
9. Kamolova Z.M., Akhmedov V.N., Beshimov I.A. "Separation of GMK Thermostable Coating Using the Extraction Method." *KarSU Bulletin. Scientific-Theoretical and Methodological Journal*, 2025, Vol. 1(2), pp. 72–75.
10. Kamolova Z.M., Akhmedov V.N., Beshimov I.A. "The Role of Liquid Glass in the Modern Development of Silicate Chemistry and Analysis of Its Development Trends." *Development of Science. Scientific Journal*, 2026, No. 5, pp. 268–273.

INSTRUCTIONS FOR AUTHORS

1. "The Baku Engineering University Journal-Chemistry and Biology" accepts original unpublished articles and reviews in the research field of the author.
2. Articles are accepted in English.
3. File format should be compatible with **Microsoft Word** and must be sent to the electronic mail (**journal@beu.edu.az**) of the Journal. The submitted article should follow the following format:

- Article title, author's name and surname
- The name of workplace
- Mail address
- Abstract and key words

4. The title of the article should be in each of the three languages of the abstract and should be centred on the page and in bold capitals before each summary.
5. **The abstract** should be written in **9 point** type size, between **100** and **150** words. The abstract should be written in the language of the text and in two more languages given above. The abstracts of the article written in each of the three languages should correspond to one another. The keywords should be written in two more languages besides the language of the article and should be at least three words.
6. . **UDC** and **PACS** index should be used in the article.
7. The article must consist of the followings:

- Introduction
- Research method and research
- Discussion of research method and its results
- In case the reference is in Russian it must be given in the Latin alphabet with the original language shown in brackets.

8. **Figures, pictures, graphics and tables** must be of publishing quality and inside the text. Figures, pictures and graphics should be captioned underneath, tables should be captioned above.
9. **References** should be given in square brackets in the text and listed according to the order inside the text at the end of the article. In order to cite the same reference twice or more, the appropriate pages should be given while keeping the numerical order. For example: [7, p.15].

Information about each of the given references should be full, clear and accurate. The bibliographic description of the reference should be cited according to its type (monograph, textbook, scientific research paper and etc.) While citing to scientific research articles, materials of symposiums, conferences and other popular scientific events, the name of the article, lecture or paper should be given.

Samples:

a) ***Article:*** Demukhamedova S.D., Aliyeva İ.N., Godjayev N.M.. *Spatial and electronic structure af monomerrik and dimeric conapeetes of carnosine üith zinc,* Journal of structural Chemistry, Vol.51, No.5, p.824-832, 2010

b) ***Book:*** Christie ohn Geankoplis. *Transport Processes and Separation Process Principles*. Fourth Edition, Prentice Hall, p.386-398, 2002

c) ***Conference paper:*** Sadychov F.S., Aydın C., Ahmedov A.İ.. Appligation of Information – Commu-nication Technologies in Science and education. II International Conference."*Higher Twist Effects In Photon- Proton Collisions", Bakı, 01-03 Noyabr, 2007, ss 384-391*

References should be in 9-point type size.

10. The margins sizes of the page: - Top 2.8 cm. bottom 2.8 cm. left 2.5 cm, right 2.5 cm. The article main text should be written in Palatino Linotype 11 point type size single-spaced. Paragraph spacing should be 6 point.
11. The maximum number of pages for an article should not exceed 15 pages
12. The decision to publish a given article is made through the following procedures:

- The article is sent to at least to experts.
- The article is sent back to the author to make amendments upon the recommendations of referees.
- After author makes amendments upon the recommendations of referees the article can be sent for the publication by the Editorial Board of the journal.